

AN ISOLATED SMALL WIND TURBINE EMULATOR

MD. ARIFUJJAMAN



**AN ISOLATED
SMALL WIND TURBINE EMULATOR**

BY

MD. ARIFUJJAMAN

A thesis

submitted to the school of Graduate Studies

in partial fulfillment of the requirements for the degree of

MASTER OF ENGINEERING

FACULTY OF ENGINEERING AND APPLIED SCIENCE
MEMORIAL UNIVERSITY OF NEWFOUNDLAND

St. John's, Newfoundland, Canada
July, 2006



Library and
Archives Canada

Bibliothèque et
Archives Canada

Published Heritage
Branch

Direction du
Patrimoine de l'édition

395 Wellington Street
Ottawa ON K1A 0N4
Canada

395, rue Wellington
Ottawa ON K1A 0N4
Canada

Your file *Votre référence*
ISBN: 978-0-494-30445-7
Our file *Notre référence*
ISBN: 978-0-494-30445-7

NOTICE:

The author has granted a non-exclusive license allowing Library and Archives Canada to reproduce, publish, archive, preserve, conserve, communicate to the public by telecommunication or on the Internet, loan, distribute and sell theses worldwide, for commercial or non-commercial purposes, in microform, paper, electronic and/or any other formats.

The author retains copyright ownership and moral rights in this thesis. Neither the thesis nor substantial extracts from it may be printed or otherwise reproduced without the author's permission.

AVIS:

L'auteur a accordé une licence non exclusive permettant à la Bibliothèque et Archives Canada de reproduire, publier, archiver, sauvegarder, conserver, transmettre au public par télécommunication ou par l'Internet, prêter, distribuer et vendre des thèses partout dans le monde, à des fins commerciales ou autres, sur support microforme, papier, électronique et/ou autres formats.

L'auteur conserve la propriété du droit d'auteur et des droits moraux qui protègent cette thèse. Ni la thèse ni des extraits substantiels de celle-ci ne doivent être imprimés ou autrement reproduits sans son autorisation.

In compliance with the Canadian Privacy Act some supporting forms may have been removed from this thesis.

Conformément à la loi canadienne sur la protection de la vie privée, quelques formulaires secondaires ont été enlevés de cette thèse.

While these forms may be included in the document page count, their removal does not represent any loss of content from the thesis.

Bien que ces formulaires aient inclus dans la pagination, il n'y aura aucun contenu manquant.


Canada

To My Parents

“Md. Abul Bashar & Rokeya Begum”

Abstract

Furling control method is the most commonly used control method by small wind turbine industry to control the aerodynamic power extraction from the wind. In this thesis, a small wind turbine with furling mechanism and its resulting dynamics are modeled on Matlab/Simulink platform. The model is simulated to regulate the speed of the wind turbine via a load control method. Tip-speed ratio and hill climbing control methods for the maximum power extraction are investigated. The wind speed data and Rayleigh distribution of St. John's, Newfoundland, is used to determine the annual energy capture. Satisfactory simulation performance leads to the implementation of an isolated small wind turbine emulator based on a separately excited DC motor to emulate and evaluate the performance of a small wind turbine using different control strategies. The test rig consists of a 3HP separately excited DC motor coupled to a synchronous generator. Wind turbine rotor and furling dynamics are incorporated in the emulator with the use of a PC based wind turbine model. A dump load is connected to the generator through a buck-boost converter controlled by a microcontroller. Emulation of the wind turbine is confirmed by running the DC motor to track the theoretical rotational speed of the wind turbine rotor. A dynamic maximum power controller is implemented and tested. The controller uses the wind speed and rotor speed information to control the duty cycle of the buck-boost converter in order to operate the wind turbine at the optimum tip-speed ratio. Test results indicate that the proposed system accurately emulates the behavior of a small wind turbine system.

Acknowledgements

This research project has been carried out at the Department of Electrical and Computer Engineering at Memorial University of Newfoundland. The financial support provided by the National Science and Engineering Research Council (NSERC), Canada is gratefully acknowledged.

My main thanks go to my supervisors Dr. Tariq Iqbal and Dr. John E. Quaicoe, without whom this thesis would have never been completed. Their overwhelming enthusiasm has kept me going when things felt tough. During my study at MUN, their extensive knowledge and experience have guided me through difficulties and encouraged me toward accomplishments. Working with Dr. Iqbal and Dr. Quaicoe has been a great pleasure and lots of fun!

I truly appreciate Jahangir Khan, who has assisted me many times during my research. I would also like to thank my housemates for their constant support. In particular, I am indebted to Wasimul Bari, for his guidance and mental support during my stay at St. John's.

Finally, thanks to my family and wife, Morsheda Mamataz, for supporting and for giving me so many good reasons not to work hard! Most of all, thanks to my parents, Md. Abul Bashar and Rokeya Begum, their love and encouragement is a deep and strong force in my life; without that, I could not have pursued my goals. I wish their acceptance of my dedicating this work to them.

Table of Contents

Abstract	i
Acknowledgements	ii
List of Figures	ix
List of Tables	xv
List of Symbols	xvi
List of Abbreviations	xxii
1. Introduction	1
1.1 Review of previous literatures	2
1.2 Organization of the thesis	7
2. Modeling and Energy Calculation of Small Wind Energy Conversion System	10
2.1 The wind energy conversion system	10
2.2 Control objectives of the wind turbine	15
2.2.1 Aerodynamic power control	16
2.2.2 Aerodynamic control strategy selection principle	19
2.2.3 Control strategy to extract maximum power	22
1. Tip-speed ratio (TSR) control	23
2. Hill climbing (HC) control	23
2.3 Modeling of the wind energy conversion system	24
2.3.1 Wind turbine	24

2.3.2	Permanent magnet synchronous generator	27
2.3.3	Rectifier	29
2.3.4	Inverter	30
2.3.5	Load	31
2.4	Energy calculation	32
2.5	Summary	34
3.	System Implementation and Simulation	35
3.1	System description	35
3.2	System implementation in Simulink	38
3.2.1	Wind turbine model	39
3.2.2	Permanent magnet synchronous generator model	39
3.2.3	Rectifier model	39
3.2.4	Inverter model	39
3.2.5	Load model	39
3.3	Simulation of the wind energy conversion system	40
3.4	Results and discussions	40
3.4.1	System stabilization	41
3.4.2	Investigation of the furling action dynamics	43
3.4.3	Energy calculation	45
3.5	Summary	46
4.	Development of a Novel Small Wind Turbine Emulator	48
4.1	Introduction	49
4.2	Basic structure of a wind turbine emulator	50

4.3	The developed wind turbine emulator	51
4.3.1	Reference rotor speed for the wind turbine emulator	55
4.3.2	Furling dynamics discretization for the wind turbine emulator	55
4.3.3	Controller algorithm for the wind turbine emulator	56
4.4	Implementation issues and calibration equations	59
4.4.1	Interfacing between the PC and power electronic circuitries	60
4.4.2	DC motor starting current	60
4.4.3	Calibration equation for the rotational speed of the motor	62
4.4.4	Calibration equation for the armature current of the motor	63
4.4.5	Calibration equation for the input and output of the phase controlled relay	64
4.5	Control program for the wind turbine emulator system	66
4.6	Power electronics for the wind turbine emulator	67
4.7	Motor parameter calculation	70
4.7.1	Armature resistance	70
4.7.2	Inertia	70
4.7.3	Back emf constant	72
4.7.4	Torque coefficient	73
4.8	Inertia disk design for the wind turbine emulator	74
4.9	Summary	74
5.	Test Results and Discussions on the Wind Turbine Emulator	76
5.1	Introduction	76
5.2	Armature current transient	77

5.3	Constant input response	78
5.4	Sudden change response	79
5.5	Summary	82
6.	Maximum Power Controller for the Emulator	83
6.1.	Introduction	83
6.2.	Maximum power control	85
6.2.1	Maximum power control algorithm	86
6.3.	Implementation of the maximum power controller power electronics	87
6.3.1	A complete power supply for the maximum power controller power electronics circuitry	89
6.3.2	DC – DC converter design	90
6.3.2.1	Inductor	93
6.3.2.2	Capacitor	95
6.3.2.3	Switch	97
6.3.2.4	Diode	98
6.3.2.5	Input filter	98
6.3.2.6	Output filter	98
6.3.3	Driver circuit for the switch	101
6.3.4	Extraction of the RPM information from the generator	102
6.3.5	PIC interfacing and programming	104
6.4.	Summary	108
7.	Results and Discussions	109
7.1	Introduction	109

7.2	Constant input response	110
7.2.1	Response to a constant wind speed of 7 m/s	110
7.2.1.1	Wind turbine emulator characteristics	110
7.2.1.2	Maximum power control	112
7.2.1.3	Maximum power controller power electronics	
	Performances	113
7.2.2	Response to a constant wind speed of 8 m/s	115
7.3	Sudden change response	117
7.3.1	Response to a step change in wind speed from 7 to 8 m/s	118
7.3.1.1	Wind turbine emulator characteristics	118
7.3.1.2	Maximum power control	119
7.4	Summary	120
8.	Conclusions	122
8.1	General summary	122
8.2	Achievements	123
8.3	Further work	126
	References	128
	Appendix A MATLAB/Simulink Wind Energy Conversion System Subsystem	
	Blocks	137
	Appendix B Wind Turbine Emulator Control Program	141
B.1	Labmaster I/O board analogue input test program	141
B.2	Labmaster I/O board analogue output test program	142

B.3	A program for control of wind turbine emulator	144
Appendix C	Program for the Maximum Power Control	149
C. 1	Program for the maximum power control	149

List of Figures

Figure 2.1 – Horizontal axis wind turbine	12
Figure 2.2 - Vertical axis wind turbine	12
Figure 2.3 – A typical wind power generation system	14
Figure 2.4 – Aerodynamic power as a function of wind speed for a typical wind turbine	16
Figure 2.5 – Horizontal furling of wind turbine	17
Figure 2.6 - Vertical furling of wind turbine	18
Figure 2.7 – Unfurled condition of a wind turbine	20
Figure 2.8 – Furled condition of a wind turbine	21
Figure 2.9 – Furling angle versus wind speed	22
Figure 2.10 – Schematic of the tip-speed ratio control of an isolated wind turbine	23
Figure 2.11 - Schematic of the hill climbing control of an isolated wind turbine	24
Figure 2.12 – Power coefficient as a function of tip-speed ratio	25
Figure 2.13 - Circuit model of a single-phase inverter	31
Figure 2.14 - Pulse width modulation	31
Figure 2.15 - Overall model of the wind energy conversion system	32
Figure 3.1 - Small wind energy conversion system	36
Figure 3.2 - Simulink diagram of the small wind energy conversion system	37
Figure 3.3 - Simulink diagram of the tip-speed ratio control of wind turbine	37
Figure 3.4 - Simulink diagram of the hill climbing control of wind turbine	38

Figure 3.5 - Step response of the turbine with the PID controller. (Wind speed increases from 9.5m/s to 10.5m/s at t= 7 s)	41
Figure 3.6 - PWM output of the inverter during tip speed ratio control (Wind speed increases from 9.5m/s to 10.5m/s at t= 7 s)	42
Figure 3.7 - Step response of the turbine with the hill climbing controller. (Wind speed increases from 9.5m/s to 10.5m/s at t=7 s)	42
Figure 3.8 - PWM output of the inverter hill climbing control (Wind speed increases from 9.5m/s to 10.5m/s at t=7 s)	43
Figure 3.9 - Step response of the turbine with the TSR controller. (Wind speed increases from 9.5m/s to 10.5m/s at t= 7 s)	44
Figure 3.10 - Step response of the turbine with the hill climbing controller. (Wind speed increase from 9.5m/s to 10.5m/s at t=7 s)	44
Figure 3.11 - Power output for the ti-speed ratio control	45
Figure 3.12 - Power output for the hill climbing control	45
Figure 3.13 - Per minute wind speed data	45
Figure 3.14 - Rayleigh distribution	45
Figure 3.15 - Power output for the tip-speed ratio control within St. John's wind speed	46
Figure 3.16 - Power output for the hill climbing control within St. John's wind speed	46
Figure 4.1 - A typical structure of wind turbine emulator	51
Figure 4.2 - Block diagram representation of the implemented wind turbine emulator	54
Figure 4.3 - Flow chart of the controller algorithm	58
Figure 4.4 - Structure of the small wind turbine emulator with peripheral	59
Figure 4.5 - Rotational speed versus voltage output from the tacho generator	62

Figure 5.5 - Variation of the rotational speed (Wind speed increases from 7m/s to 8m/s at t=1100 s)	81
Figure 5.6 - Representation of the expected furl dynamics (Wind speed increases from 7m/s to 8m/s at t=1100 s)	81
Figure 5.7 - Variation of the armature current after a step change in the load	82
Figure 6.1 - Structure of the maximum power controller	85
Figure 6.2 - Flow chart of the maximum power controller	86
Figure 6.3 - Schematic of the controller power electronics circuitry	88
Figure 6.4 - Schematic of the power supply for the controller power electronics	90
Figure 6.5 - Schematic of a buck-boost converter	90
Figure 6.6 - Schematic of the converter stage with peripheral	100
Figure 6.7 - Schematic of the driver stage of DC – DC converter	101
Figure 6.8 - Characteristic of the RPM signal extraction circuit	102
Figure 6.9 - Schematic of the RPM information extraction stage with peripheral	103
Figure 6.10 - A picture of the RPM information extraction circuit	104
Figure 6.11- Interfacing of the PIC with peripheral	105
Figure 6.12 - Flow chart of for maximum power the controller code	106
Figure 6.13 - A circuit diagram of the maximum power controller power electronics	107
Figure 6.14 - A photo of the maximum power controller power electronics	108
Figure 7.1 - Wind speed profile applied to the wind turbine emulator	111
Figure 7.2 - Variation of the armature current of the DC motor	111
Figure 7.3 - Variation of the rotational speed of the DC motor	111
Figure 7.4 - Expected furling dynamics of the wind turbine emulator	111

Figure 7.5 - Variation of the tip-speed ratio with time	112
Figure 7.6 - Duty cycle variation from the PIC with time	112
Figure 7.7 - PWM output of the PIC	113
Figure 7.8 - Amplified signal applied to the PIC	114
Figure 7.9 - Transformer output (upper) and Schmitt trigger output (lower)	114
Figure 7.10 - Gate drive signal for the MOSFET switch	114
Figure 7.11 - Wind speed profile applied to the wind turbine emulator	115
Figure 7.12 - Variation of the armature current of the DC motor	115
Figure 7.13 - Variation of the rotational speed of the DC motor	115
Figure 7.14 - Expected furling dynamics of the wind turbine emulator	115
Figure 7.15 - Variation of the tip-speed ratio with time	116
Figure 7.16 - Duty cycle variation from the PIC with time	116
Figure 7.17 - PWM output of the PIC	116
Figure 7.18 - Amplified signal applied to the PIC	117
Figure 7.19 - Transformer (upper) and Schmitt trigger output (lower)	117
Figure 7.20 - Gate drive signal for the MOSFET switch	117
Figure 7.21 - Wind speed profile applied to the wind turbine emulator (Wind speed increases from 7m/s to 8m/s at t=480 s)	118
Figure 7.22 - Variation of the armature current of the DC motor	118
Figure 7.23 - Variation of the rotational speed of the DC motor	119
Figure 7.24 - Expected furling dynamics of the wind turbine emulator	119
Figure 7.25- Variation of the tip-speed ratio with time	120
Figure 7.26 - PWM wave from the PIC	120

Figure 7.27 - Gate drive signal for the MOSFET Switch	120
Figure A.1 - Subsystem “Wind Turbine”	137
Figure A.1 - Subsystem “Permanent Magnet Generator”	138
Figure A.2 - Subsystem “Rectifier”	138
Figure A.3 - Subsystem “Inverter”	139
Figure A.4 - Subsystem “Load”	139
Figure A.5 - Subsystem “Measurement Block”	140

List of Tables

Table 2.1 - A Typical comparison of small and large wind turbines	13
Table 2.2 - Control method of commercially available small wind turbines	18
Table 6.1 - Component of the DC – DC converter and filters	99

List of Symbols

Symbols

ρ	Air density
θ	Furling angle
λ	Tip speed ratio
ω_m	Angular velocity of wind turbine rotor
λ_{abc}^g	Amplitude of flux linkages in matrix form
ω_r	Rotor angular velocity of the generator
λ_m	Amplitude of the flux linkages
α	Delay angle
δ	Shear exponent
ω_{noload}	No load speed of the motor
A	Cross sectional area of the wind turbine
B	Damping constant
C	Capacitor of the converter
C_p	Power coefficient
C_{pb}	Betz constant
C_t	Torque coefficient
D	Duty cycle

$e(t)$	Error value
$E_{L,energy}$	Energy of the inductor
f_s	Switching frequency
G_f	Generator frequency
$H(s)$	Continuous furl dynamics
$H(z)$	Discrete furl dynamics
H_1	Reference height
H_2	Height of the tower
i	Load current
i_{abc}^g	Stator current of the PMSG in matrix form
I_R	Rectifier current
i_q^g	Zero sequence current in quadrature axis
i_d^g	Zero sequence current in direct axis
ΔI_L	Ripple current
I_0	Output current of the converter
$I_{L,rms}$	RMS current through the inductor
$I_{L,avg}$	Average current through the inductor
$I_{L,peak}$	Peak current through the inductor
$I_{c,rms}$	RMS current through capacitor

$I_{c,p-p}$	Peak to peak current through capacitor
$I_{SW,rms}$	RMS current through switch
$I_{SW,peak}$	Peak current through switch
$I_{SW,avg}$	Average current through switch
$I_{D,avg}$	Average current through diode
$I_{D,peak}$	Peak current through diode
$I_{C_1,rms}$	RMS current through the input filter capacitor
$I_{C_1,p-p}$	Peak to peak RMS current through the input filter capacitor
J	Moment of inertia of the generator
J_m	Moment of inertia of the motor
J_w	Moment of inertia of the wind turbine
K_t	Torque coefficient of the motor
K_e	Back emf constant of the motor
K_p	Proportional gain
L	Inductor of the converter
L_q^g	Stator inductance in quadrature axis
L_d^g	Stator inductance in direct axis
L_L	Load inductance
m	Modulation index
M	Mass of the wind turbine rotor

p	Differential operator
P	Number of pole of the PMSG
P_{mean}	Mean output power
P_{load}	Load power
P_{aero}	Aerodynamic power
r	Current ripple ratio
R	Radius of wind turbine rotor
R_{abc}^s	Stator resistances of the PMSG in matrix form
R^s	Stator phase winding resistance
R_L	Load resistance
R_a	Armature resistance of the motor
R_{disk}	Radius of the disk
T_w	Wind turbine torque
T_e	Electromagnetic torque in rotor reference frame
T_i	Integral time
T_d	Derivative time
T_s	Sampling time
T_m	Mechanical time constant of the motor
T_{ON}	ON time of the converter
T_{OFF}	OFF time of the converter

$u(t)$	Output of the PID controller
u_0	Base value of the control signal
u_c	Controller output voltage
V	Wind speed
V_n	Normal wind speed to the rotor plane
V_{abc}^g	Terminal voltages of the PMSG in matrix form
V_q^g	Terminal voltage of the PMSG in quadrature axis
V_d^g	Terminal voltage of the PMSG in direct axis
V_s^g	Stator output voltage of the PMSG
V_R	Rectifier voltage
V_{dc}	DC voltage of a source
V_{sine}	Predefined sine wave
$V_{\text{triangular}}$	Triangular carrier signal
V_{AA}	Output PWM wave
$V_{A,peak}$	Peak value of the PWM wave
V_a	Motor armature voltage
V_{ip}	Voltage input to the PIC
V_L	Load voltage
V_1	Wind speed of St. John's, Newfoundland

V_2	Scaled wind speed of St. John's, Newfoundland
V_0	Output voltage of the converter
V_d	Diode voltage
$V_{i(\max)}$	Maximum input voltage of the converter
ΔV_r	Maximum ripple voltage
V_{noload}	No load voltage of the motor armature
X_{c_2}	Capacitive reactance of the output filter
X_{L_2}	Inductive reactance of the output filter
Z_0	Surface roughness

List of Abbreviations

Abbreviations

AC	Alternating Current
A/D	Analogue to Digital
C	C programming language
DC	Direct Current
D/A	Digital to Analogue
ESR	Equivalent Series Resistance
F/V	Frequency to Voltage
HC	Hill Climbing
HP	Horse Power
I/O	Input Output
IM	Induction Motor
IC	Integrated Circuit
kW	Kilo watt
KHz	Kilo Hertz
MOSFET	Metal Oxide Field Effect Transistor
MPP	Maximum Power Point
MPPT	Maximum Power Point Tracker
MPC	Maximum Power Controller
P	Proportional
PSF	Power signal feedback
PI	Proportional Integral
PID	Proportional Integral Derivative
PMSG	Permanent Magnet Synchronous Generator

PWM	Pulse Width Modulation
PC	Personal Computer
PIC	Peripheral Interface Controller
QBASIC	Quick Beginner's All-purpose Symbolic Instruction Code
RPM	Rotation per Minute
RMS	Root Mean Square
SWTE	Small Wind Turbine Emulator
SRF	Self Resonant Frequency
TSR	Tip speed ratio
WT	Wind turbine
WTE	Wind Turbine Emulator
ZN	Ziegler-Nichols

Chapter 1

Introduction

Wind technologies have been developing rapidly over the last few decades. As a source of energy, wind is renewable, cost-effective and causes little harm to nature in comparison to other conventional sources of energies. Canada has a great potential for electricity generation from wind. A current survey (April, 2006) indicates that Canada had installed 260 MW of new wind energy capacity and expects 250 MW of additional capacity to be installed by the end of 2006 [1]. Also it should be mentioned that Canada is the 14th largest producer of wind energy in the world [2].

Wind turbines are used to generate electricity from wind. From the electrical engineering perspective, it can be defined as a device that converts wind energy into electrical energy. Electricity generation using wind energy is crucial for remote or isolated locations removed from the grid. There are lots of remote and isolated places around the world where a small-scale wind power generation can be connected together to meet the users' load demand. Small wind turbines are least expensive, composed of very few moving

parts and mainly designed for long life [3]. They can be installed on roof tops with smaller tower arrangement and also have very little environmental pollution. Due to a rapid increase in electricity generation from wind and the ease of use of small wind turbine systems, recent R & D activities involve the investigation of the behavior of small wind turbines.

Small wind turbines can operate with either fixed-speed or variable-speed. One problem with fixed-speed wind turbines is that it affects the power quality of the grid due to turbulence and the stochastic nature of wind [4]. On the other hand, variable speed wind turbines can be controlled by power electronic equipment, and by changing the rotor speed, power fluctuations can be minimized. Also energy production from a variable speed wind turbine is much greater than the fixed speed wind turbine [5].

The primary task of a wind turbine is to generate electricity from the wind and to supply the produced power to the user. Control of a wind turbine is an integral part of the wind power generation system for proficient operation of the wind turbine, to ensure the maximum power production and finally, maximum energy capture from a wind turbine system. In order to avoid problems at installation, it is necessary to test the power electronics and study the performance of the controller in a laboratory environment. The subject of this thesis is therefore to develop a laboratory model that emulates the steady state and dynamic behavior of a small wind energy system.

1.1 Review of Previous Literatures

As indicated above, a variable-speed wind turbine system can produce more energy than a fixed speed wind turbine. However, there is no specific gain on the energy capture

capability of a variable-speed wind turbine over a fixed-speed wind turbine. A variable-speed wind turbine can produce 2-6% more energy than a fixed-speed wind turbine [6], while the increase in energy can be around 39% [7]. Depending on the site condition and design parameters the energy capture can vary between 3-28% [8]. Thus variable-speed wind turbine hold promise for increased energy capture and further research is required to explore this potential.

The control action of a wind turbine is an essential part of the wind energy system. According to past research, with proper control of the wind turbine it is possible to increase the energy capture. A proper control of the wind turbine will cause no extra pressure on the electrical and mechanical parts of the wind turbine, thus increasing the ability to maximize the power extraction from a wind turbine system [9], [10]. As far as the aerodynamic power control of a small wind turbine is concerned, there are several ways of performing this task. Hoffmann and Mutschler [8] have shown that active stall, passive stall and pitch control on wind turbines can reduce the aerodynamic power. The associated problems with this scheme are the need for a good understanding of the airfoil design and the complex control system which sometimes tends to increase the cost of the installation. Further investigation shows that there are four main types of aerodynamic control methods for a small wind turbine system: furling (horizontal/vertical); flapping; passive pitching and soft stall. These control methods that are being used in most commercially available small wind turbines, mostly for their over speed and power control capacity [11]. It should be mentioned that the furling control method has received a lot of attention [11, 12, 13]. For this reason, this research focuses on the modeling and implementation of a wind turbine with furling mechanism and its resulting dynamics.

The control task should also ensure maximum power extraction and maximization of the energy capture by the wind turbine. There are several ways to extract maximum power from the wind turbine system, Tip Speed Ratio (TSR) control, power signal feedback (PSF) control and Hill Climbing (HC) control [14]. The problem associated with the TSR control is that it needs information about the instantaneous wind speed. In practice, it is quite difficult to measure the wind speed accurately because the wind turbine experiences a different wind on its rotor than an anemometer installed close to the wind turbine [15]. The HC method is based on the measurement of power. Two consecutive power measurements are used to determine the change in the power and the controller continuously searches for the peak output power [16,17], thus ensuring the operation at the maximum power point. With a proper controller it is possible to maximize the energy capture by the wind turbine. From this point of view a HC algorithm can work better compared to the TSRcontrol method. There are mainly three methods to determine the annual energy capture from a small wind energy conversion system namely, the swept area of the rotor method, the power curve method, and the use of the manufacturers published estimates [18, 19]. As a result of the stochastic nature of the wind, the power output of the wind turbine could vary even if the average wind speed is the same. In order to simplify this difficulty, the manufacturer and testing laboratories often sort a series of power measurements into the corresponding interval or register of wind speed and the technique is called method of bins [20]. This research uses the method of bins to calculate the annual energy capture by the modeled wind turbine.

Large wind turbines are complex in operation, deploy a multitude of control methods and operate mainly in grid-connected mode. On the other hand, small wind turbines can be

used for stand-alone as well as grid-connected applications. In order to avoid problems at installations and later use, it is necessary to emulate the steady state and dynamic behavior of the system in a laboratory environment. This can be achieved by developing a wind turbine emulator which will reflect the actual behavior of a wind turbine. The main use of a wind turbine emulator is to help design and test the wind turbine controller. Several researchers are working on the control of wind turbine by implementing the control schemes in a simulator. These investigations are mainly focused on the 5 kW or more rated wind turbine [21], [22]. Research need to be further extended to small wind turbines to effectively understand and characterize the behavior and control of such wind turbines.

A wind turbine is a highly nonlinear system and in order to build an emulator system that represents a realistic wind turbine, several dynamics should be included in the model. Several steady state wind turbine models have been used in the emulator platform based on the power speed characteristics [22], [23] and [24], torque coefficient based wind turbine model [21], [25] and [26], power coefficient and pitch angle based wind turbine model [27]. However the problem with static modeling is that the static behavior is unable to reflect the different dynamic aspects of a wind turbine which could be a vital issue during operation. In some publications, the dynamic aspects are incorporated with the model in different ways: elastic model of the turbine shaft [28]; mechanical balance equation [29], [30] for the turbine torque; and aerodynamic, oscillatory and dynamic torque to combine the wind turbine torque [31]. Passive pitching mechanism and rotor blade inertia have been considered with the wind turbine model which can be a well thought-out more generalized approach for a small wind turbine emulator system [32]. A

review of research on the development of wind turbine emulators given by A. D. Diop, et. al. [33], shows that the furling action is still not considered in the wind turbine emulator research area. Although static and dynamic aspects have been incorporated in some of the models developed in the literature, there is scope for further development and This work extends the development of a wind turbine emulator system to include both furling and rotor dynamics.

Maximum Power Point Tracking (MPPT) needs to be incorporated with any wind turbine system to maximize the power production. There are several ways to track the Maximum Power Point (MPP) of a wind turbine. A wind speed estimation based MPPT algorithm is investigated that employs principles of the generator and turbine characterization [34]. Wind speed is determined iteratively from the total generated power and the $C_p - \lambda$ profile of the turbine in use and based on this information, optimum TSR is maintained. The controller further needs to address several real time dynamic conditions, i.e., torque disturbances due to tower shadow effect, effect of wind gusts etc. Hysteresis maximum power point tracking scheme is another suitable option to track the maximum power. A hysteresis maximum power tracking scheme which works on the two modes of operation of the hysteresis loop is investigated in the past work [35]. Increment and decrement of the output power is governed by the equations and based on the demand, output current of the inverter is controlled. A well explanation is necessary to determine the various parameters as these parameters govern the dynamic performance of the controller. Authors of paper [36] proposed that if the DC bus voltage of the wind turbine is constant to any desired value then the maximum power could be achieved by forcing the DC current at its maximum value. However, the controller might fail to work for a wind gust

situation that needs to be considered. In this research work, the optimum TSR control has been chosen due to ease of implementation, although this technique is not good for practice as described above.

1.2 Organization of the Thesis

The basic purpose of this research work is to propose a stand-alone wind turbine emulator system which incorporates over speed control, isolated supply for system power electronics and maximum power extraction. A small Wind Turbine Emulator (WTE) needs to be developed in the lab environment to simulate the practical behavior of the system. In order to extract the maximum power out of the system, a maximum power point extractor is of importance. Associated power electronics and controller performance need to be addressed. Hence, the development of the power electronics for an isolated system is also a main part of the thesis. The proposed WTE consists of a 3HP separately excited DC motor coupled to a synchronous generator. A dump load is connected to the generator through a buck-boost converter controlled by a microcontroller. Wind turbine rotor and furling dynamics are incorporated in the emulator with the use of a PC based wind turbine model. The MPP controller, i.e., Maximum Power Controller (MPC) uses the wind speed and rotor speed information to control the duty cycle of the buck-boost converter in order to operate the wind turbine at the optimum TSR. The details of the development of the WTE system are described in the thesis as follows:

In Chapter 2, a small wind turbine with furling mechanism and its resulting dynamics are modeled on a Matlab/Simulink platform. A model wind turbine in conjunction with the electrical subsystem is developed. The model is simulated to regulate the speed of the

wind turbine via a load control method. TSR and HC control methods for maximum power extraction from a small wind turbine are implemented and investigated through simulation.

In chapter 3, several tests are performed in order to determine a suitable control strategy for the small wind energy conversion system based on annual energy capture. Wind speed versus power curve and annual energy capture of the system for each control method is determined for wind conditions in St. John's, Newfoundland. The wind speed data and the Rayleigh distribution of St. John's, Newfoundland, are used in this research to determine the annual energy capture.

In chapter 4, a small wind turbine emulator based on a separately excited DC machine is described to emulate the steady state and dynamic behavior of a WT. The proposed experimental rig consists of a PC, Lab Master I/O board, power electronics circuitry and a 3HP separately excited DC motor which drives a synchronous generator. The proposed model and the integration of the various subsystems of the small wind turbine emulator are presented in the chapter.

In chapter 5, the performance of the emulator is investigated. Test results for furling action, response to step changes in wind speed, and sudden load changes are presented and discussed in the chapter.

In chapter 6, a maximum power controller based on a microcontroller and the load side of the WTE is developed. The maximum power extractor consists of a generator coupled to the motor shaft and a dump load connected to the generator through a microcontroller controlled DC-DC converter. The topology selection and design of the DC-DC converter are described. Several real time issues and implementation details of each stage are

described. To ensure maximum power extraction, a dynamic controller is proposed which compares the actual TSR with an optimum TSR and uses the difference to control the Pulse Width Modulation (PWM) duty cycle of the DC-DC converter through a programmed microcontroller. The basic structure of the controller and the algorithm used to ensure the maximum power extraction are discussed in the chapter.

In chapter 7, the global results of the proposed system with wind speed variations are presented. The performance of the complete system under constant and sudden wind speed changes are evaluated. The results of the investigation show that the proposed system emulates accurately the characteristic of a small stand-alone wind turbine system and the MPC extract the maximum power from the system.

Finally, a summary of the work presented in the thesis, as well as an outline of the achievement and contribution of the work are highlighted in chapter 8. The chapter also includes suggestions for further investigations.

Chapter 2

Modeling and Energy Calculation of Wind Energy Conversion System

In this chapter, the modeling equations of a small wind turbine system as well as the electrical system mathematical equations and description are presented. A brief description of the aerodynamic power control, i.e., furling control method, which was one of the main interests of this work, is presented. Two dynamic controller selection principles for extracting the maximum power from the system are also discussed. In the end, a procedure to calculate the energy capture from such a small wind energy conversion system is presented.

2.1 The Wind Energy Conversion System

The importance of renewable energy is no longer questionable for electricity generation. In Canada, renewable energy consists mainly of wind power, biomass, and solar energy. Solar potential appears very limited in the Atlantic region due to

extended cloudy periods during the year. There is little hope of solar power due to its very high cost. Micro hydro and ocean energy systems could meet some of the local needs of electricity. This would, however, be seasonal and other forms of power generation may be required during some months of the year. Further R&D would be needed to exploit geothermal power.

Wind energy has the potential to provide mechanical energy or electricity without generating pollutants. Historically it has been used in many countries, especially, the Netherlands, as a source of mechanical energy, e.g. grinding corn or pumping water. In Canada, as in many other countries, wind energy has also been used to produce electricity. A lot of research has been carried out to prove the effectiveness of wind energy from large wind energy conversion systems but unfortunately not much research has been conducted on wind energy generation from small systems. Renewed interests have recently been generated in utilizing the energy of wind for wind pumps and sailing boats in many countries, especially, Netherlands.

Wind electricity for decentralized system or hybrid generation of electricity using other energy sources complementary to wind energy has now been given some attention and this could be suitable in low wind regimes for localized small grid systems or battery charging. For low wind speed, wind pumps could also be a viable option. Wind turbine system can be classified in a number of ways as follows.

1. According to the rotational axis of the rotor.
 - a) Horizontal axis
 - b) Vertical axis.
2. According to the size and capacity

a) Small wind turbine

b) Large wind turbine

3. According to their speed of rotation

a) Fixed speed wind turbine

b) Variable speed wind turbine

The horizontal axis wind turbines (whose rotational axis is parallel to the wind) is shown in Figure 2.1 and the vertical axis wind turbine (whose rotational axis is perpendicular to the wind) is shown in Figure 2.2 [18]. In addition, the wind turbine rotor can be propelled either by drag forces or by aerodynamic lift. The horizontal or vertical axis drag based designs operate with low speed and high torque, which can be

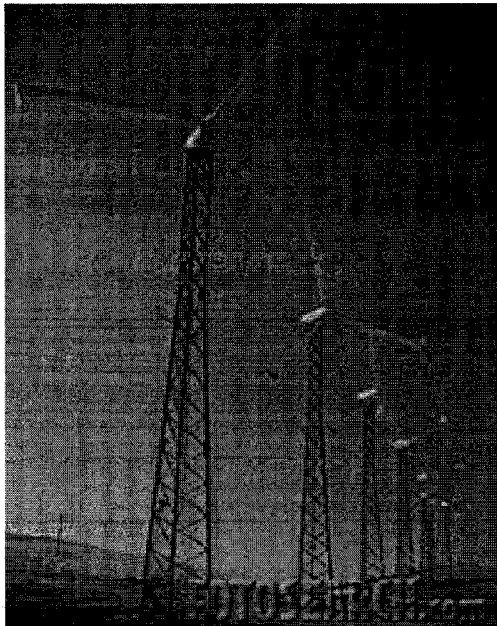


Figure 2.1 Horizontal axis wind turbine



Figure 2.2 Vertical axis wind turbine

useful mainly for grinding grains and pumping water. On the other hand, the horizontal and vertical axis lift based designs operate with high speed and low torque and are suitable for electricity generation. A wind turbine system can be classified as small or large depending on the rotor diameter, and capacity of generator. A typical

configuration and design aspect of small and large wind turbines is shown in Table 2.1.

Table 2.1 A Typical comparison of small and large wind turbines

Criteria	Small	Large
Power	Less than 10Kw	660 KW ~ 2 MW+
Diameter	1 ~ 7m	10 ~ 100m
Hub height	~ 30m	~ 130m
Over speed control	Furling control, Flapping control, Passive pitching control, Load control	Pitch to stall, pitch to feather
Generator	DC Alternator, Permanent Magnet Alternator	Induction Generator, Synchronous Generator
Application	Home, Farms, Remote Application	Central station wind farm, Community wind

The most useful classification in wind turbine industry is based on speed. Wind turbines can operate with either fixed-speed or variable-speed. In a fixed-speed large wind turbine, the generator (induction generator) is directly connected to the grid. One of the disadvantages of a fixed speed wind turbine is that the turbulence of the wind will result in power fluctuations, and thus affect the power quality of the grid [37]. In a variable-speed wind turbine, the generator is controlled by power electronic equipment, which makes it possible to control the rotor speed so that power fluctuations caused by wind variations can be more or less absorbed by changing the

rotor speed [38]. Compared to the fixed-speed wind turbine, the variable-speed wind turbine provides advantages such as higher energy production and improved power quality [39, 5].

Small wind turbine systems can be tied to the grid or it can work isolated. Several issues need to be addressed when a small wind turbine is connected to the grid. One of the major issues is the flicker production. Due to the load flow changes in the grid, the output voltage of the wind turbine fluctuates and induce flicker in the output. In addition, the stochastic nature of the wind, wind gradient and tower shadow effect contribute to inducing flicker in a grid connected wind turbine. Variable-speed wind turbines can mitigate the flicker phenomenon more than the constant speed wind turbine [40]; however, the phenomenon requires attention, particularly in small wind turbine connected to the grid. A typical arrangement of an isolated small wind energy system shown in Figure 2.3 consists of a wind turbine, a generator, power electronic converter and a maximum power extractor to extract the maximum power from the wind turbine. A battery arrangement is essential for an isolated small wind energy conversion system, while for a grid connected wind turbine, a transformer is required at the output to raise the level of the voltage.

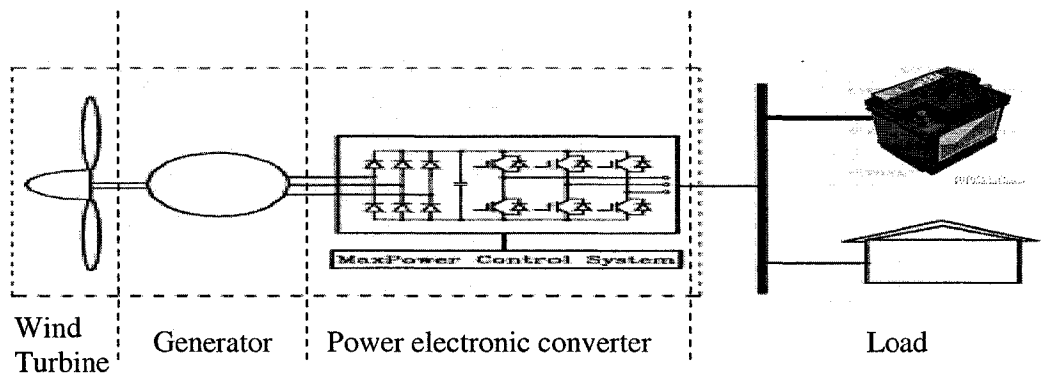


Figure 2.3 A typical wind power generation system

2.2 Control Objectives of the Wind Turbine

The control task of a wind turbine is essential for a number of reasons which can be summarized from earlier research as follows [9, 10]:

- Maximize the energy capture by the wind turbine by tracking the maximum power point. The simplest approach is to track the maximum power coefficient point.
- The wind is stochastic in nature; therefore, it produces lots of torque or power peaks and creates stress on the mechanical parts as well as cause power fluctuations in the grid.
- The wind turbine should be controlled to limit the power extracted from the wind to the nominal value of the wind turbine.
- Reduce the drive-train transients.
- Stabilize the system under all operating conditions.
- Control the grid voltage and power by regulating the output of the wind turbine.

Instead of focusing on the complete control task, this research work deals with some specific aspects under certain assumptions which can be summarized as follows.

- The wind turbine considered is a direct drive system and gear box dynamics can be ignored.
- The small wind turbine system considered operates in the isolated mode.
- Grid voltage, current and power fluctuations are not considered.

Using the above assumptions, the control objectives in this work deal mainly with

- Reducing the aerodynamic power of the wind turbine during high wind speed, and
- Maximizing the energy capture by extracting the maximum power from the wind turbine.

In order to achieve the control objectives, the control task was subdivided into two sections namely, aerodynamic power control and maximum power extraction from the wind turbine. Discussions and approaches considered to achieve the control task are presented in the following sections.

2.2.1 Aerodynamic Power Control

The aerodynamic power produce by the wind turbine varies with the third power of the wind speed and a typical power produce at the wind turbine shaft by the wind is shown in Figure 2.4 [41].

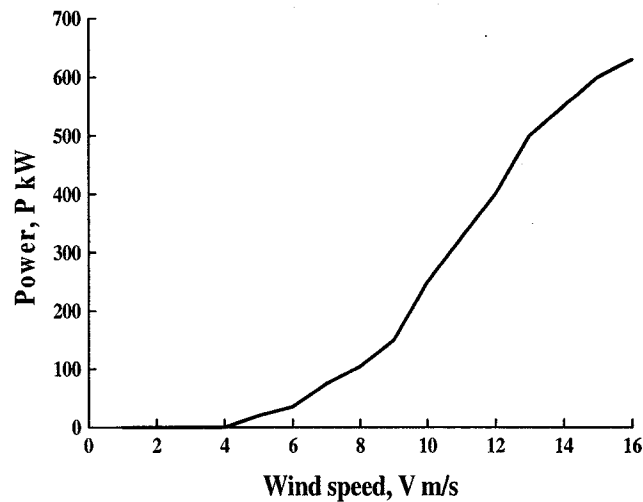


Figure 2.4 Aerodynamic power as a function of wind speed for a typical wind turbine

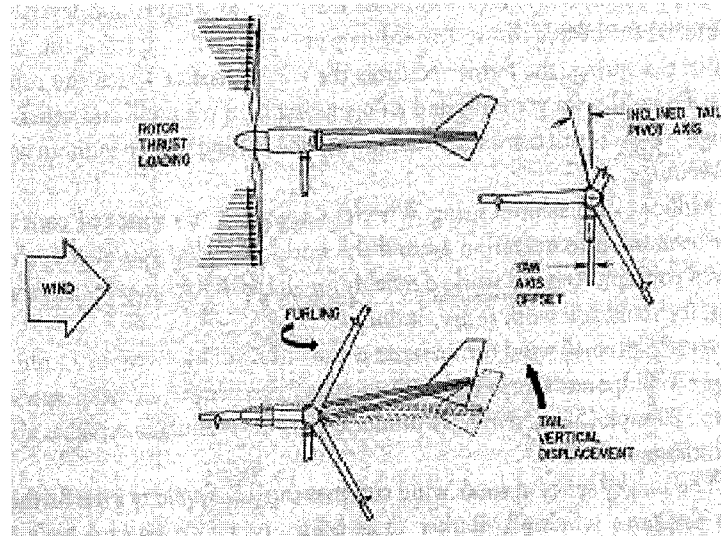


Figure 2.5 Horizontal furling of wind turbine

As stated above, one of the most important tasks of a control strategy for wind turbines is to limit the power input to the turbine to a level that reduces the stress on the mechanical and electrical components of the turbine. This must be achieved by reducing the power extracted from the wind. Hoffmann and Mutschler [8] have shown that active stall, passive stall and pitch control on wind turbines can reduce the aerodynamic power. The associated challenges with this scheme are the need for a good understanding of the airfoil design and the complex control system which sometimes tends to increase the cost of the installation. Furling control is another suitable option to reduce the aerodynamic power. In the furling control method, the rotor furls or turns away from the direction of the wind as the wind speed increases. This causes the effective wind speed to decrease on the rotor plane and thus lower the aerodynamic power of the wind turbine. This turn away action is normally termed as furling action. Depending on the turn away direction, furling can be subdivided into two methods: horizontal and vertical furling method. In the horizontal furling method the rotor turns away from the wind in a direction that is horizontal to the rotor plane

(Figure 2.5) and for the vertical furling, rotor turns away from the wind in a direction that is vertical to the rotor plane (Figure 2.6) [18].

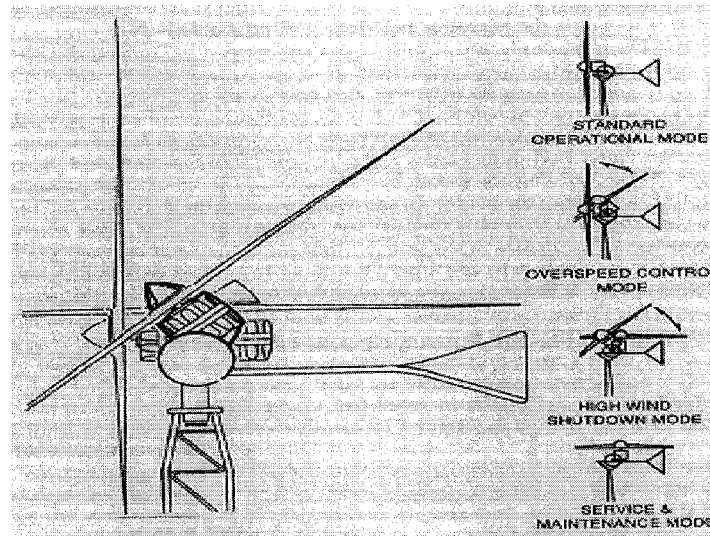


Figure 2.6 Vertical furling of wind turbine

The furling control method has received a lot of attention [11, 12, 13] and is extensively used in commercially available small wind turbine. As part of this research, a survey of the type of furling control method used by wind turbine manufacturers in commercially available small wind turbines was carried out. Table 2.2 gives the different wind turbine manufacturers along with their controlling method.

Table 2.2 Control method of commercially available small wind turbines

Manufacturer	Rated Power	Model	Horizontal furling	Vertical furling
Aeromax Corporation (www.aeromaxenergy.com)	1.3 kW	LAKOTA	Yes	
Point power systems (www.pointpowersystems.com)	1 kW	PPS 1 kW	Yes	
	6.2 kW	PPS 6.2 kW	Yes	

West wind (www.west-wind.com)	3 kW	3kW	Yes	
	5 kW	5 kW	Yes	
	10 kW	10 kW	Yes	
Bergey wind power (www.bergey.com)	BWC XL.1	1 kW	Yes	
	BWC Excel-S	10 kW	Yes	
Land mark wind (www.landmark-halle.de)	1.5 kW	Inclin 1500 neo		Yes
	3 kW	Inclin 3000 neo		Yes
	6 kW	Inclin 6000 neo		Yes
Synergy Power corporation (www.synergypowercorp.com)	3 kW	S20000		Yes
Southwest wind power (www.windenergy.com)	.9 kW	Whisper H40		Yes
	1 kW	Whisper H80		Yes
	3 kW	Whisper H175		Yes

2.2.2 Aerodynamic Control Strategy Selection

Principle

Most of the small wind turbines use an upwind rotor configuration with a tail vane for passive yaw control. This allows the rotor to furl in high wind and hence achieve both power regulation and over speed protection. The aerodynamic power available from the wind depends on the air density, cross section area of the wind turbine rotor, and the wind speed. Assuming that the wind speed is normal to the rotor plane, the power available from the wind is given by [19]

$$P_{aero} = 0.5\rho V^3 A \quad (2.1)$$

where, ρ is the air density ($\sim 1.293 \text{ kg/m}^3$),

A is the cross sectional area of the wind turbine rotor, i.e., πR^2 ,

V is the wind velocity (m/s).

The ratio of the power extracted from the wind to the power available from the wind is referred to as the power coefficient, C_p [42]

Hence, the aerodynamic or mechanical power extracted from the wind turbine is given by [42, 43]

$$P_{aero} = C_p 0.5 \rho V^3 A \quad (2.2)$$

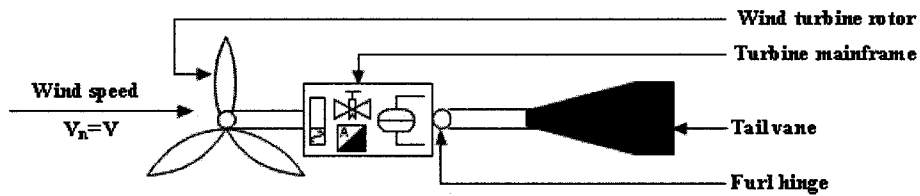


Figure 2.7 Unfurled condition of a wind turbine

When the wind speed increases, the wind turbine moves to an angle θ along its horizontal axis because of the furling action. Figure 2.7 and 2.8 illustrates the unfurled and furled conditions of the wind turbine. The effective speed on the rotor plane in the furled condition (Figure 2.8) becomes [12]

$$V_n = V \cos \theta \quad (2.3)$$

Substituting (2.3) in (2.2) the aerodynamic power extracted from the wind turbine can be expressed as

$$P_{aero} = C_p 0.5 \rho (V \cos \theta)^3 A \quad (2.4)$$

An entire furling model has been developed which requires Lagrangian approach to derive the basic equations of motion of the furling mechanism and computer code *YawDyn* to characterize the turbine power output and the corresponding aerodynamic

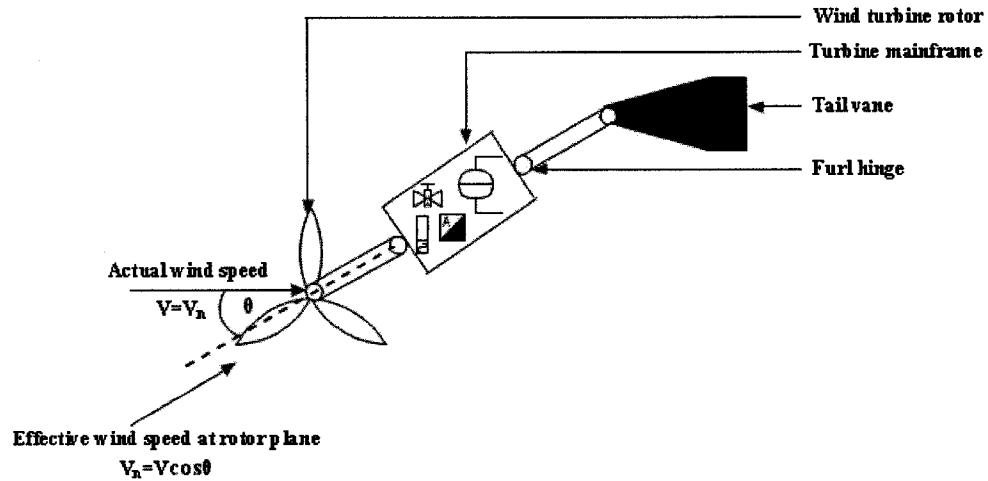


Figure 2.8 Furled condition of a wind turbine

forces on turbine [44]. From 5, it can be seen that by controlling the furl angle (θ), the aerodynamic power production from the wind can be controlled. In this research work, instead of modeling the furling action, a simple model based on the relationship between the wind speed and furling angle is used. A typical curve between wind speed and furl angle for an 8 kW wind turbine was taken from the literature [45, 46]. It was found that the fifth order expression in (2.5) is sufficient to represent the relationship between the wind speed (V m/s) and furling angle (θ^0)

$$\theta = -0.00017327V^5 + 0.0085008V^4 - 0.12034V^3 + 0.4501V^2 + 1.0592V + 0.38972 \quad (2.5)$$

where, θ is the furling angle in degree and V is the wind speed in m/s. The actual data and approximated model curve are presented Figure 2.9.

The R^2 value and goodness of fit of the model was found as 98.6% and less than 0.0001, thus validating the modeling approach.

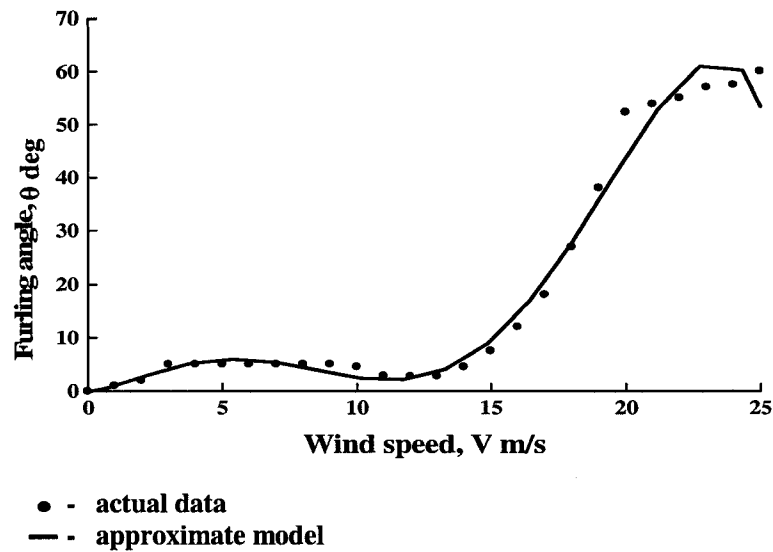


Figure 2.9 Furling angle versus wind speed

2.2.3 Control Strategy to Extract Maximum Power

The crucial part to maximize the energy capture by a small wind turbine is the selection of proper control strategy. The control strategy should ensure that the load demand is met and the ratings of the electrical and mechanical parts are not exceeded. In addition, for a stand-alone variable-speed wind turbine connected to a load, the control strategy should ensure that maximum power is extracted from the wind turbine. Dynamic modeling and simulation is required to determine a suitable controller for the wind turbine connected to a load. In this research work, the over speed control was achieved by the furling control method described in section 2.2.2. The furling control method does not provide the maximum output from the turbine system to the connected load. There are three main approaches to extract the maximum power from the wind turbine system namely, the tip-speed ratio (TSR) control, power signal feedback (PSF) control and hill-climbing control (HC) [14]. In this research, the TSR and HC control strategies were investigated.

1. Tip-Speed Ratio (TSR) Control

In the TSR control, the wind turbine rotor speed is regulated to maintain an optimum TSR. It should be noted that the value of the optimum TSR varies from one turbine to another. In this control strategy, the current value of the TSR is calculated and compared with the optimum TSR and a controller controls the load connected to the system. The operation of the wind turbine at an optimal tip speed ratio will ensure that maximum energy is extracted from the wind. A schematic of the overall system is shown in Figure 2.10.

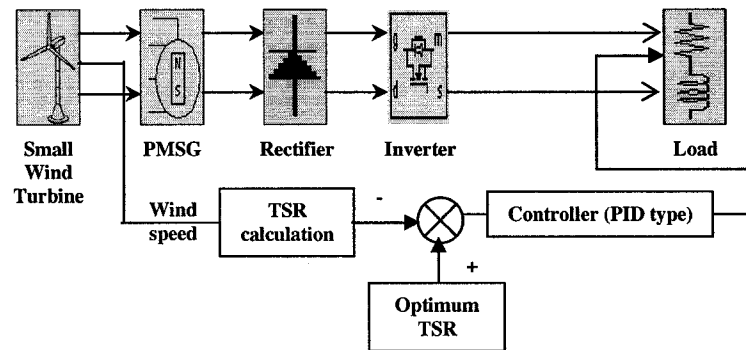


Figure 2.10 Schematic of the tip-speed ratio control of an isolated wind turbine
Tip speed ratio control method needs the information about the instantaneous wind speed. In practice, it is quite difficult to measure the wind speed accurately because the wind turbine experiences different wind profiles on its rotor than an anemometer installed close to the wind turbine [15].

2. Hill climbing (HC) Control

The hill climbing method is based on the measurement of power. Two consecutive power measurements are used to determine the change in the power and a controller continuously adjusts the load to ensure operation at the MPP [16, 17]. A schematic of the hill climbing controller is given in Figure 2.11.

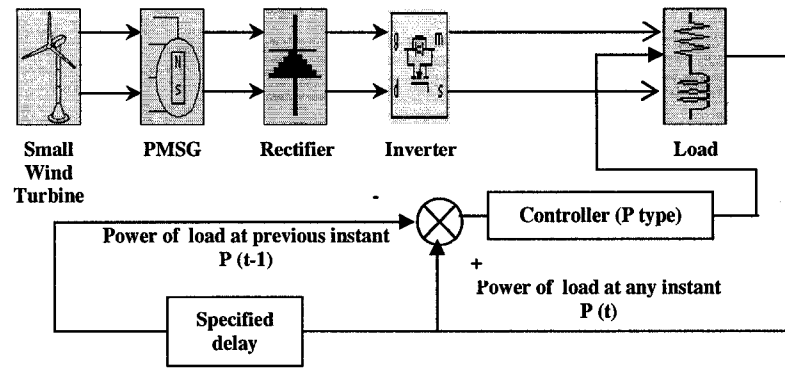


Figure 2.11 Schematic of the hill climbing control of an isolated wind turbine

2.3 Modeling of the Wind Energy Conversion System

The small wind energy system consists of a small wind turbine, Permanent Magnet Synchronous Generator (PMSG), rectifier, inverter and a passive load is modeled in this section. The model of the overall system is a combination of the modeling equations of the various subsystems. The following subsections provide the details of the modeling equations of the subsystems.

2.3.1 Wind Turbine

The wind turbine was being modeled in this research rated at 10 kW similar to Bergey EXCEL and incorporate furling mechanism. The equations for modeling of a wind turbine system is well understood and found extensively in the literature [11, 12, 42, 43]. The modeling approach is mainly dependent on the necessary output defined by the researcher. In this research, the torque produced by the wind turbine system was connected to a PMSG, leading to a torque output based model. The modeling equations are described below.

The relationship between the power coefficient and tip-speed ratio for a typical wind turbine has been taken from the literature [13]. A model for the power coefficient (C_p) has been calculated and the curve generated by the model and the actual data are presented in Figure 2.12. A statistical analysis shows that the R^2 value of the model is 99.8% and goodness of fit is less than 0.0001, which proves that the predicted model for C_p with the fitted coefficients is fairly good enough to represent the actual value.

The modeling equations has been found as

$$C_p = 0.00044\lambda^4 - 0.012\lambda^3 + 0.097\lambda^2 - 0.2\lambda + 0.11 \quad (2.6)$$

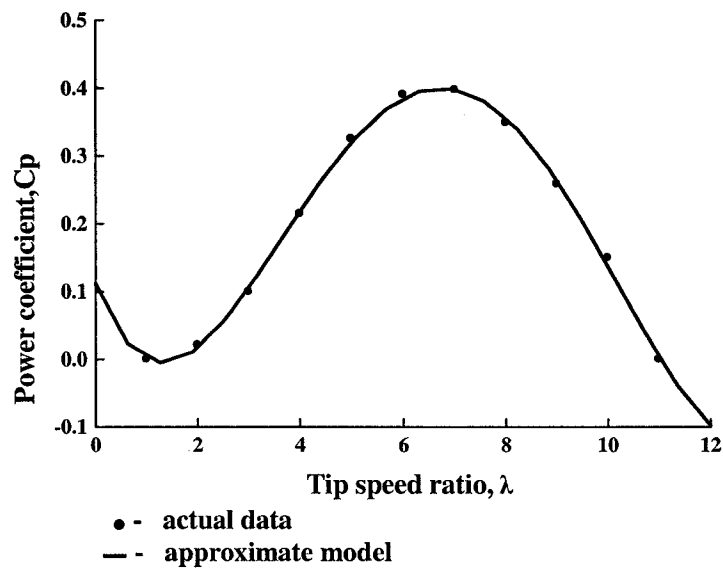


Figure 2.12 Power coefficient as a function of tip-speed ratio

It should be noted that the maximum value of the power coefficient is limited by Betz formula and is known as Betz limit. This power coefficient has a constant

magnitude $C_{pb} = \frac{16}{27} = 0.59$ [42]. Nevertheless, in practice, it is not possible to reach

the Betz limit. However, with a well designed machine this value can be assumed to be 0.45.

The output aerodynamic power extracted from the wind turbine can be expressed as

$$P_{aero} = 0.5\rho AC_p(\lambda)V^3 \quad (2.7)$$

The torque produced by the wind turbine is given by

$$T_w = \frac{P_{aero}}{\omega_m} \quad (2.8)$$

where, ω_m is the angular velocity of the wind turbine rotor (rad/s.). Also, the tip-speed ratio λ is given in terms of the rotor speed, ω_m and wind speed, V (m/s) as

$$\lambda = \frac{R*\omega_m}{V} \quad (2.9)$$

where, R is the radius of the wind turbine rotor (~ 3.2004 m).

Substituting (2.9) and (2.7) in (2.8), the torque term can be expressed as

$$T_w = \frac{0.5\rho AC_p(\lambda)V^3}{\omega_m} = 0.5\rho AR \frac{C_p(\lambda)}{\lambda} V^2 \quad (2.10)$$

$$\text{or, } T_w = \frac{0.5\rho AC_t(\lambda)V^2}{\omega_m} \quad (2.11)$$

where, $C_t(\lambda)$ is the ratio of the power coefficient $C_p(\lambda)$ to tip-speed ratio (λ), and is referred to as the torque coefficient. When the wind speed increases, the wind turbine moves to an angle θ along its horizontal axis because of furling action. The effective wind velocity at the rotor plane is given by (2.5). Incorporating the furling action, the final expression of the torque is obtained as

$$T_w = 0.5\rho ARC_t(\lambda)*(V \cos \theta)^2 \quad (2.12)$$

A second order dynamics is often used for robotics and gearing design [63]. As the relationship of the wind speed and furling angle will act like a motion of the wind turbine rotor thus a second order dynamics could be considered for the furling action. By this assumption, a second order dynamics ($H(s)$) for the furling action was considered as

$$H(s) = \frac{1}{1.3s^2 + s + 1} \quad (2.13)$$

2.3.2 Permanent Magnet Synchronous Generator

A permanent magnet machine is of primary importance to this research because of its low initial cost and simplicity of structure. Energy converters using permanent magnets come in a variety of configurations and are described by such terms as motor, generator, alternator, stepper motor, linear motor, actuator, transducer, control motor, tachometer, and brushless dc motor. The Permanent Magnet Synchronous Generator (PMSG) has been modeled in the rotor reference frame. The terminal voltage equations of a permanent magnet synchronous generator can be described as a set of matrix form [43]

$$[V_{abc}^s] = -[R_{abc}^s][i_{abc}^s] + P[\lambda_{abc}^s] \quad (2.14)$$

Assuming that zero sequence quantities are not present and applying Park's transformation, the terminal voltage of the PMSG in the rotor reference frame can be expressed as [43,47]

$$V_q^s = -(R^s + pL_q^s)i_q^s - \omega_r L_d^s i_d^s + \omega_r \lambda_m \quad (2.15)$$

$$V_d^s = -(R^s + pL_d^s)i_d^s + \omega_r L_q^s i_q^s \quad (2.16)$$

where, R^s is the stator phase winding resistance ($\sim 0.5 \Omega$),

L_q^s is the stator inductance in the quadrature axis (~ 0.00448 H),

L_d^s is the stator inductance in the direct axis (~ 0.00448 H),

ω_r is the rotor angular velocity of the generator (rad/s),

λ_m is the amplitude of the flux linkages (~0.39 v-s/rad) established by a permanent magnet as viewed from the stator phase windings,

p is operator $\frac{d}{dt}$.

The electromagnetic torque in the rotor reference frame is given as [43, 48]

$$T_e = \frac{3}{2} * \frac{P}{2} * \left[(L_d^s - L_q^s) i_q^s i_d^s - \lambda_m i_q^s \right] \quad (2.17)$$

where, P is the number of poles of the PMSG (~ 38).

In a gearless wind turbine the relation between the rotor angular velocity of the generator ω_r and mechanical angular velocity of the rotor ω_m can be expressed as

$$\omega_r = \omega_m \quad (2.18)$$

The rotational speed and the torque are related as

$$T_I = Jp\omega_m - T_e + B\omega_m \quad (2.19)$$

where, T_I is the input torque to the machine and J is the moment of inertia (~ 25 kg.m²). This input torque corresponds to the torque produced by the wind turbine T_w .

A small friction term, B (~0.00035 N.m.rad/s), has been added in the generator to make the model more realistic. T_w is the torque produced by the wind turbine and serves as the input to the PMSG. The wind turbine considered has no gearbox.

Assuming that the output stator voltages of the generator are sinusoidal, the rotor reference frame equations reduce to the following [43]

$$V_q^s = V_s^s \quad (2.20)$$

$$V_d^s = 0 \quad (2.21)$$

For a practical permanent magnet synchronous machines, it can be assumed that

$L_d^s = L_q^s = L^s$ [43]. Substituting (2.20) and (2.21) into (2.15) gives [43]

$$V_q^s = - \left[\frac{(R^s + pL^s)^2 + \omega_r^2 (L^s)^2}{(R^s + pL^s)} \right] i_q^s + \omega_r \lambda_m \quad (2.22)$$

Equation (2.22) resembles a linear equation if the term $\omega_r^2 (L^s)^2$ is neglected. In

order for this approximation to be valid, it is required that V_q^s , ω_r and T_e be equal to

or greater than zero [43]. Thus, neglecting $\omega_r^2 (L^s)^2$, $L_d^s = L_q^s = L^s$ and substituting

(2.20) in (2.22), gives [43]

$$V_s^s = -(R^s + pL^s) i_q^s + \lambda_m \omega_r \quad (2.23)$$

Considering the rotor reference frame quantities and the assumption of non-existence

of zero-sequence current the AC power output of the synchronous generator can be

expressed as [43]

$$P_{ac} = \frac{3}{2} (V_q^s i_q^s + V_d^s i_d^s) \quad (2.24)$$

2.3.3 Rectifier

The expression for the average output voltage of a three-phase, 6-pulse uncontrolled

rectifier can be found in the literature [43, 49]. If the commutation angle is neglected,

the rectifier output voltage expression is given by

$$V_R = \frac{3\sqrt{2} * V_s^s}{\pi} \quad (2.25)$$

Assuming that the output current of the rectifier is continuous and ripple-free, the dc output power of the rectifier is given by

$$P_{dc} = V_R I_R \quad (2.26)$$

where, I_R is the dc output current.

Neglecting losses in the rectifier, the dc output power of the rectifier is equal to the ac input power to the rectifier. Equating (2.26) and (2.24) gives

$$V_R I_R = \frac{3}{2} (V_q^s i_q^s + V_d^s i_d^s) \quad (2.27)$$

Since from (2.21) V_d^s is zero, (2.27) reduce to [43]

$$V_R I_R = \frac{3}{2} * V_q^s i_q^s \quad (2.28)$$

The direct axis current may be expressed as [43]

$$i_d^s = i_q^s \tan \alpha \quad (2.29)$$

Since $\alpha = 0$ for an uncontrolled rectifier, the direct axis current can be written as

$$i_d^s = 0 \quad (2.30)$$

And the rectifier output current is given by

$$I_R = \frac{P_{load}}{V_s^s} \quad (2.31)$$

2.3.4 Inverter

The power inverter was modeled assuming the basic principle of pulse width modulation (PWM) operation. Figure 2.13 is the circuit model of a single-phase inverter, and Figure 2.14 is the principle of pulse width modulation.

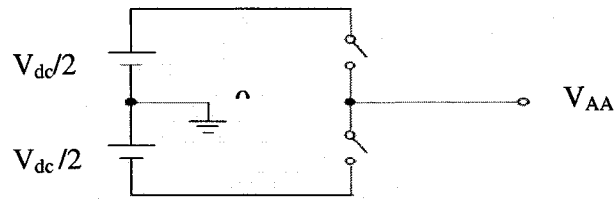


Figure 2.13 Circuit model of a single-phase inverter.

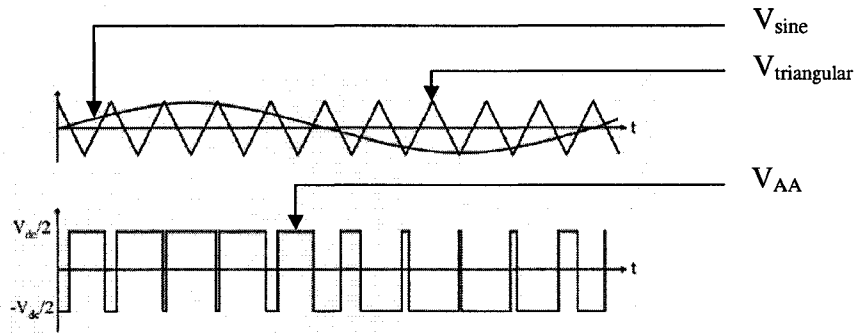


Figure 2.14 Pulse width modulation

As shown in Figure 2.14, the inverter output voltage obtained as follows:

$$\text{When } V_{\text{sine}} > V_{\text{triangular}}, V_{AA} = \frac{V_{dc}}{2}$$

$$\text{When } V_{\text{sine}} < V_{\text{triangular}}, V_{AA} = \frac{-V_{dc}}{2}$$

Modulation index (m) is defined as

$$m = \frac{V_{\text{sine}}}{V_{\text{triangular}}} = \frac{V_{AA, \text{peak}}}{\frac{V_{dc}}{2}} \quad (2.32)$$

2.3.5 Load

A simple series $R_L L$ load is assumed and is modeled by the simple equation

$$V_L = i_L R_L + L_L \frac{di_L}{dt} \quad (2.33)$$

where, V_L is the load voltage and i_L is the load current.

The complete wind turbine and electrical components mathematical equations have been formulated above which was used in this research. With the above expressed modeling equations, the overall system is presented in Figure 2.15.

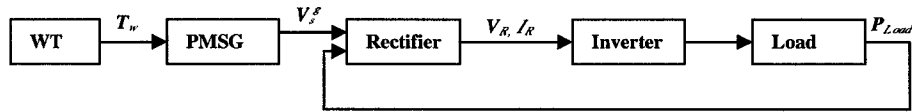


Figure 2.15 Overall model of the wind energy conversion system

2.4 Energy Calculation

In order to deploy a wind energy system it is necessary to know the annual energy output for best fit in terms of installment cost, economies of various sizes and brands of wind machines. The problem becomes more difficult when the wind energy system is small. Therefore, the expected energy output values of a system supplied by the manufacturer are calculation based. Three general approaches are used to determine the annual energy capture from a small wind energy conversion system. The first approach uses the swept area of the rotor method. In this method, when the average wind speed of a particular site, Rayleigh distribution and rotor diameter are known, the intercepted wind energy of the wind turbine is determined. A general assumption is that a sophisticated rotor can capture 40 percent of the energy of the wind, thus leads the energy capture capacity by the wind turbine. The second approach uses the power curve method. In this method, a series of power measurements are sorted into corresponding intervals or register of wind speed. The technique is called the method of bins [50]. By multiplying bin by bin of the generated power curve and Rayleigh distribution, a mean output power can be determined and the annual energy capture

was obtained from the mean output power and the total number of hours in a year. In this work, a power curve method was selected based on a bin width of 1 m/s. The average generated power was determined through simulation. Rayleigh distribution parameters for one year of wind speed in St. John's, Newfoundland were used and the annual energy capture was calculated using Bin's Power Curve method as follows[50]. Wind speed data was recorded at a 10m height for a period of a year. The average per minute time series wind speed data for a year is scaled to 30 meter height. Rayleigh distribution was considered for the wind speed data and equations to find wind speed at 30 meter height can be computed as [50, 51]

$$\frac{V_2}{V_1} = \left(\frac{H_2}{H_1} \right)^\delta \quad (2.34)$$

where, V_1 is the wind speed data of 1 year recorded at 10m height (For St. John's, Newfoundland),

V_2 is the scaled wind speed data,

δ is the shear exponent,

H_1 is the reference height,

H_2 is the height of the tower

To calculate the shear exponent (δ) the following formula was employed [51];

$$\delta = 0.096 \log_{10}(Z_0) + 0.016 (\log_{10}(Z_0))^2 + 0.24 \quad (2.35)$$

where, Z_0 is the surface roughness. (Typical value of surface roughness for St. John's city is taken 6 meter) .

The mean output power (P_{mean}) is calculated by the following formula

$\Sigma(\text{Average power for a particular wind speed} * \text{No. of times for a particular wind speed to occur within one year}) / (\Sigma \text{the time for which the particular wind speed occurs in one year})$

The mean energy output is calculated using the following formula

$$\text{Annual energy output} = P_{mean} * 8765 \quad (2.36)$$

where, P_{mean} is the mean power out put.

The third approach simply uses the manufacturers published estimates [11,12].

2.5 Summary

This chapter has discussed the aerodynamic as well as maximum power control from a small wind energy conversion system. The wind turbine incorporates furling mechanism and the system has been modeled using Matlab/Simulink. Two dynamic controllers based on the TSR and HC control are discussed. To calculate the annual energy capture from such a small system, the Bin's Power curve method is presented.

Chapter 3

System Implementation and Simulation

The purpose of this chapter is to investigate the expected dynamic performance of the small wind energy conversion system and determine the energy capture by the Tip-Speed Ratio (TSR) and Hill Climbing (HC) control strategy. This study focuses on 1) stabilization of the overall system after a sudden increase in wind speed, 2) study of the furling dynamics and aerodynamic power drop due to the furling action, and finally 3) comparison of the energy capture by the TSR and HC control method. In order to make the comparison, the wind turbine system remains the same for the two methodologies. The assumption in this work is that the dynamics of the rectifier and converter are very fast as compared to the dynamics of the wind turbine system.

3.1 System Description

A stand-alone variable speed wind turbine when connected to a load should be controlled to extract the maximum power. Dynamic modeling and simulation is required to

determine a suitable controller of a wind turbine connected to a load. The wind turbine used in this work is considered as a direct drive system. The generator is connected to the load through a rectifier and an inverter. The torque produced by the wind turbine is used as the input torque to the Permanent Magnet Synchronous Generator (PMSG) and the voltage produced by the PMSG is rectified and passed through an inverter to the load. A maximum power point extractor is necessary to extract the maximum power from the system. In this work, the maximum power extractor controls the load connected to the system in order to achieve the maximum power extraction. The load was considered as an RL type used for residential purpose. A complete schematic of the system is shown in Figure 3.1 and the Simulink realization is given in Figure 3.2.

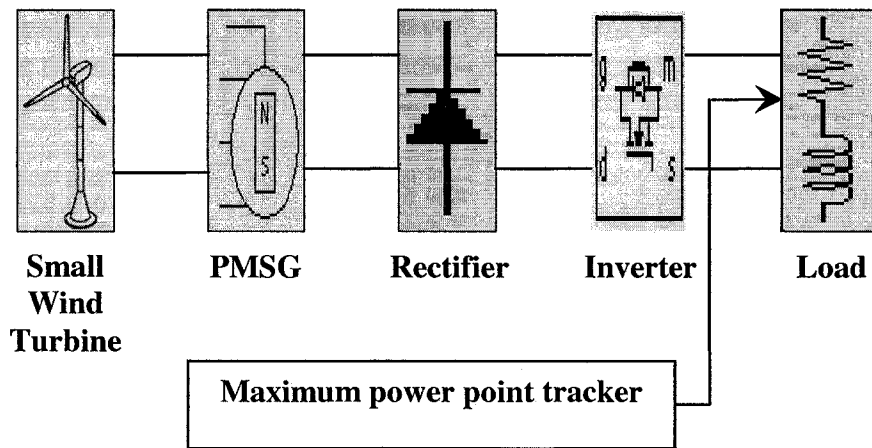


Figure 3.1: Small wind energy conversion system

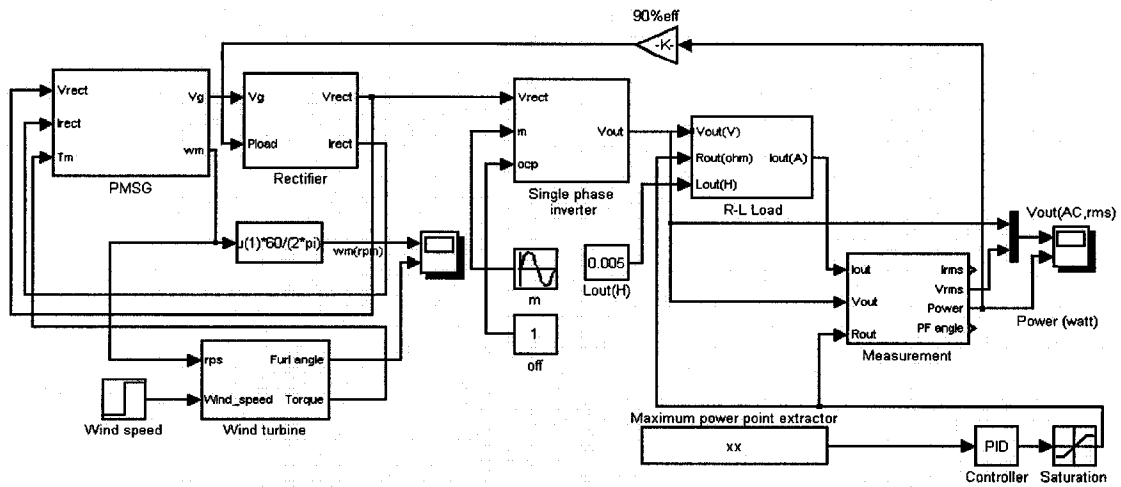


Figure 3.2: Simulink diagram of the small wind energy conversion system

Figure 3.3 shows the actual Simulink realization with the TSR control. The actual TSR of the wind turbine from the wind turbine block is compared with the optimum TSR of 7 and also a PID controller was used to control the load.

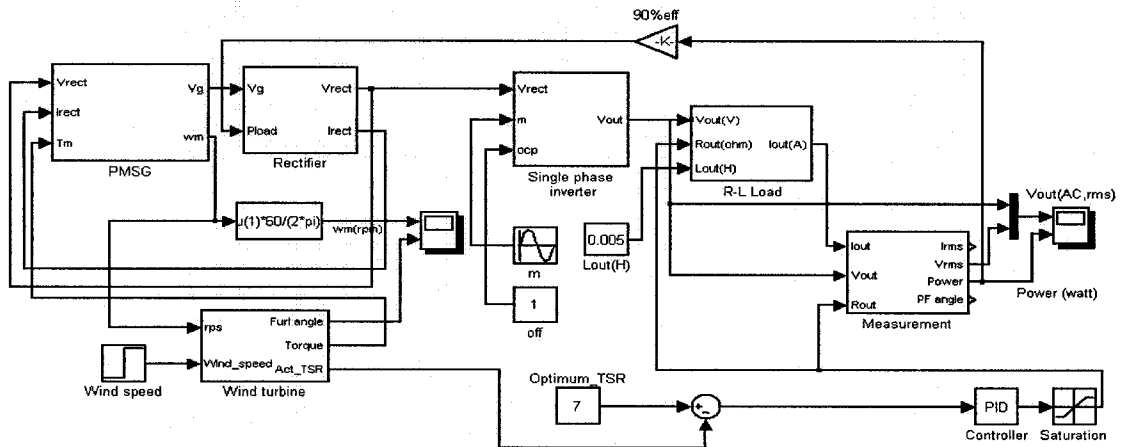


Figure 3.3: Simulink diagram of the tip-speed ratio control of wind turbine

Figure 3.4 gives the actual Simulink realization of the HC control of the wind turbine. The output power was delayed by 0.1 second and based on the difference of power; a proportional controller controlled the load connected to the system.

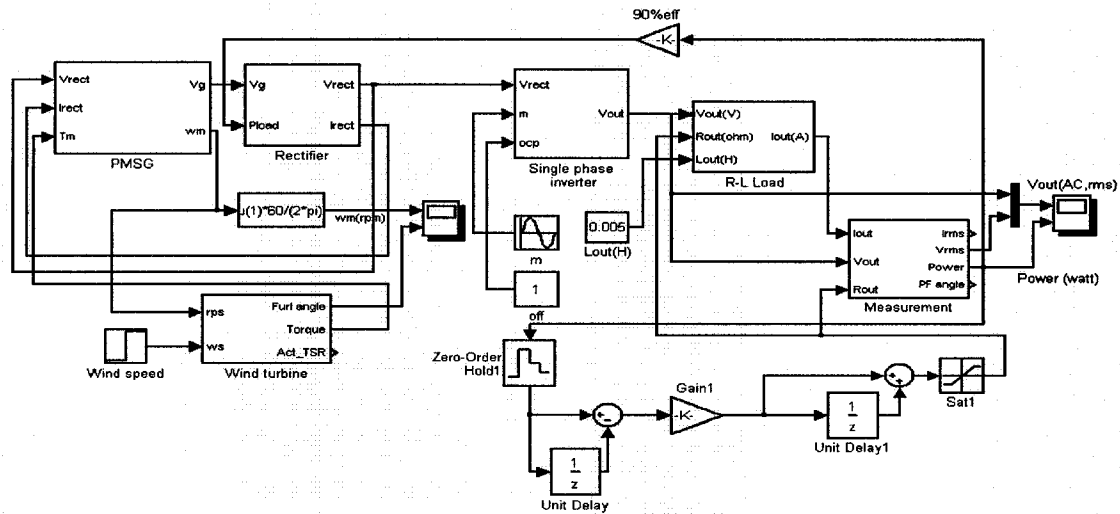


Figure 3.4: Simulink diagram of the hill climbing control of wind turbine

3.2 System Implementation in Simulink

A small wind turbine system along with its various components was discussed and its mathematical models were formulated in chapter 2. The system described in the chapter 2 was implemented and simulated using Matlab-SimulinkTM. MATLAB version 6.5.0.18091 3a (R13) and Simulink version 5.0 (R13) were employed. The equations were implemented using the built in library blocks in Simulink and several of the equations were combined to form a subsystem. By connecting several subsystems, a complete model was developed. Several limiters and memory element blocks were used to overcome convergence problems.

3.2.1 Wind Turbine Model

Based on the mathematical equations (2.6) to (2.13) described in the section 2.3.1, the wind turbine model was developed. The equation used to model the power coefficient variations with TSR is described by (2.6). The complete detail of the subsystem is given in Appendix A (Figure A.1).

3.2.2 Permanent Magnet Synchronous Generator Model

The torque produced by the wind turbine rotor was applied as the input torque for the generator and as the system was a direct drive, gear box dynamics were not considered. The PMSG has been modeled by (2.14) to (2.24) described in section 2.3.2, and subsystem of the PMSG is explained in Appendix A (Figure A.2).

3.2.3 Rectifier Model

The equations (2.25) to (2.31) were used to model the rectifier subsystem depicted in section 2.3.3 and the detail is shown in Appendix A (Figure A.3). Dynamics of the rectifier were neglected since it is much faster as compared to the PMSG.

3.2.4 Inverter Model

A simple PWM approach was used to model the inverter and the subsystem, as shown in Appendix A (Figure A.4).

3.2.5 Load Model

Equation (2.33) of section 2.3.5 was used to model the load and Figure A.5 (Appendix A) explains the load model.

A measurement block was used to calculate the RMS value and the Simulink built in library was used to model the block. Figure A.6 (Appendix A) is the Simulink representation of the measurement subsystem.

3.3 Simulation of the Wind Energy Conversion System

Simulation of the integrated system was slow and different integration algorithms were combined to avoid the convergence problem. The TSR control strategy was simulated using “Fixed step/ODE 4 (Runge-Kutta)” method while the HC strategy was simulated using “Fixed step/ODE 4 (Dormand-Prince)” method. The relative and absolute tolerance was taken as 0.00001 and 0.001. The simulation time for both strategies was 17 seconds. The TSR strategy takes around 35 minutes and the HC strategy takes around 15 minutes to complete simulation of 17 seconds wind data. An Intel (R) Celeron (R) CPU 1.7 GHz, 256 MB of RAM computer was used for the simulation.

3.4 Results and Discussions

Various issues could be studied to evaluate the performance of the wind energy conversion system. Effect of the wind speed and tuning of the controller parameters are the two most significant factors to be studied in the simulation. A wide range of wind speed was used to simulate the system thus helping to evaluate the performance of the integrated system. The furling dynamics and the effect of furling action on power production was also investigated. The control action for both the TSR and HC has been discussed in the chapter 2. The following section is the discussion of the simulation

results. As stated earlier, the main objectives of the simulation were to investigate the different control task and study, how effectively they work.

3.4.1 System Stabilization

In the first strategy (TSR), a PID controller was used to adjust the load. Several methods exist to guess the initial parameter of a controller. In this research work, the Ziegler-Nichols (ZN) method was used to calculate the controller parameter and suitable controller parameters were found to be; $K_p = 2.31$; $K_i = 49.5$; $K_d = 0.01675$. Figures 3.5 and 3.6 show results of the simulation of the TSR control strategy. A step change in wind speed from 9.5 m/s to 10.5 m/s was applied to the system at 7 seconds after the start of simulation. Within 17 seconds all the quantities reach new steady state values and the system stabilizes. The generator speed (RPM) increases with the increase in wind speed and settles to a new stable state of 285 rpm within 10 seconds (Figure 3.5). Figure 3.4 shows the output power and the load voltage of the PWM inverter and the conclusion is the same. The system initial start up transient is also shown in Figure 3.6.

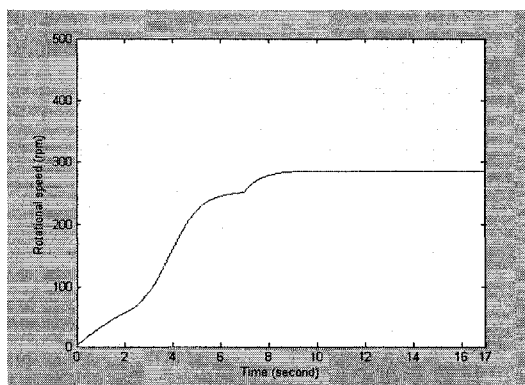


Figure 3.5: Step response of the turbine with the PID controller. (Wind speed increases from 9.5m/s to 10.5m/s at $t=7$ s)

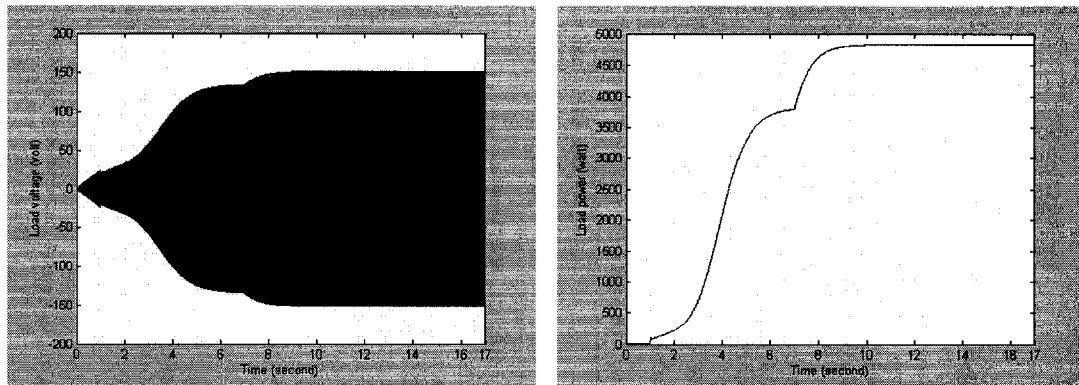


Figure 3.6: PWM output of the inverter during the tip-speed ratio control (Wind speed increases from 9.5m/s to 10.5m/s at $t=7$ s).

As stated in chapter 2, the TSR control strategy needs the usually unavailable information about the rotor speed. So, the HC method was investigated, which works on the measurement of power. A proportional controller was used and a suitable gain of the controller was found to be 0.009. Figure 3.7 and 3.8 shows the simulation results. A step input of 9.5 m/s to 10.5 m/s was applied at $t=7$ s. The rotor speed gradually increases and settles to a new stable value of 285 rpm. (Figure 3.7).

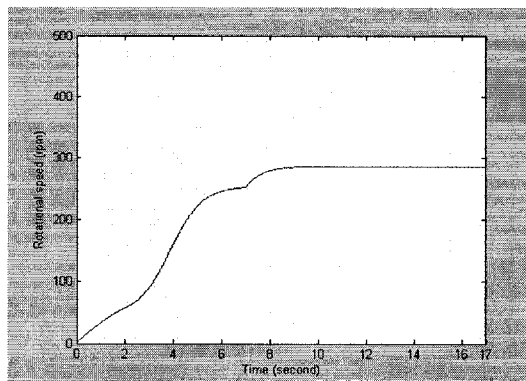


Figure 3.7: Step response of the turbine with the hill climbing controller. (Wind speed increases from 9.5m/s to 10.5m/s at $t=7$ s)

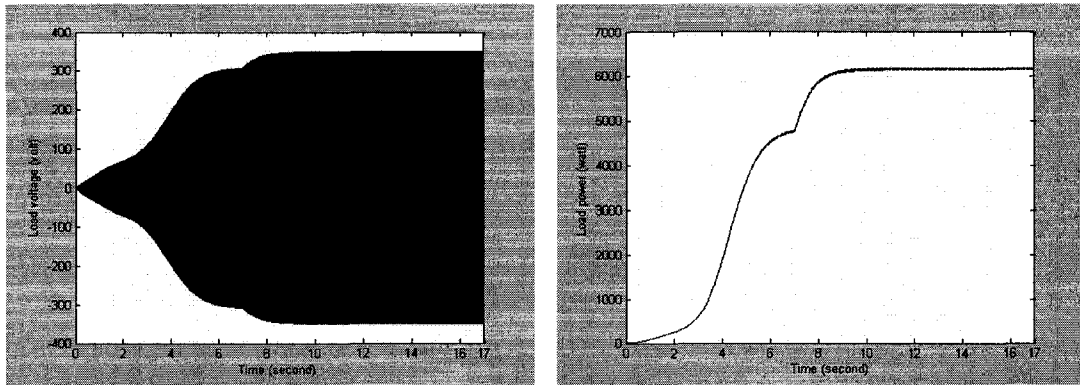


Figure 3.8 PWM output of the inverter the hill climbing control (Wind speed increase from 9.5m/s to 10.5m/s at $t=7$ s)

In Figure 3.8, the load voltage gradually increases and after a short time it reaches a stable value. It represents the initial transient of the system. The same conclusion can be drawn for the power. It should be noted that the steady state response of the two control strategies is similar and the only difference is in their steady state values. The transient response of the PMSG and rectifier was neglected during this simulation. The HC algorithm also behaves like a bang-bang controller in an effort to extract power from the wind turbine. The advantages of the HC algorithm are that it does not need the wind speed and rotor speed information. The controller parameter values of the HC control are harder to obtain than the TSR control, as there is no well established method to determine the gain of such controller.

3.4.2 Investigation of the Furling Action Dynamics

As stated in chapter 2, a second order furling dynamics was introduced to the wind turbine model by maintaining that the furling action should be attained within a reasonable time. The value of the furl angle with a step change in the wind speed settles

to a new stable value within 10 second for both the TSR (Figure 3.9) and HC control (Figure 3.10) strategy.

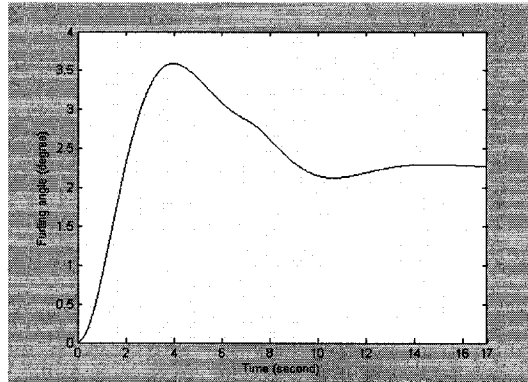


Figure 3.9 Step response of the turbine with the tip-speed ratio controller. (Wind speed increases from 9.5m/s to 10.5m/s at t= 7 s)

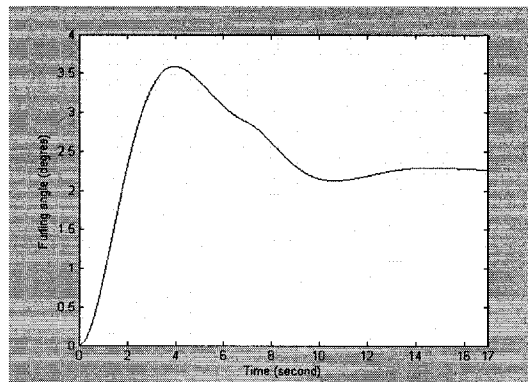


Figure 3.10 Step response of the turbine with the hill climbing controller. (Wind speed increases from 9.5m/s to 10.5m/s at t=7 s)

In order to investigate the power drop due to the furling action phenomena, power production by the wind turbine for several different wind speeds was required. To get the power output values for each strategy, several wind speeds of fixed interval were used in the simulation. The corresponding power output for the TSR strategy at 2 m/s intervals of wind speed is shown in Figure 3.11. It can be seen from the Figure 3.11 that above 21m/s the power suddenly dropped, i.e., furling activates when the wind speed exceeds that

value. The same conclusion can be drawn for the hill climbing strategy shown in Figure 3.12. The figure shows that the power drops after the furling speed is attained.

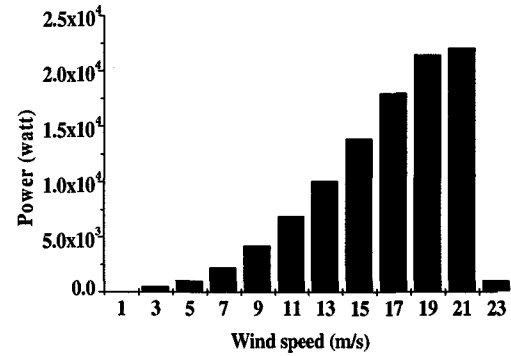
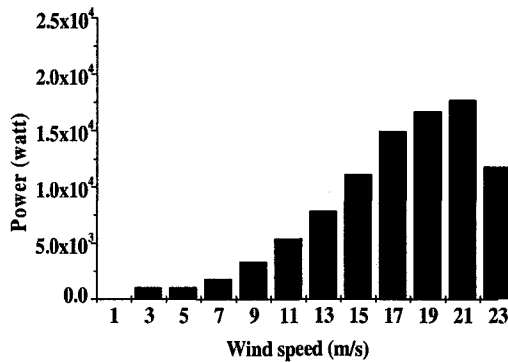


Figure 3.11 Power output for the tip-speed ratio control. **Figure 3.12** Power output for the hill climbing control

3.4.3 Energy calculation

To calculate the annual energy from the wind turbine a power profile was first produced by employing several constant wind speeds to the modeled small wind energy conversion system and observing the corresponding output power. The average wind speed data (sample per minute) for a year is scaled to 30 meter height and it is presented in Figure 3.13. The corresponding Rayleigh distribution considering bin width as 1 m/s is given in Figure 3.14.

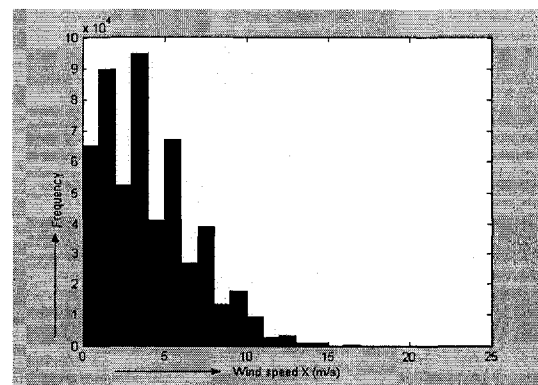
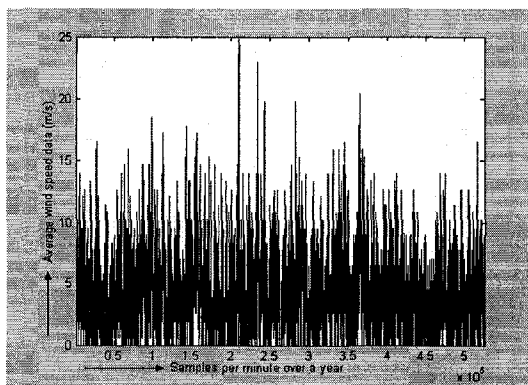


Figure 3.13 Per minute wind speed data

Figure 3.14 Rayleigh distribution

The maximum wind speed at the proposed site near St. John's, Newfoundland, was found to be around 17 m/s, so the annual energy was calculated up to this limit. As the simulation figure and wind speed are all the same for the two systems, a comparison was performed by calculating the annual energy capture. The expected power profile for the TSR control and HC controls for discrete wind speeds at the site near St. John's, Newfoundland, are shown in Figure 3.15 and Figure 3.16 respectively.

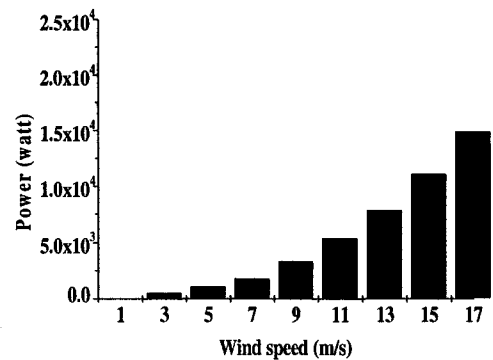
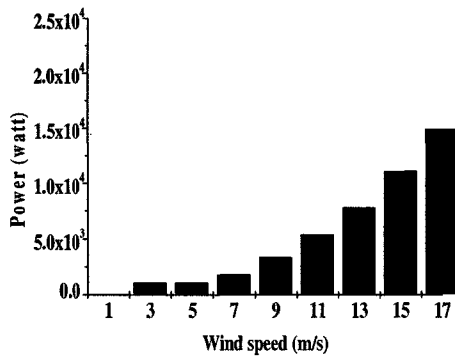


Figure 3.15 Power output for the tip-speed ratio control within St. John's wind speed.

Figure 3.16 Power output for the hill climbing control within St. John's wind speed

The annual energy capture was calculated using (2.36) and it was found that the HC control strategy gives 4.94% more energy than the TSR control strategy. Thus the hill climbing control strategy offers reduced cost/energy advantage compared to the TSR control strategy.

3.5 Summary

The effectiveness of the two control strategies for small wind turbine with respect to their annual energy capture is investigated. Dynamic modeling and control of the small wind

turbine with furling dynamics is described in the previous chapter and the energy is calculated using the Bin's power curve method. Two dynamic controllers are implemented and their operations are investigated through simulation. Furling action is initiated in case of high wind speed and it reaches a steady state within 10 seconds. Practical wind speed data and Rayleigh distribution of St. John's, Newfoundland, are used to determine the annual energy capture. It is found that the HC control leads to a better annual energy capture than the TSR control.

Chapter 4

Development of a Novel Small Wind Turbine Emulator

The development of a novel small wind turbine emulator is described in this chapter. Firstly, the basic structure of a wind turbine emulator is described. A detailed literature review on the developed wind turbine emulator by past research and the novel wind turbine emulator developed in this research are described in the wind turbine emulator section. Later on in this chapter, implementation details of the wind turbine emulator with several implementation issues and the power electronics of the emulator are described. Finally, the experimental procedures to calculate the motor parameters and the design of an inertia disk are presented. The key aspect of this chapter is to develop a test bed for a small wind turbine system to evaluate the steady state and dynamic behavior of a wind turbine.

4.1 Introduction

Chapter 2 describes the modeling of the wind energy conversion system and chapter 3 evaluates the performance of the system through simulation. Several issues could have been raised in order to install a wind turbine system for actual use. Simulation should be the first step before deploying any wind turbine system. It is necessary to emulate the steady state and dynamic behavior of the system in a laboratory environment to avoid the problems at installation. This can be achieved by developing a Wind Turbine Emulator (WTE) which will reflect the actual behavior of wind turbines. The main use of a WTE is to help the design and test the wind turbine controller. Several researchers are working on an emulator, but these investigations are mainly focused on the 5 kW or more rated wind turbines [21], [22]. Research needs to be further extended on small wind turbines to effectively understand and observe the behavior and control of such wind turbines. As stated in chapter 2, the control task should ensure that no electrical or mechanical part of the wind turbine is exceeding its limits due to the variations in wind speeds. Also, it has been described that most of the commercially available small wind turbines have the furling control method to reduce the aerodynamic power or to avoid the over speed situation. The design of a maximum power controller for such wind turbines is still a research issue. This chapter describes the implementation of a small WTE including its aerodynamic power control method, i.e., furling control method. In this research work, investigations were carried out by running a separately excited DC motor such that it followed the theoretical rotational speed of the wind turbine rotor. To represent the wind turbine rotor inertia, a large inertia disk was designed and coupled with the system which represents the inertia of a small wind turbine rotor.

4.2 Basic Structure of a Wind Turbine Emulator

A WTE is fundamentally a demonstration of a practical wind turbine in a laboratory environment. The general structure of a WTE consists of a PC where the model and characteristics of the wind turbine are written either in high or low level language, a motor drive to represent a wind turbine rotor, feedback mechanism from the drive, and power electronics equipment to control the drive. The feedback signal is normally acquired by a PC through an A/D converter and the signal for driving the power electronics equipment comes from the PC through a D/A converter. A detailed literature review has shown that all the components in the system are similar except the use of an AC or a DC drive to simulate the wind turbine rotor. Prior to 1980, Adjustable Speed Drives (ASD) implemented with DC drives had significant advantages over other types of AC drives. Recently, researchers more often choose an AC drive mainly due to the benefit of low cost and low maintenance in contrast to a DC drive. Beside this, the DC drive may be bulky and costly. But the primary disadvantages of the AC drive are that the speed control of the AC drive requires expensive power electronic equipment and the control is more complex than the DC drive. Also it should be noted that the AC drive is not suitable to operate below 1/3 of its base speed, i.e., it will not properly reflect the actual turbine characteristic below 1/3 of its base speed. On the other hand, the DC drive is easy to understand and the speed or torque control is less complex. A DC drive can operate more accurately at low speeds. Finally, in a DC drive, the torque and speed can be controlled directly by controlling the armature current and voltage respectively. The cost of the controlling equipment of a DC drive is lower than the cost of an AC drive. Due to the above-discussed reasons, this research used a separately excited DC drive to reflect a wind

turbine rotor. It has been found that most of the DC drive-based WTEs are controlled by the armature current [32, 29, 25], and few researchers have considered the armature voltage control [21] to operate the DC drive. A typical structure of a WTE system is shown in Figure 4.1.

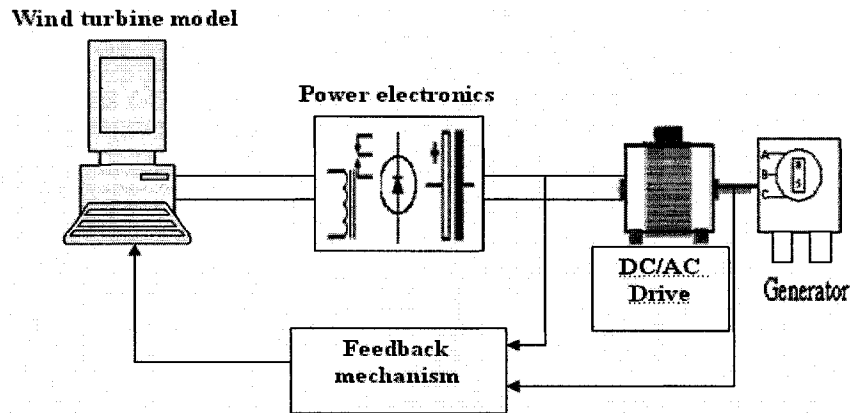


Figure 4.1 A typical structure of wind turbine emulator

4.3 The Developed Wind Turbine Emulator

In order to enhance the research and development on wind turbines, it is necessary to better understand the steady state and dynamic behavior of wind turbines. Typically, a wind turbine is a highly nonlinear system and to represent a realistic wind turbine several dynamics should be included in the model. Several wind turbine models have been used in the emulator platform based on the steady state and dynamic model. A brief literature review about the emulator is as follows:

A WTE has been developed based on an induction motor (IM) which is rated at 125 HP [22]. The WT model is incorporated in the PC using a static speed vs. power curve and no mechanical control is incorporated with the model. At any given wind speed, the operating point of the wind turbine is determined by the intersection point of load and turbine characteristics. The feedback from the IM motor has been taken as torque

and speed which determines the required torque for the wind turbine. The 3 phase IGBT converter is triggered on the base of the controlled stator current. The modeled IM based on several assumptions and programming has been done in C language, which can be considered as a mid level language. Information regarding the mechanical power control has not been described. Further research has been carried out [23, 24] based on the rating of a 10HP induction machine and using the same control strategy that has been described in the previous work [22]. The parameter value of the IM is considered to be known in advance rather than using any experimental procedure. The problem with this research is that it does not reflect any small wind turbine behavior which is essential in the development of the small wind turbine industry. To implement the control task, a cascaded mode has been considered which increases the program complexity.

A more generalized approach has been developed by Nichita [52]. The proposed system has been implemented using a DC motor and the WTE consists of a real time software emulator and an electromechanical tracking system. By taking the reference from the wind turbine model the total structure can be implemented either in torque control or speed control mode which gives a lot of flexibility to the control.

Research by Rabelo [28] emulates a wind turbine with a separately excited DC motor rated at 7.5KW. In this work, the armature control method has been applied to control the DC motor and the wind turbine model is based on both the steady state and dynamic behavior. The steady state torque has been passed through a 3 mass model which represents the wind turbine, gear box and generator moments of inertia and the elastic shafts connecting them. For mechanical power control, pitch angle control method has been incorporated with the wind turbine steady state model. The controller

for the DC machine has been done with the frequency response method. Both steady state and dynamic behavior have been described in their proposed system. The control has been performed using the armature voltage control method, i.e., by controlling the speed of the separately excited DC motor.

Research has been carried out by Manwell, [53] on a wind/diesel system where the WTE mainly based on the steady state characteristics. A 40 kW DC motor has been used to simulate the wind turbine behavior and the model of wind turbine based on the power coefficient vs. tip-speed ratio curve. The reference torque of the wind turbine is compared with the torque of the DC motor and based on this comparison, the controller determines the DC motor torque.

A research by Pierik [32] has considered the passive pitching mechanism to the wind turbine model and the rotor dynamics have been taken into account. A separately excited DC motor has been used to emulate the wind turbine and the motor is controlled using the armature current. A flywheel at the motor shaft that represents the inertia of a wind turbine rotor. Aerodynamic torque of the wind turbine is calculated from the motor rotational speed and considered as the reference torque of the wind turbine. Based on the difference of reference torque and the torque produced by the motor, the DC motor armature current is controlled.

A simple model of the wind turbine has been proposed by Barrero [31]. To represent the torque dynamics; oscillatory, aerodynamic and dynamics components of the wind turbine torque are considered. The DC motor is controlled using the armature current.

Researcher Battaiotto [29] has carried out a research work on the WTE by considering a separately excited DC motor. The control of the DC motor has been carried out

through the armature current. To implement the control strategy, a dual DSP board is used which increases the total cost of the emulator system.

A brief review of research on the development of the WTE is given by A. D. Diop, et. al. [33], which shows that the furling action is still not considered in the WTE raised area. From the previous investigations, it is viewed that although the static and dynamic aspects have been incorporated in the model in some way or other, there is always a scope to develop further. In this work, a novel small wind turbine emulator system was developed which incorporate various features. Varying aerodynamic power of the wind turbine due to furling action and resulting dynamics were incorporated in the emulator with the use of a PC based wind turbine model. The shaft torque of the separately excited DC motor was determined from the armature current and the parameters of the DC motor were obtained by experimentation. In order to reflect the inertia of a small wind turbine, an inertia disk was designed and coupled to the generator shaft. A gain scheduled digital PI controller was designed to track the theoretical rotational speed of the wind turbine rotor by the DC the motor. The basic structure of the small WTE developed in this research is presented in Figure 4.2. The following section describes the implementation process.

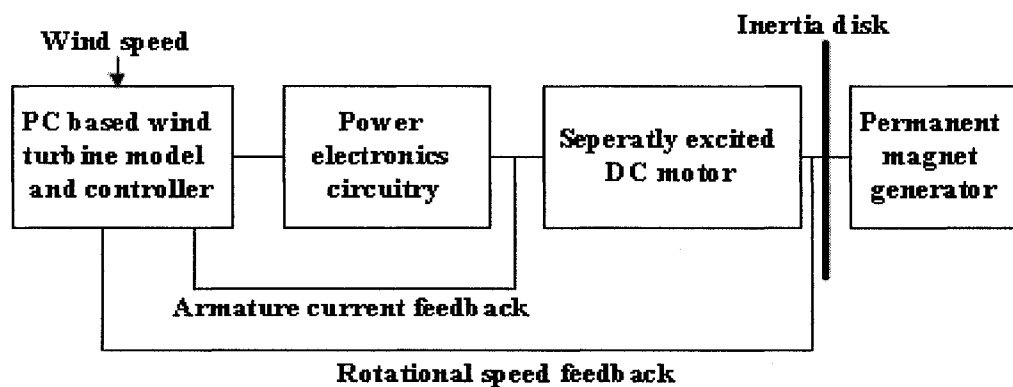


Figure 4.2 Block diagram representation of the implemented wind turbine emulator

4.3.1 Reference Rotor Speed for the Wind Turbine

Emulator

As stated in chapter 2, modeling equations of the wind turbine is well understood and found extensively in the literature. The wind turbine model used in this research was implemented in QBASIC 4.5 and the equations are described in section 2.3.1. From (2.11), the theoretical rotational speed of the wind turbine can be written as

$$\omega_m = \frac{0.5 * \rho * A * C_p(\lambda) * (V \cos \theta)^3}{T_w} \quad (4.1)$$

i.e., This speed serves as the reference speed of the rotor in a specific wind speed. The relation between the power coefficient and tip-speed ratio has been presented by (2.6) and relation of wind speed and furling angle is labeled by (2.5).

4.3.2 Furling Dynamics Discretization for the Wind

Turbine Emulator

To incorporate with a digital system, a continuous function should be converted to a discrete equivalent of the continuous function. The second order furling dynamics has been presented by (2.13). A zero order hold method for 0.1 second sampling time was used to convert the continuous dynamics of the furling action to its discrete equivalent ($H(z)$) given by (4.2) which was derived from (2.13) and then converted to a difference equation form.

$$H(z) = \frac{0.003747 * z + 0.003652}{z^2 - 1.919 * z + 0.926} \quad (4.2)$$

4.3.3 Controller Algorithm for the Wind Turbine Emulator

To implement a digital control algorithm, it is necessary to convert the discrete equivalents of the analogue controller is essential. A simple controller used most of the time is a PI/PID controller, as it is easy to implement and needs less computing power. In the time domain, the PID controller equation can be written as [54]

$$u(t) = K_p * e(t) + \frac{K_p}{T_i} * \int_0^t e(t) dt + K_p * T_d \frac{de(t)}{dt} + u_0 \quad (4.3)$$

Where, $u(t)$ is the output of the PID controller at any instant t .

K_p is the proportional gain of the PID controller.

T_i is the integral time of the controller.

T_d is the derivative time of the controller.

$e(t)$ is the error between reference and actual control variable.

In order to implement the controller in a PC, an approximation of the continuous function of (4.3) is required. Approximation of the integral and derivate term of (4.3) can be written as

$$\frac{de(t)}{dt} \approx \frac{e(t) - e(t-1)}{T_s} \text{ and } \int_0^t e(t) dt \approx T_s \sum_0^t e(t) \quad (4.4)$$

Where, T_s is the sampling time.

$e(t-1)$ is the previous state error.

From the above approximation, the discrete equivalent of the continuous PID controller algorithm can be written as

$$u(t) = K_p * e(t) + \frac{K_p * T_s}{T_i} \sum_0^t e(t) + \frac{K_p * T_d \{e(t) - e(t-1)\}}{T_s} + u_0 \quad (4.5)$$

where, u_0 is the base level of the control signal.

(4.5) can be easily implemented using a PC and this form of the PID controller equation is called the positional PID controller algorithm. One of the major drawbacks of the positional algorithm is that the value of u_0 is sometimes hard to determine and needs a lot of trial and error. By shifting one sampling interval of the PID controller equation written in (4.5), it can be written as

$$u(t-1) = K_p * e(t-1) + \frac{K_p * T_s}{T_i} \sum_0^{t-1} e(t-1) + \frac{K_p * T_d \{e(t-1) - e(t-2)\}}{T_s} + u_0 \quad (4.6)$$

Subtracting (4.5) from (4.6) gives

$$u(t) = u(t-1) + K_p * [e(t) - e(t-1)] + \frac{K_p * T_s}{T_i} e(t) + \frac{K_p * T_d}{T_s} * [e(t) - 2e(t-1) + e(t-2)] \quad (4.7)$$

(4.7) describes the velocity PID controller equation. There are several advantages of the velocity PID algorithm over the positional PID algorithm such as:

- The summations of errors are not explicitly calculated so there is an anti reset wind up accumulated with this controller algorithm.
- A base value is not required for velocity PID controller algorithm, i.e., it depends on the previous state value and no prior assumption is necessary.

Due to the above reasons, the velocity PID controller algorithm was used to track the theoretical rotational speed of the wind turbine rotor by the DC motor. As there are three types of controllers (P, PI, PID) which can be implemented, the obvious question that could arise is which controller would be the most suitable to implement. A proportional only controller is the easiest to tune but the problem could arise is that it

is hard to achieve zero steady state error with only proportional control. On the other hand a PID controller is the most complicated to tune and the derivative term might be effected by the noise. To avoid these complexities, a PI controller was used as it has the ability to turn steady state error zero and is also less complex to tune. Although, it should be noted that a PID controller will be able to give a better performance than a PI controller. Due to the use of a PI controller, the derivative term will become zero, and (4.7) will be reduced to

$$u(t) = u(t-1) + K_p * [e(t) - e(t-1)] + \frac{K_p * T_s}{T_i} e(t) \quad (4.8)$$

A flow chart for the controller algorithm and the basic structure of the WTE including the controller in conjunction with the peripheral is given in Figure 4.3 and 4.4 respectively.

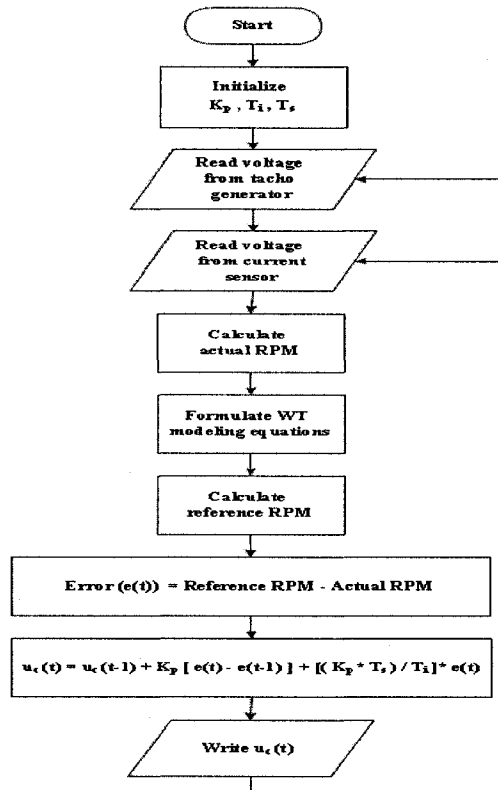


Figure 4.3 Flow chart of the controller algorithm

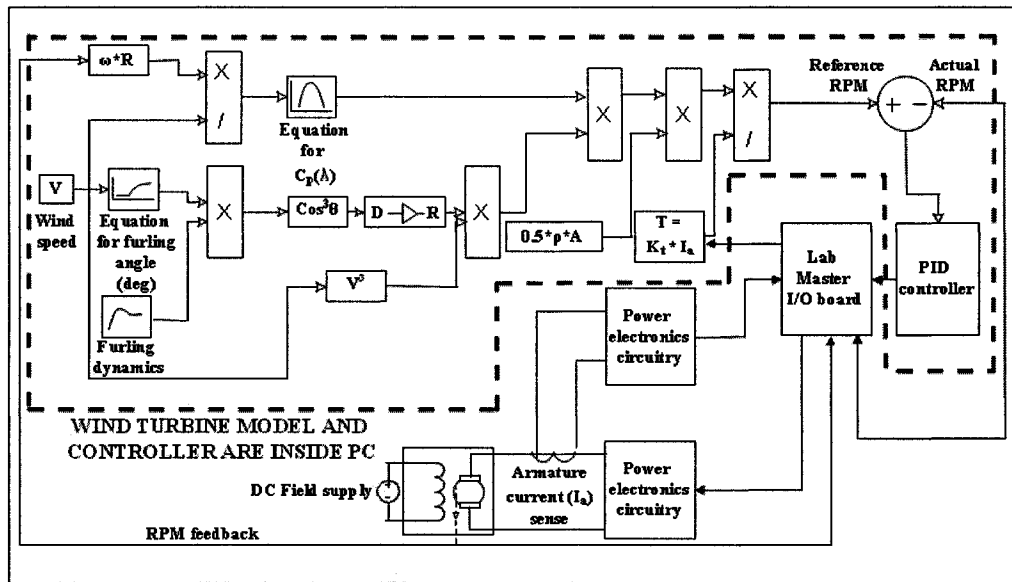


Figure 4.4 Structure of the small wind turbine emulator with peripheral

4.4 Implementation Issues and Calibration

Equations

Before implementation of such a real time system, several possible issues (motor current and speed) need to be addressed and resolved. Variables from the peripheral were essential for the controller algorithm as shown in Figure 4.3. Related calibration equations were also absolutely necessary. In this research work, the motor speed and armature current information was required to determine the voltage across the motor. Motor torque was calculated using the armature current measurement of the motor. A phase controlled relay was used to apply the voltage across the motor. A calibration equation was also required as the relation between the input and output voltage of a phase controlled relay is not linear. The following sections are the description of such issues which were taken into consideration during the implementation.

4.4.1 Interfacing between the PC and Power Electronic Circuitries

A real time system consists of various analogue and digital circuitry and whenever a PC based system is developed, it is necessary to make an interface between the peripheral circuitries and a PC. The circuitry that was used to control the DC motor is analogue in nature and if any quantity is feedback to a PC, the analogue voltage and current should be converted to the digital equivalent of the analogue value. A digital to analogue converter can serve this purpose and also an analogue to digital converter can do the reverse. There are several I/O cards commercially available which can be used for this purpose. In this research work, a Scientific Solutions LabMaster I/O board [56] was used to interface the PC and the power electronics.

The board has 8 channels for analogue to digital conversion and 2 independent digital to analogue converter channels. A communication program is required to send the data to an output channel and acquire the data from an input channel. The board can be configured between different voltage ranges by setting appropriate jumpers. A range between 0 to 10 volts was used and the feedback voltages were lowered or higher within this range. It should be noted that any voltage spikes on any channel can damage the channel, so necessary precaution should be taken.

4.4.2 DC Motor Starting Current

Due to the large inertia of the WTE, which is mainly because of the flywheel, the motor responds very slowly. Even if the dynamics of the motor are slow, an armature surge current could develop [54] and may cause the motor armature circuit damage. The fact is that the armature resistance of the DC motor is quite low. As a result,

during the initial start up it draws a large current that can damage the motor. A small increase in armature voltage could lead to a large armature current, and finally end up by burning the motor. Therefore, limitation of initial armature current is essential. There are several ways to limit the initial inrush current in the motor armature. Current limiting can be achieved by limiting the reference of a cascaded current regulating system [56, 57] or it can be achieved by a parallel interventionist system [56, 58]. However, the drawback of the first method is a complex controller. The problem raised by the interventionist system is that, to perform the current limit effectively, the first over shoot of the current should be allowed [57,58]. Also complex analogue circuitry could be an issue to implement such methods. A simple solution to above mentioned problems could be to limit the current within the digital controller algorithm which will effectively eliminate complex electronics circuitry. Several research papers discuss how to limit the initial current to a motor by the digital algorithm [56, 57, 59]. The authors of a paper [59] proposed a simple technique. It is well understood that even if the armature voltage increases very slowly with time, it will make a very fast changes in the motor armature current. A solution to this problem could be, if the armature current at any instant is too large then apply a slightly smaller amplitude voltage to the motor in the next sampling instant. In this research work, the simplest approach was selected. The motor armature voltage was supposed to be dictated by the controller output. A gradual increase in voltage, which was dependent on the controlled voltage, was determined at the output of the controller. At any particular instant t , the difference of the voltage between the instant t and $(t-1)$ was calculated for both the controlled and linear voltage. The strategy was: the difference in the voltage between the instant t and $(t-1)$ will be compared for both

the controlled and linear voltage. And then, the smaller difference in voltage applied to the motor armature. Initially the controller will be producing a large variation in the output until it sets to a fixed controlled value. Therefore, the difference between the instant t and $(t-1)$ of the controlled voltage will be higher and the linear voltage will slowly speed up the motor, thus limiting the armature current. It was observed that by using this technique, motor armature current was limited and worked effectively.

4.4.3 Calibration Equation for the Rotational Speed of the Motor

A tacho generator was attached to the motor shaft to generate a voltage corresponding to the rotational speed. It produced voltage between 0 and 10 volts. Several voltages

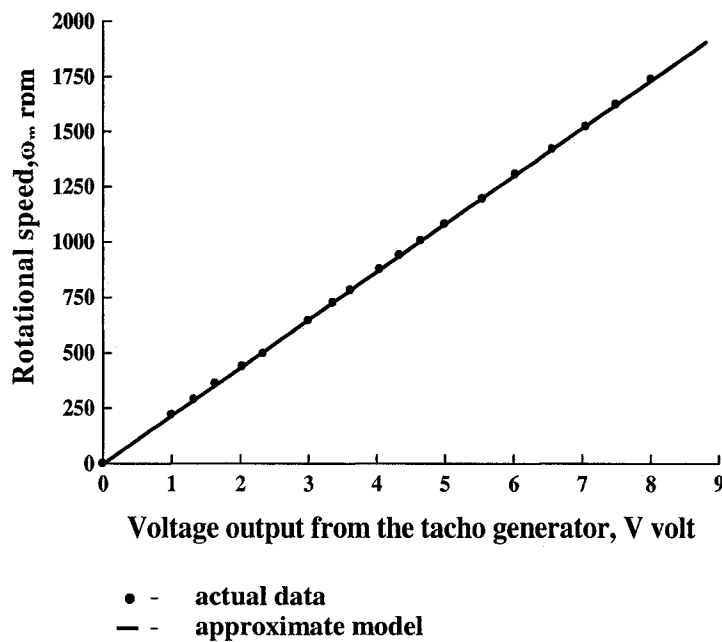


Figure 4.5 Rotational speed versus voltage output from the tacho generator

were applied to the motor armature and the tacho generator voltages were recorded. It should be noted that the armature voltage was increased using the PC to avoid error. A model for rotational speed vs. tacho output was calculated and the curve generated by the model and the actual data are presented in Figure 4.5. A statistical analysis shows that the R^2 value of the model is 99.9% and goodness of fit is less than 0.0001, which proves that the predicted model for the rotational speed with the fitted coefficients is fairly good. The resulting calibration equation was

$$\omega_m = 216.18 * V - 0.9919 \quad (4.9)$$

4.4.4 Calibration Equation for the Armature Current of the Motor

A current sensor was used to sense the motor armature current. The armature current was used to calculate the torque produce by the motor.

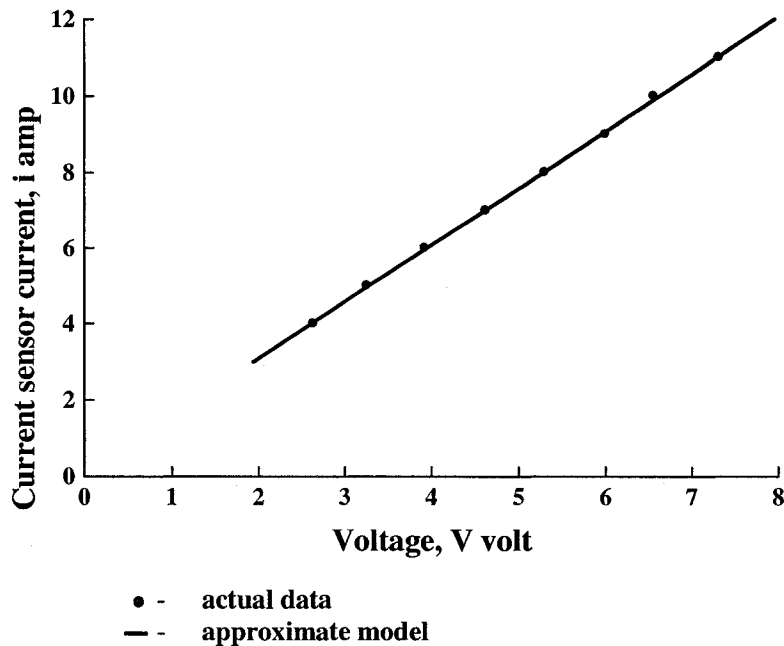


Figure 4.6 Current sensor current versus voltage.

Varying current were passed through the current sensor and corresponding output voltages were recorded. A statistical model was also developed to find out the calibration equation and found to be

$$\text{Current}(i) = 1.4956 * \text{Voltage} + 0.0895 \quad (4.10)$$

The experimental data and predicted model curve are shown in Figure 4.6.

4.4.5 Calibration Equation for the Input and Output of the Phase Controlled Relay

The output of the controller was applied to the phase controlled relay. The relay can accept the voltage 2-10 volts and output in between 0 to 120 volts. When using such a phase controlled relay, a problem could arise. The problem is that the relation between

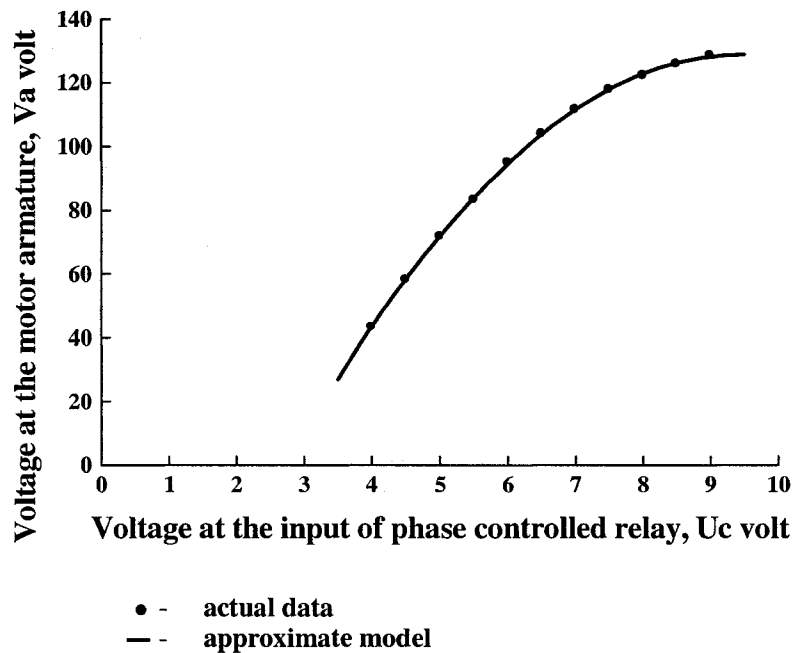


Figure 4.7 Voltage at the motor armature versus voltage at the input of the phase controlled relay.

the input and output of the relay is not linear. It is exponential nature. Due to this reason, a calibration equation was necessary to perfectly reflect the actual controller voltage and the relay input. The actual data and the approximate model are shown in Figure 4.7 and the equation found to be

$$V_a = -2.9*(u_c)^2 + 54*u_c - 130 \quad (4.11)$$

where, u_c is the control voltage.

With this equation, the actual armature voltage could be found but the voltage range of the Lab master I/O board was 0 to 10 volts. So another relation was still required to obtain the actual controller output. The actual data and approximate model are represented in Figure 4.8. The fitted equation was found to be

$$u_c = 0.00001*(V_a)^3 - 0.0021*(V_a)^2 + 0.18*(V_a) - 0.64 \quad (4.12)$$

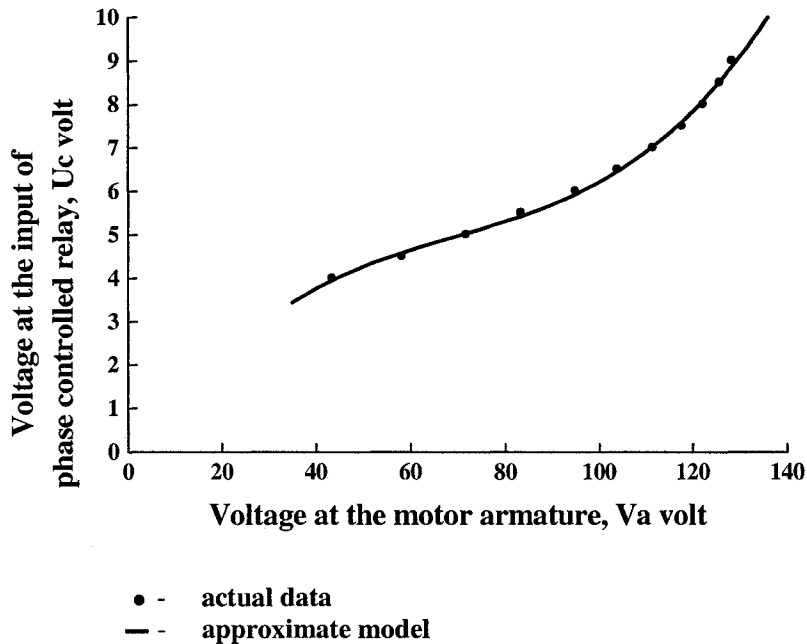


Figure 4.8 Voltage at the input of the phase controlled relay versus voltage at the motor armature.

4.5 Control Program for the Wind Turbine

Emulator

After determining the calibration equations, the controller algorithm coding was done in QBASIC 4.5. QBASIC has been extensively used due to ease of use. The tacho

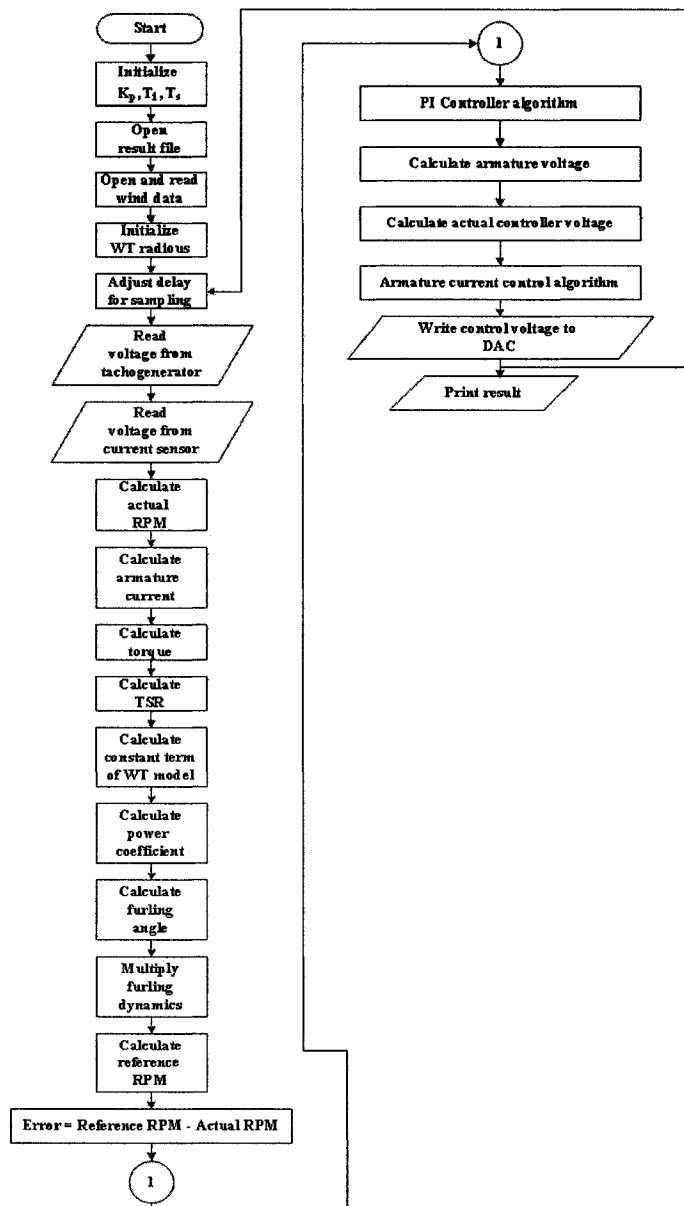


Figure 4.9 Flow chart of the complete emulator program.

generator and current sensor output was feedback to PC via the LabMaster I/O board. This feedback was connected to 2 input channels of the LabMaster I/O board by maintaining that feedback voltage should be within 0 – 10 volts. The controller voltage output was sent to one of the DAC channels of the board and the complete program for sending and receiving data has been given in Appendix B. The complete model of the wind turbine system was then written and the controller algorithm was implemented. The mathematical equations for the wind turbine system have been described in section 2.3.1. To determine the sampling time, the program delay was adjusted by observing the total time to complete the loop and it was adjusted by 0.1 second. The wind data file was the input to the program and the outputs were also recorded to a file. The current limitation algorithm was written after the final controller output. The controller parameters were adjusted to get the best result. The complete program is given in appendix B and a flow chart is given in Figure 4.9.

4.6 Power Electronics for the Wind Turbine Emulator

The small WTE (SWTE) developed in this research consists of a 3HP separately-excited DC motor which drives a constant field excited three phase synchronous generator. A simple power electronics schematic of the test-rig is shown in Figure 4.10 and the test-rig picture is given in Figure 4.11

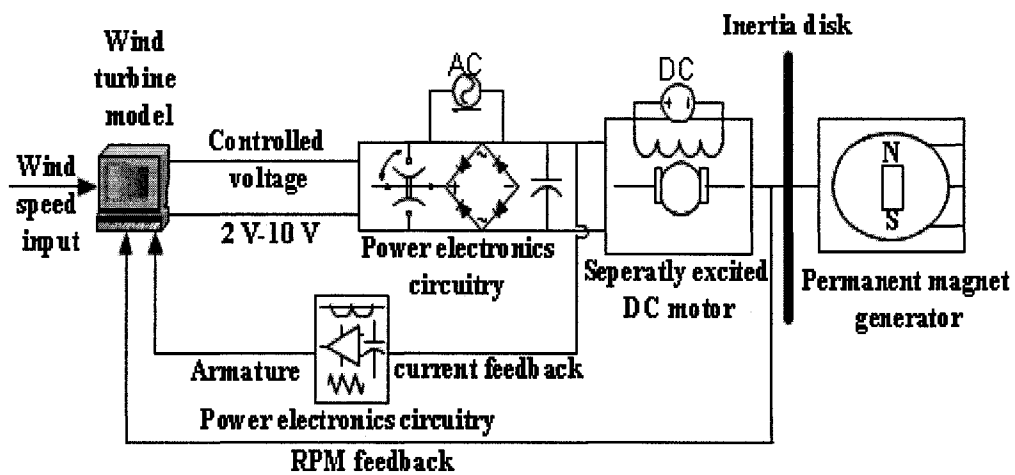


Figure 4.10 Small wind turbine emulator structure

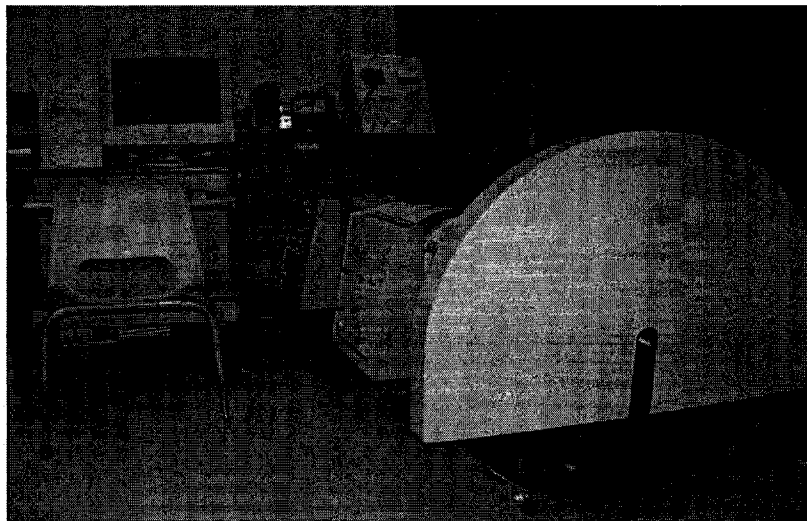


Figure 4.11 Photograph of the Test-Rig

The controller produced the required control voltage to trigger the phase controlled relay. A simple amplifier and a filter circuit were used in conjunction with the current sensor. Saturation of the armature current was eliminated by adjustment the gain of the amplifier stage. It was observed that the voltage of the tacho generator was almost ripple free so a filter was avoided in that portion. The output of the phase controlled relay was rectified and then filtered using a capacitor to remove the noise from the rectified voltage. A circuit breaker was necessary during tuning of the controller

parameters and was used in the armature side of the system. Figure 4.12 shows the power electronics schematic diagram of the emulator and the pictorial presentation is in Figure 4.13. A large inertia disk was coupled to the system through a flexible coupling to reflect the inertia of a real wind turbine rotor. The disk is made of cast steel C10/20. Two bearings were used to support the system and a spider coupling was used to couple the disk with the synchronous generator and the shaft of the disk.

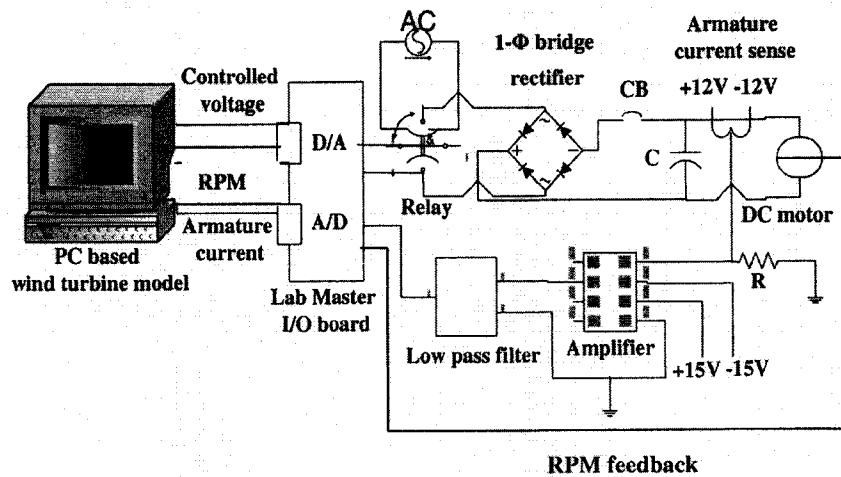


Figure 4.12 Schematic of the wind turbine section of the emulator.

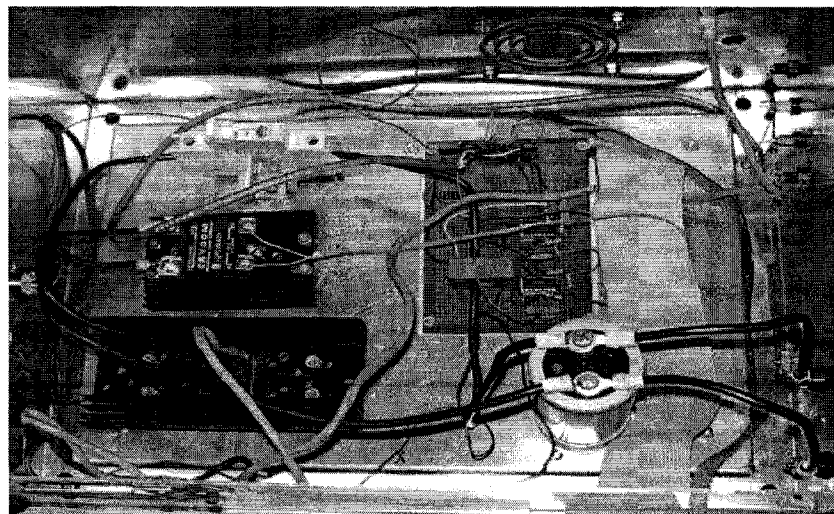


Figure 4.13 Photograph of the wind turbine emulator power electronics

4.7 Motor Parameter Calculation

The separately excited DC motor used in this research is rated at 3 HP and the parameters of the motor were determined through experimentation rather than assuming the value provided by the manufacturer. The following procedure was used to obtain the parameters.

4.7.1 Armature Resistance

The armature resistance of the motor was determined by applying a DC voltage at the armature terminal and measuring the corresponding current. The experimental recorded values are shown in Figure 4.14. In order to reduce the error on the armature resistance, several readings were taken and a mean value was considered which was found as 0.4 ohm.

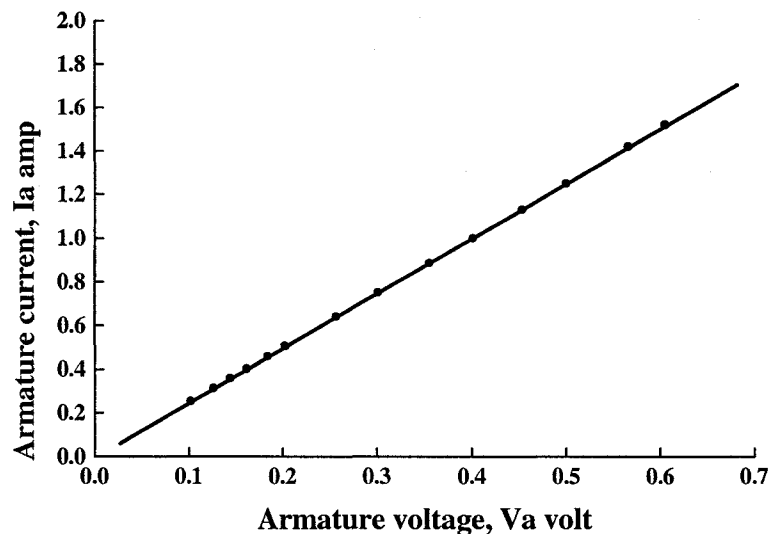


Figure 4.14 Experimental curve to determine the armature resistance.

4.7.2 Inertia

Several methods exist to determine the inertia of a DC drive. A review of the existing methods by Lin [60] found that most methods lead to uncertainty in the parameters. In

this research a general approach was considered which is based on the following equation [60]:

$$J_m = \frac{T_m * K_t * K_e}{R_a} \quad (4.13)$$

where, J_m is the moment of inertia of the motor,

T_m is the mechanical time constant of the motor,

K_t is the torque co-efficient of the motor,

K_e is the back emf constant of the motor,

R_a is the armature resistance of the motor.

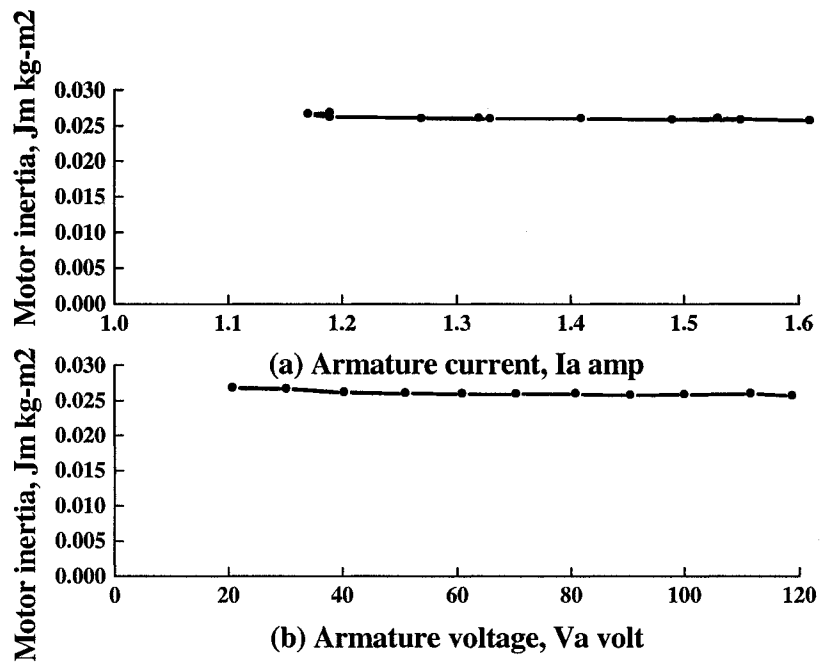


Figure 4.15 Variation of the motor inertia with, (a) armature current; (b) armature voltage

The mechanical time constant of the motor was determined by rotating the motor to its base speed and then shut down the power and recording the time it takes to reach 36.3% of its base speed [60]. It was found that the inertia of the motor was almost

constant regardless of the variations in the motor armature voltage or current. A mean value was used to minimize the error and the inertia of the motor was 0.026042 kg-m². The variation of motor inertia with respect to the armature current and voltage are shown in Figure 4.15a and 4.15b respectively.

4.7.3 Back Emf Constant

The back emf constant was calculated as follows [61]

$$K_e = \frac{V_{no\ load}}{\omega_{no\ load}} \quad (4.14)$$

where, $V_{no\ load}$ is the no load voltage of the armature and $\omega_{no\ load}$ is the no load speed of the motor [61]. It can be found that back emf constant is more or less constant regardless the variation of the armature voltage and current. The back emf constant of the motor was found to be 73.167 v/krpm. The experimental back emf constant with the variation of armature current and voltage are shown in Figure 4.16a and 4.16b respectively.

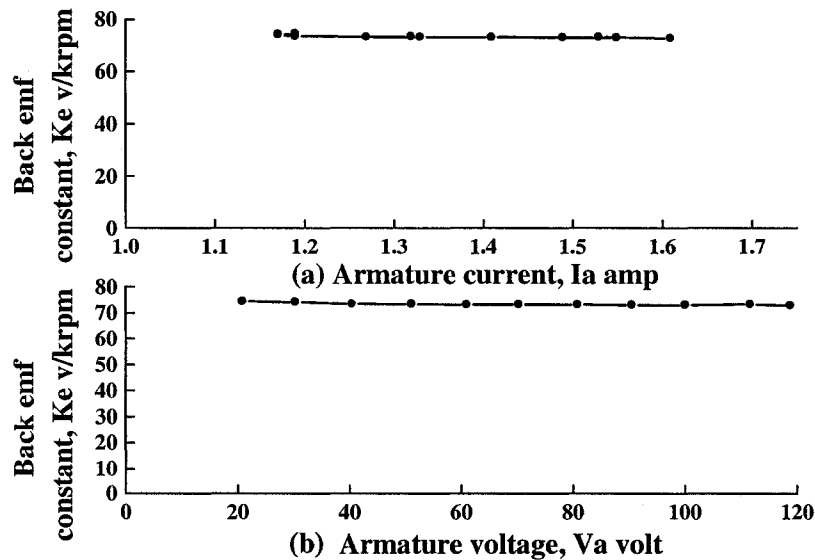


Figure 4.16 Variation of the back emf constant with, (a) armature current; (b) armature voltage

4.7.4 Torque Coefficient

The torque co-efficient was calculated as described below [61].

$$K_t = 9.5439e-3 * K_e \quad (4.15)$$

where, K_e is the back emf constant in V/krpm.

The experimental torque coefficient with the variation of armature current and voltage are presented in Figure 4.17a and 4.17b respectively and the value was found as 0.0711 kg.m/A.

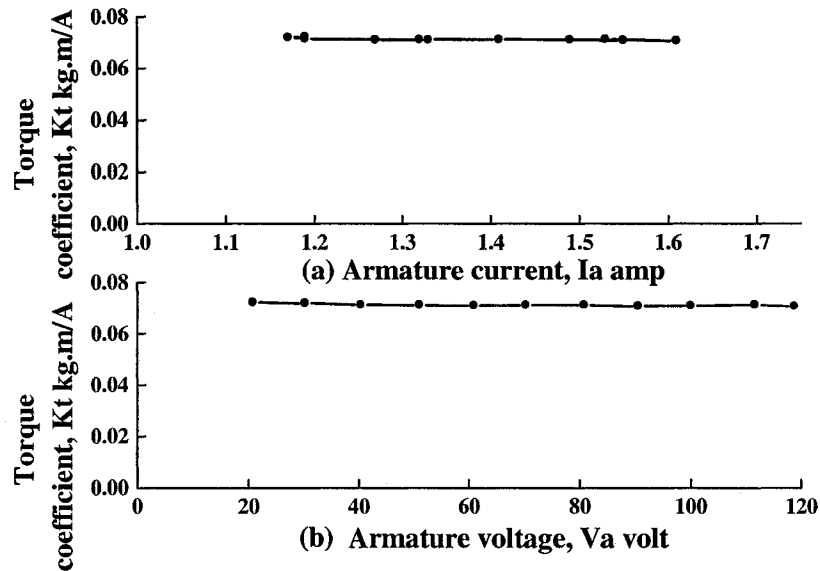


Figure 4.17 Variation of the torque coefficient with , (a) armature current; (b) armature voltage

In order to reduce the error several readings have been taken for emf constant and torque coefficient, and a mean value has been taken used in WTE code.

4.8 Inertia Disk Design for the Wind Turbine

Emulator

The inertia of the wind turbine was a critical part of the research. It largely depends on the rotor radius, blade length and material. An extensive review indicates that the information available regarding the moment of inertia of the wind turbine rotor is not adequate. An assumed value based on the practical experimentation was considered in this research. The inertia disk was designed using the following approach.

For a solid cylinder, the inertia is given by [62]

$$J_w = \frac{1}{2} * M * (R_{disk})^2 \quad (4.16)$$

where, M is the mass of the solid disk and R_{disk} is the radius of the disk

Mass = Volume * Density

Cast steel C10/20 was considered for the disk. From (4.16) the thickness was calculated by choosing suitable radius and it was found that a disk of around 46 kg adequately represents the inertia of such 2.2 kW small wind turbines.

4.9 Summary

A WTE is a strong platform for testing and observing the wind turbine behavior. This chapter describes the novel small wind turbine emulator for small wind turbine system where aerodynamic power is controlled through furling control and the resulting dynamics are also incorporated in the small wind turbine model. To reflect the inertia of the wind turbine rotor an inertia disk is incorporated with the system. A digital PI controller is designed to make sure that the theoretical rotational speed of the wind turbine rotor will be followed by the separately excited DC motor, i.e., emulate the

wind turbine characteristics. Several implementation issues are addressed and solutions are described. The system design, model and associated power electronics are discussed and developed.

Chapter 5

Test Results and Discussions on the Wind Turbine Emulator

This chapter provides some small wind turbine emulator test results and discusses some implementation issues. During test it was required to limit the initial armature current of the DC motor and to follow the theoretical rotational speed of the wind turbine rotor. Response of the system with a step change in wind speed and load was observed and discussed.

5.1 Introduction

The small Wind Turbine Emulator (WTE) described in the previous chapter was implemented and tested in a laboratory environment. A simple gain scheduled digital PI controller was designed to control the speed of the DC motor, which is the same as the required rotation of the wind turbine rotor. The reference output voltage from the PC was

applied to the phase controlled relay using the Lab Master I/O board. The rectified output voltage of the phase controlled relay was applied to the motor armature. The speed control was implemented in QBASIC 4.5 and the initial inrush of the armature current of the motor was controlled through coding, which decreases the necessity of any extra circuitry. The following section is the discussion of the emulator objectives and how the objectives were attained from the proposed WTE system.

5.2 Armature Current Transient

As stated in chapter 4, initial current of the motor armature could damage the armature circuit; therefore some sort of precaution needs to be considered. In this research work, a simple code was used to limit the initial inrush of armature current, which eliminated the need of extra circuitry. A constant wind speed of 7 m/s was applied to investigate the armature current variation and the result is shown in Figure 5.1. It can be seen that the

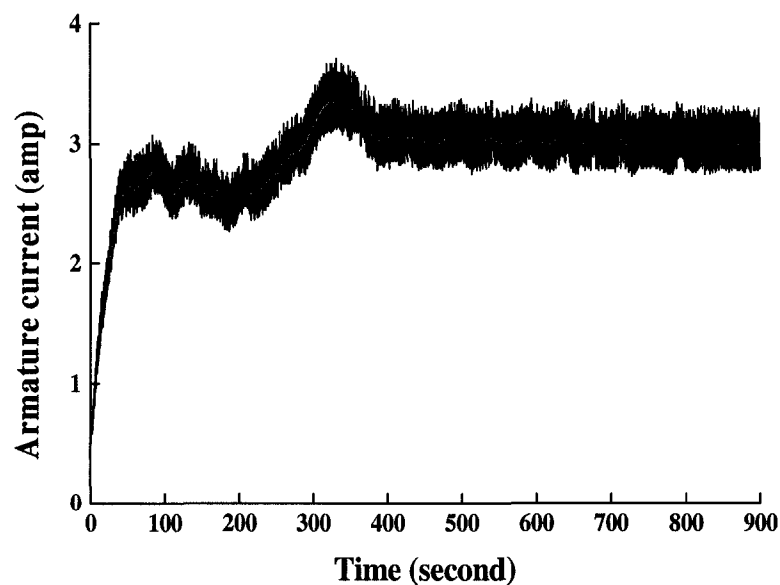


Figure 5.1 Variation of the armature current during the starting period of the DC motor

controller is able to maintain the armature current within a limit and works effectively. System stabilization was also achieved as, after some initial transient, armature current settles to a new value and remains more or less constant. The measured current was filtered using the averaging technique.

5.3 Constant Input Response

In order to test a WTE in a laboratory environment, the first obstacle is to reflect the wind turbine characteristics perfectly. In a real situation, whenever wind flows through a rotor plane, the rotor starts to move and produces power at the shaft. Therefore, a developed WTE should perfectly follow the theoretical rotational speed of the rotor for a particular wind speed or a change in the wind speed. To investigate this ability, a constant wind speed (7 m/s) was applied to the emulator model and the corresponding reference rotor speed (upper trace), actual rotational speed (middle trace) of the motor and error (lower trace) are presented in Figure 5.2. It is shown that after 7 minutes the motor tracks the

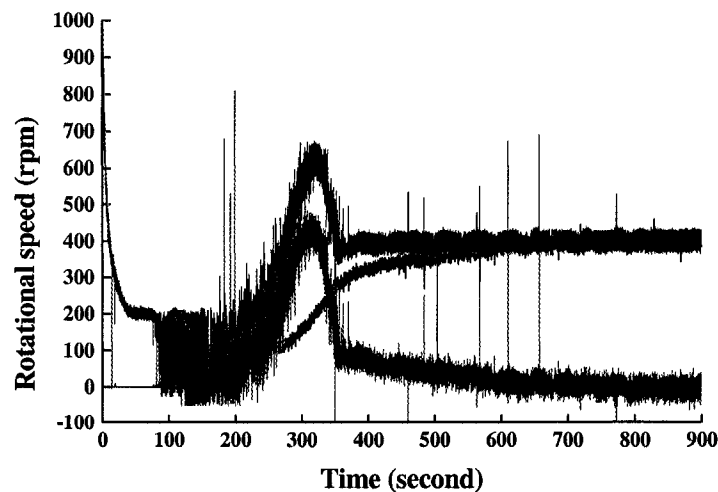


Figure 5.2 Variation of the rotational speed (for a wind speed of 7m/s)

theoretical rotor speed and remains more or less constant. It should be noted that there was some initial transient, and this was due to the large inertia of the inertia disk. Figure 5.3 represents the expected furling dynamics. The value of the furling angle is 5.6° and is the same as predicted from (2.5) in chapter 2.

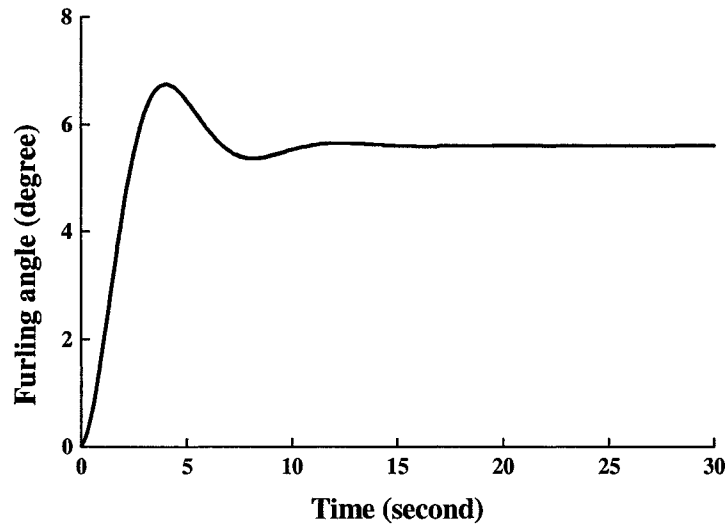


Figure 5.3 Representation of the expected furl dynamics (for a wind speed of 7m/s)

5.4 Sudden Change Response

To evaluate the system performance, a sudden change in the input provides more insight into the transient condition. The main objectives of the WTE controller design were, to track the theoretical rotational speed of the wind turbine rotor, to achieve the expected dynamics of the furling mechanism and to observe the transient response of the armature current for a sudden change in the load. A step increase in the wind speed (from 7 to 8 m/s at $t=1100$ seconds) was applied to the emulator as shown in Figure 5.4. The corresponding reference rotor speed (upper trace), actual rotational speed (middle trace) of the motor and error (lower trace) are presented in Figure 5.5. It can be seen that, after a

step change in the wind speed, within 3 minutes the motor speed follows the reference rotor speed and the error becomes more or less zero. Due to the large inertia of the wind turbine rotor, it takes 3 minutes to reach a stable value. It should be noted that due to the large inertia of the rotor blade of a wind turbine, in a practical situation, the rotor can not move instantly and it will take some time to follow the changing wind speed. Figure 5.6 represents the expected furling dynamics of the wind turbine. After an increase in the wind speed, within 20 seconds the rotor reaches to a new furling angle 4.6° and the angle remains stable as predicted by (2.5). Figure 5.7 represents the variation of the armature current after a step change in the load. As long as the load changes, the armature current settles to a new higher value and the system stabilizes. The measured current was smoothed by the averaging technique. For an initial guess of the PI controller parameter values, the Ziegler-Nichols method was applied and finally, after several trials and errors, a suitable set of parameters, were found to be $K_p = .0000003$ and $K_i = .0000002$.

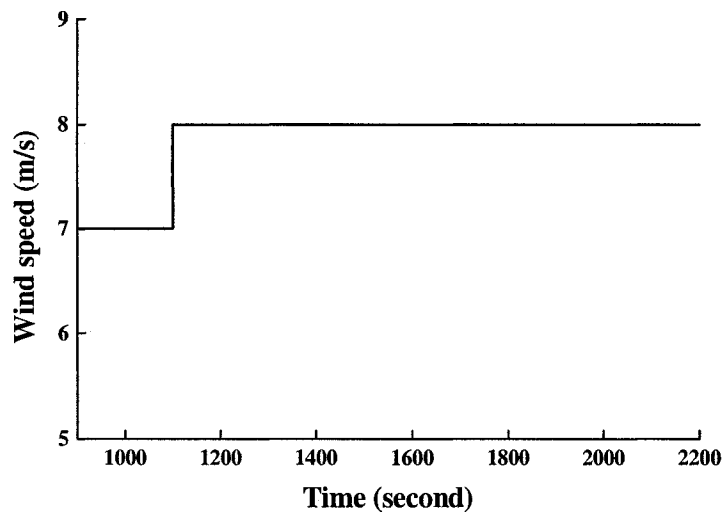


Figure 5.4 Wind speed profile applied to the wind turbine emulator (Wind speed increases from 7m/s to 8m/s at t=1100 s)

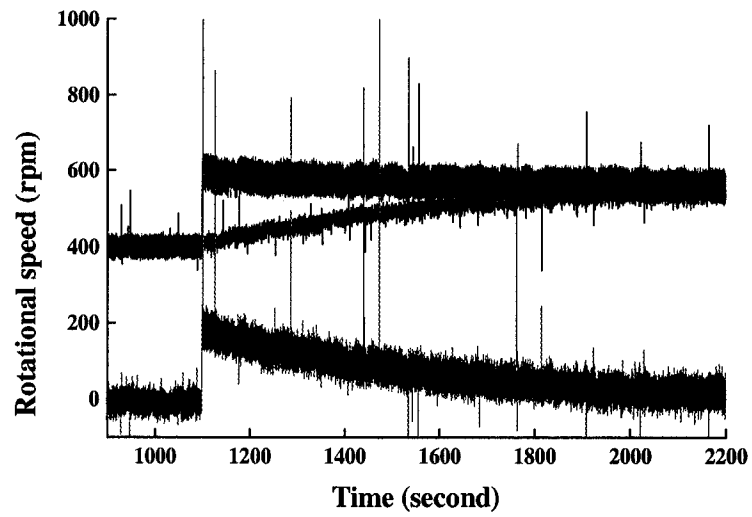


Figure 5.5 Variation of the rotational speed (Wind speed increases from 7m/s to 8m/s at $t=1100$ s)

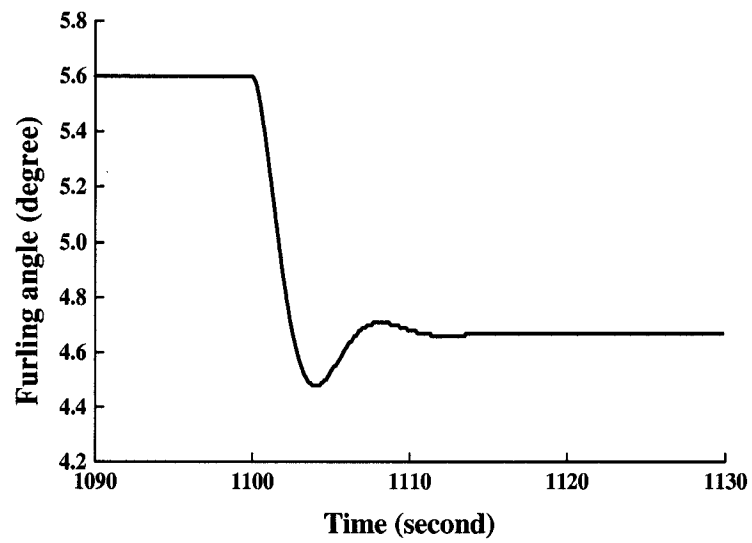


Figure 5.6 Representation of the expected furl dynamics (Wind speed increases from 7m/s to 8m/s at $t=1100$ s)

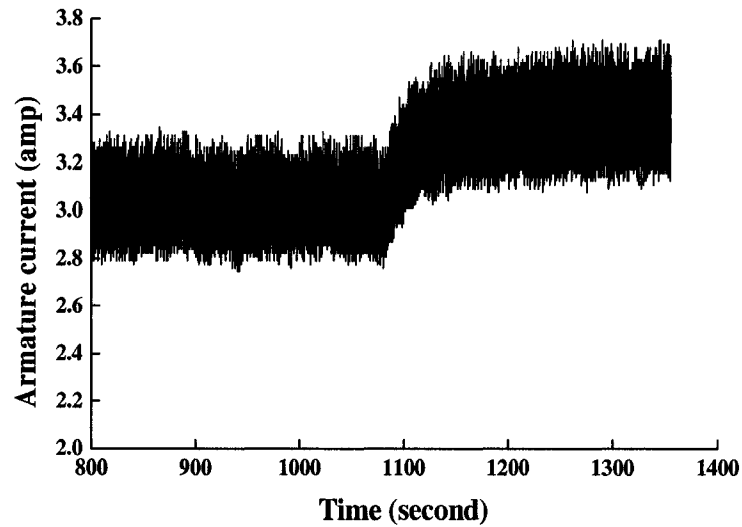


Figure 5.7 Variation of the armature current after a step change in the load

5.5 Summary

The small WTE described in chapter 4 and the results are discussed in this chapter. The initial armature current of the DC motor is limited to an acceptable range and found to be stable after a step change in the load. The theoretical rotational speed of the wind turbine rotor is followed by the DC motor, thus emulates the behavior of a wind turbine. Expected furling dynamics are also attained. The performances of the wind turbine emulator are investigated using both a fixed wind speed and a step change in the wind speed and found to be acceptable.

Chapter 6

Maximum Power Controller for the Emulator

This chapter provides the description of the maximum power controller and related power electronics for the wind turbine emulator. The first section is the motivation, challenges, and details of the study to be conducted on the wind turbine emulator. Secondly, a controller to achieve the maximum power extraction from the wind turbine emulator is described. Later on in this chapter, there is a summary of the maximum power controller power electronics followed by the detailed description and implementation are presented.

6.1 Introduction

A complete wind turbine emulator system was developed and its performance has been investigated in the previous chapters (chapter 4 and chapter 5). It was found that the developed wind turbine emulator accurately represent the characteristics of a wind

turbine. However, in actual practice, a Maximum Power Controller (MPC) is necessary to extract the maximum power from a wind turbine. Also, it has been stated earlier that Canada has a great potential to generate electricity using wind power. There are lots of remote and isolated places all around the world where small-scale wind power generation can be used to meet the users' load demand. Testing of the power electronics and the controller performance in a laboratory environment is required to avoid problems at installation. This research focuses on the small wind turbine systems which are mainly used to supply a single user's load demand and further investigation can be carried for remote or isolated locations. In remote locations it is desirable to power the associated power electronics circuitry of the wind turbine from the wind turbine itself. As far as the power production is concerned, it is always desirable to extract the maximum power from the wind turbine. In the above discussions, several issues have been raised and need to be solved, i.e., the design of maximum a power controller for the proposed small wind turbine emulator system, the design of a power supply for the power electronics circuitry, and a complete implementation of the controller power electronics of the WTE. On the strength of the above analysis, a maximum power extractor in conjunction with the load was designed and implemented. The variable AC voltage produced by the wind turbine was rectified and passed through a DC-DC converter. A dump load was connected to the output of DC-DC converter and a microcontroller was used to control the Pulse Width Modulation (PWM) duty cycle of the converter. The key objectives of this chapter can be summarized as follows:

- Design of a maximum power controller

- Implement of the controller power electronics

The following sections describes the implementation of the maximum power controller and the development procedure of the controller power electronics.

6.2 Maximum Power Control

It has been discussed in chapter 2, the maximum power from a wind turbine system can be extracted by operating the wind turbine system at its optimum TSR. And from Figure 3.1 it was found that maximum power could be extracted from the proposed system by forcing the wind turbine to operate near TSR of 7, i.e., optimum TSR.

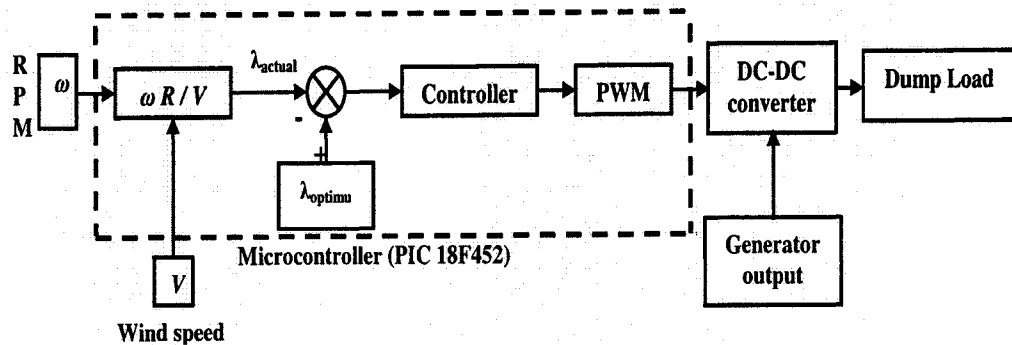


Figure 6.1 Structure of the maximum power controller

Therefore, in order to extract the maximum power, an optimum TSR control was selected. The actual TSR of the wind turbine is compared with the optimum TSR and the controller controls the duty cycle of the converter as required. The PWM wave created by the microcontroller switches the converter to control the dump load connected to the system. The microcontroller was programmed using MikroBasic 2.0.0.4. The basic structure of the maximum power controller is shown in Figure 6.1.

6.2.1 Maximum Power Control Algorithm

A digital PI controller was used to ensure the maximum power extraction by controlling the duty cycle of the converter. The advantages and disadvantages of a PI controller were described in chapter 2. The control algorithm is expressed by (4.8). The controller accepts the RPM information and calculates the desired TSR of the WT. It is then compared with the optimum TSR of the WT, i.e., 7 and determines the duty cycle as required. The control algorithm is simple and is shown in a flow chart by Figure 6.2.

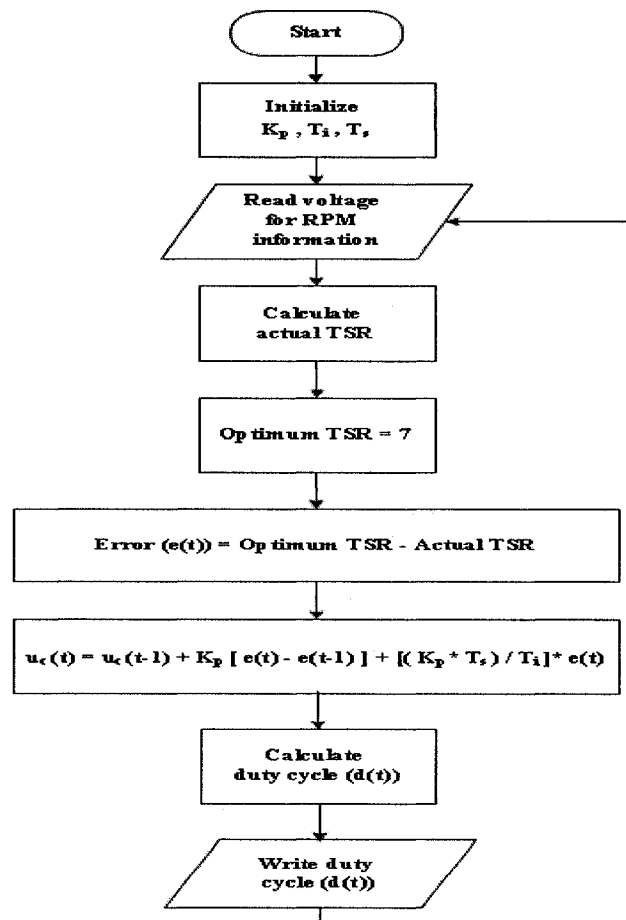


Figure 6.2 Flow chart of the maximum power controller

6.3 Implementation of the Maximum Power Controller Power Electronics

The following section is a summary of the MPC power electronics and a power scheme for the associated circuitry of the MPC that was designed during this work .

The separately excited DC motor was coupled to a generator. The output of the synchronous generator was first rectified by a 3-phase rectifier and then passed through a DC-DC converter. The topology selected was the buck-boost converter, as the variation of wind speed and expected output voltage were not known in advance. The duty cycle of the converter was controlled by a microcontroller (PIC 18F452) and the output of the converter was connected to a dump load. In order to resolve the driving issue of the MOSFET a simple approach was selected. An opto-coupler was used to separate the ground of the PIC and driver stage. In order to power the opto-coupler and driver an isolated supply was built using a single output +5V to +15V commercially available dc-dc converter. The generator RPM was determined from its output voltage. The single-phase voltage of the generator was lowered using a transformer and then it was converted into square wave using a Schmitt trigger. The square wave pulses were converted into an analog voltage using a frequency to voltage converter. Resulting analog voltage was supplied to the microcontroller.

The reference voltage for the Schmitt trigger was also generated using a voltage divider and output of the dc-dc converter. The variable frequency of the pulses was converted to

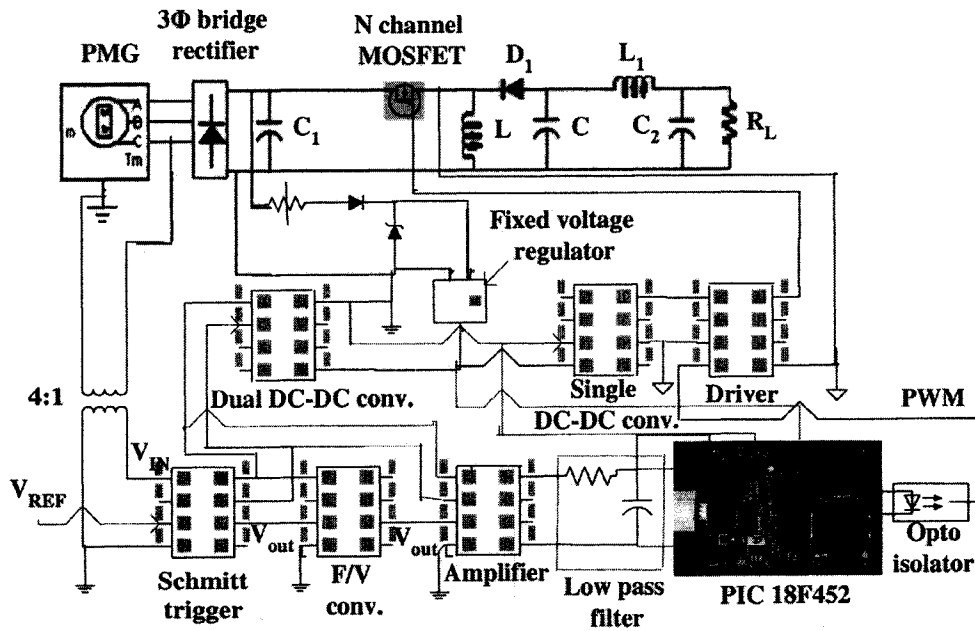


Figure 6.3 Schematic of the controller power electronics circuitry

voltage using an F/V converter IC. An amplifier stage was necessary to amplify the low voltage to 0V – 5V range. A dual output (+5 to +15/-15) dc-dc converter was used to power the Schmitt trigger, F/V converter and amplifier. A fixed voltage regulator was used to supply the necessary +5 volts to the dc-dc converters and the PIC. A 3- Φ bridge rectifier was used to convert the ac voltage to DC and a variable resistor and zener diode combination was used to regulate the input DC voltage variation to the acceptable input voltage level of the fixed voltage regulator. A schematic of the MPC power electronics and power scheme is given in Figure 6.3 and from the above discussion, the implementation stages can be subdivided into several sections as follows:

1. A complete power supply for the MPC power electronics circuitry
2. Design of a DC-DC converter
3. A driver circuit for the MOSFET switch

4. Extraction of the RPM information from the generator
5. PIC interfacing and programming

The following sections are the description of the procedures for the development of stages.

6.3.1 A Complete Power Supply for the Maximum Power Controller Power Electronics Circuitry

Assuming that the wind turbine will be operated in an isolated mode, a means to power up the integrated power electronics circuitry was required. It was found that several commercially available ICs in power electronics circuitry accept different voltage level. Therefore, a proper power supply was needed. To achieve that, the output of the generator was rectified using a 3 phase bridge rectifier and this large voltage used to power up the whole circuitry by some necessary steps. The output from the rectified DC was lowered by using a simple resistor and zener diode combination to make sure that the variation of the voltage should not exceed the acceptable voltage level of the voltage regulator. The regulator can accept an input variation of 7 – 15 volts and produce a regulated output voltage of 5 volts. The 5 volts level of the regulator was increased using a commercially available isolated dc-dc converter (+5 to +15/-15) to supply other ICs in the circuit. The supply was needed for the RPM extraction stage, the driver and PIC stage. Two of the voltage regulators were required as the complete circuit draws a lot more current than a regulator can supply. The complete power scheme that was used during implementation is shown in Figure 6.4.

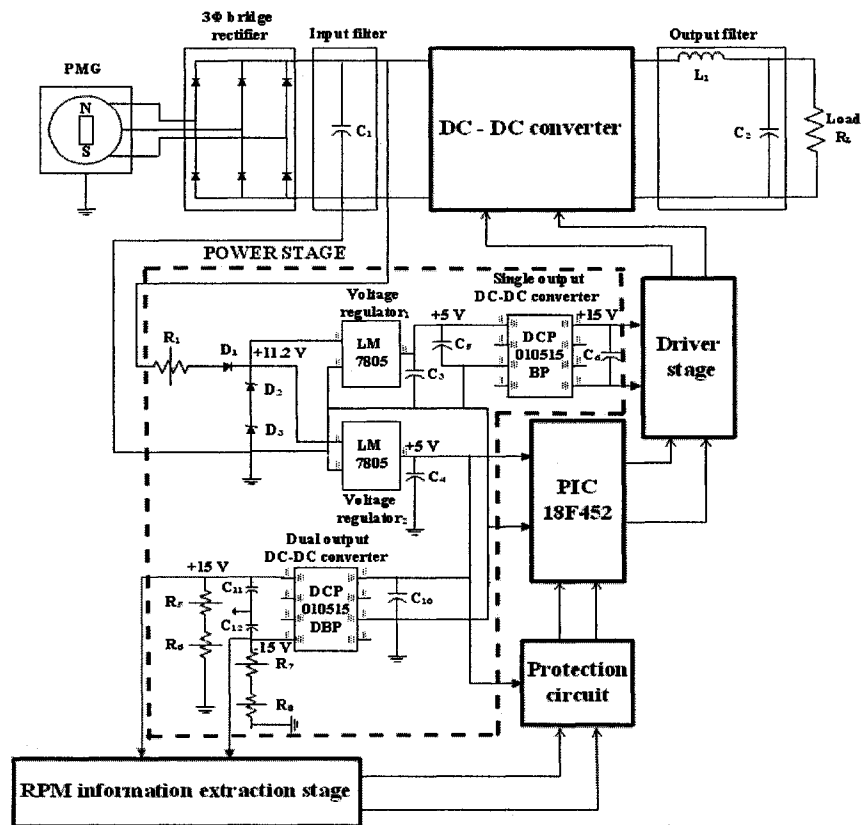


Figure 6.4 Schematic of the power supply for the controller power electronics

6.3.2 DC - DC Converter Design

The output voltage variation of the wind turbine was not known in advance, so the selected topology of the DC – DC converter was buck-boost, as it has the ability to increase or decrease the voltage level at its output. The schematic of a buck-boost converter is shown in Figure 6.5

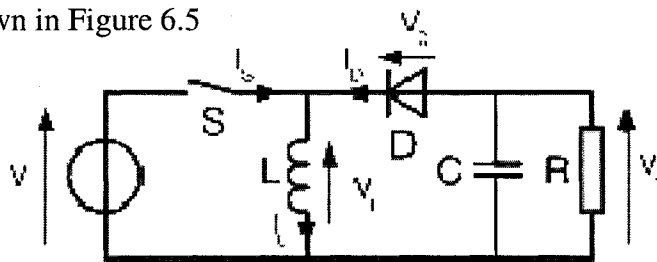


Figure 6.5 Schematic of a buck-boost converter

The basic principle of operation of a buck-boost converter is as follows. When the switch is ON, as the input is directly connected to inductor L, it acquires energy from the source and the output capacitor supplies energy to the load. The free wheeling diode is reverse biased. And when the switch is OFF, the diode is forward biased and inductor (L) transfers energy to the output capacitor (C) and, finally to load. From the principle, one point is clear enough; that the energy that is being supplied to the load depend upon the ON time and OFF time of the switch. The ON and OFF time of the DC-DC converter can be related with the term named duty cycle. Duty cycle (D) can be defined as the cycle of the ON time over the summation of the ON and OFF times, i.e.,

$$Duty_cycle(D) = \frac{T_{ON}}{T_{ON} + T_{OFF}} \quad (6.1)$$

where, T_{ON} is the total ON time of the converter.

T_{OFF} is the total OFF time of the converter.

PWM is a common technique used extensively in industry to control the duty cycle of a converter. The basic of the PWM control technique is to control the duty cycle of the switching frequency for a control variable. In this research work, a controlled voltage at the output of the DC – DC converter was not the main objective. The objective was to control the duty cycle of the converter to maintain the optimum TSR and to ensure the maximum power extraction.

A buck–boost converter produces a voltage of opposite polarity with respect to the input, where as a buck or boost converter can produce a voltage of either opposite or negative voltage at the output. Instead of going through all required aspects, a straight forward design was done by considering the voltage and current rating and it should be noted that in addition to the converter, a simple input and output filter was designed to make the voltage ripple as smaller as possible.

During the design of the converter with a wide input range, the design should be based on the worst condition so that the components will be working even if the worst condition occurs. A buck-boost converter should be designed based on the minimum input voltage because at this voltage, current through the switch is maximum. Before starting the design procedure, several assumptions need to be made:

- Switching frequency is 100 KHz
- Output voltage would be more or less 120 volt
- Minimum input voltage is 50 volt
- Maximum input voltage is 120 volt
- Maximum output current 13 amps
- Current ripple cycle at the maximum load (r) is 0.3
- Maximum duty cycle = 0.7

The following equations were used to calculate the component values of the DC – DC converter.

6.3.2.1 Inductor (L)

An inductor is the main component that supplies the energy to the output circuit and also plays a vital role to reduce the output current ripple. The selection of an inductor should be such that it is as close as possible of the calculated value. If the inductor used is less than the calculated value it will produce more ripples at the output current and if the inductor used is more than the calculated value, it may force the converter to change the states between continuous and discontinuous modes of operation. The value of the inductor (L) was calculated as [64]

$$L = \frac{V_0 + V_d}{I_0 * r * f_s} (1 - D)^2 * 10^6 \quad (6.2)$$

Where, L is the inductor in μH

V_0 is the output voltage in volt

V_d is the diode voltage in volt

D is the duty cycle

I_0 is the output current in amp

r is the current ripple cycle at the maximum load

f_s is the switching frequency in Hz

After calculation of the inductor, a proper selection was required based on different aspects of the inductor. The following are the points that should be considered carefully during the selection of a proper inductor.

- The RMS current rating of the inductor should be equal to or greater than the maximum switch current to avoid the saturation of the inductance [64].
- A larger value will increase the total cost and size.
- The DC and AC resistance of the inductor should be considered as they increase with increase in temperature [65].
- It is good in practice to operate the inductor below its Self Resonant Frequency (SRF) [65].
- The saturation current of the inductor should be taken into consideration.
- Finally, the selected inductor should have the proper energy handling capacity.

The ripple current (ΔI_L) of the inductor is given by [64]

$$\Delta I_L = \frac{V_0 + V_d}{L * f_s} * (1 - D) * 10^6 \quad (6.3)$$

The RMS ($I_{L,rms}$), average ($I_{L,avg}$) and peak current ($I_{L,peak}$) in ampere through the inductor can be found from (6.4), (6.5) and (6.6) respectively [64].

$$I_{L,rms} = \frac{I_0}{1 - D} * \sqrt{1 + \frac{r^2}{12}} \quad (6.4)$$

$$I_{L,avg} = \frac{I_0}{1 - D} \quad (6.5)$$

$$I_{L,peak} = \frac{I_0}{1-D} * \left[1 + \frac{r}{2} \right] \quad (6.6)$$

As the energy handling capacity ($E_{L,energy}$) of the inductor is essential so it was calculated by (6.7) and finally a proper inductor was selected.

$$E_{L,energy} = \frac{I_0 * E_t}{8 * (1-D)} * \left[r * \left(\frac{2}{r} + 1 \right)^2 \right] \quad (6.7)$$

It is also known that a dc-dc converter can operate in either continuous or discontinuous conduction mode and it was found that the calculated inductor value meets the continuous conduction opecylen. For a continuous conduction the inductor should meet the requirement described by (6.8) [66].

$$L \geq \frac{-V_0 * T_s}{2 * I_{ob}} * \frac{V_{i(max)}^2}{(V_0 - V_{i(max)})^2} \quad (6.8)$$

6.3.2.2 Capacitor (C)

During the selection of the capacitor several issues also need to be addressed. The value of C should have low Equivalent Series Resistance (ESR) so that it will do most of the filtering. Also, as long as the current and voltage rating is concerned, it should have the ability to maintain the worst case current. To select the starting current, a good rule of thumb is to start from a simple relation between the output voltage and the voltage ripple at the output [67]

$$\frac{\Delta V_r}{V_0} \leq 1\% \quad (6.9)$$

Where, ΔV_r is the maximum (p-p) ripple voltage in volt

In this research work a cycle of 0.5% was considered. A simple equation was used to calculate the value of ESR in ohm (Ω) as [66]

$$ESR \leq \frac{\Delta V_{r,max}}{\left(\frac{I_{0(max)}}{1-D_{max}} + \frac{\Delta I_0}{2} \right)} \quad (6.10)$$

$$\text{Or, } ESR \leq \frac{\Delta V_{r,max}}{I_{l,peak}} \quad (6.11)$$

A good rule of thumb is to decrease the ESR by 30 to 50% of the actual calculated value[66]. Therefore the calculated ESR was lowered to 40%.

The value of the output capacitor was calculated as [66, 67]

$$C \geq \frac{I_{0,max} * D_{max}}{f_s * \Delta V_{r,max}} \quad (6.12)$$

A 10 ~ 20 times bigger capacitor is often used in practice [66]. After several trials and errors, and based on the available ESR value, a suitable capacitor was selected.

It should be noted that during the selection of a capacitor, the current rating needs to be considered. The RMS ($I_{C,rms}$) and peak to peak current ($I_{C,p-p}$) of the output capacitor were calculated by (6.13) and (6.14) respectively [64].

$$I_{C,rms} = I_0 * \sqrt{\frac{D + \frac{r^2}{12}}{1-D}} \quad (6.13)$$

$$I_{C,p-p} = \frac{I_0}{1-D} * \left[1 + \frac{r}{2} \right] \quad (6.14)$$

6.3.2.3 Switch

The RMS ($I_{SW,rms}$), peak ($I_{SW,peak}$) and average current ($I_{SW,avg}$) through the switch were calculated by (6.15), (6.16) and (6.17) respectively [64].

$$I_{SW,rms} = \frac{I_0}{1-D} * \sqrt{D * \left[1 + \frac{r^2}{12} \right]} \quad (6.15)$$

$$I_{SW,peak} = \frac{I_0}{1-D} * \left[1 + \frac{r}{2} \right] \quad (6.16)$$

$$I_{SW,avg} = I_0 * \frac{D}{1-D} \quad (6.17)$$

6.3.2.4 Diode

The Peak ($I_{D,peak}$) and average current ($I_{D,avg}$) of the diode were calculated by (6.18) and (6.19) respectively [64]

$$I_{D,peak} = \frac{I_0}{1-D} * \left[1 + \frac{r}{2} \right] \quad (6.18)$$

$$I_{D,avg} = I_0 \quad (6.19)$$

6.3.2.5 Input Filter

A capacitor was used as the input filter and the RMS ($I_{C_1,rms}$) and peak to peak current ($I_{C_1,p-p}$) of the input capacitor were calculated from (6.20) and (6.21) as [64]

$$I_{C_1,rms} = \frac{I_0}{1-D} * \sqrt{D * \left[1 - D + \frac{r^2}{12} \right]} \quad (6.20)$$

$$I_{C_1,p-p} = \frac{I_0}{1-D} * \left[1 + \frac{r}{2} \right] \quad (6.21)$$

6.3.2.6 Output Filter

A LC filter was designed to minimize the ripple voltage at the output and it was considered that the maximum ripple is 0.1 volt. A minimum required damping was

considered as 0.1 volt. The L_1 and C_2 values can be calculated to maintain the assumed required damping as [68]

$$\text{Minimum required damping of the filter} = \frac{X_{C_2}}{X_{C_2} + X_{L_1}} \quad (6.22)$$

Where $X_{L_1} = 2\pi f_s L_1$; f is the switching frequency.

$$X_{C_2} = \frac{1}{2\pi f_s C_2} \quad (6.23)$$

By selecting a C_2 value for the filter, the corresponding L_1 can be found.

Using (6.1) to (6.13) buck-boost converter and filters was designed. A schematic is shown in Figure 6.6. Components used for the DC – DC converter along with their suppliers are presented in Table 6.1:

Table 6.1: Component of the DC – DC converter and filters

Symbol	Parameter	Value	Unit	Rating		Supplier (Part no.)
				Current (amp)	Voltage (volt)	
C_1	Capacitor	10000	μF		250	Digikey (P10091-ND)
SW	MOSFET			80	500	Digikey

	Switch					(IXFN80N50-ND)
L	Inductor	30	μH	120		CWS Inc. (E70340-013)
D	Diode			60	400	Digikey (60EPF04-ND)
C	Capacitor	10000	μF		250	Digikey (P10091-ND)
L_1	Inductor	1.2	μH	21.01		Digikey (308-1004-1-ND)
C_2	Capacitor	68	μF		250	Digikey (P5927-ND)

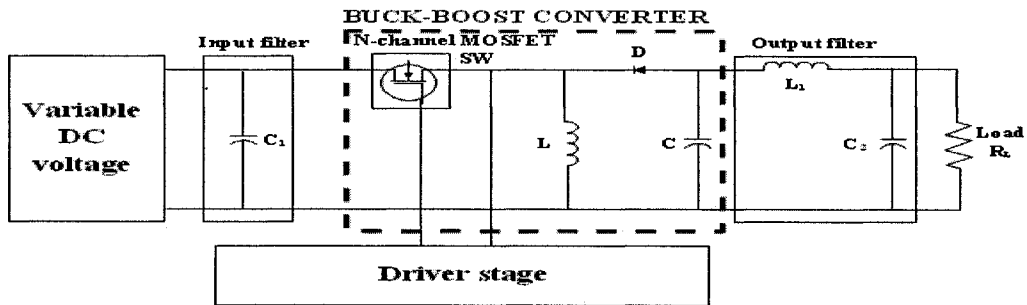


Figure 6.6 Schematic of the converter stage with peripheral

6.3.3 Driver circuit for the Switch

The PWM signal generated by the PIC was not adequate to switch the gate of the MOSFET switch. Therefore, a gate driver circuit was necessary. The main purpose of the driver circuit is to supply the necessary voltage and current to the gate of the MOSFET. The MOSFET used with the DC-DC converter needed a gate signal of 12 to 18 volts. A nominal voltage of 15 volt was selected and the driver circuit was powered from one of the outputs of the isolated supply discussed in section 6.3.1. A proper isolation is often necessary to protect the PIC and other signal circuitry. Several research and application notes are available to assemble a gate drive circuit and the minimum requirement of current for the driver circuit. Isolation between the PWM signal and drive circuit was performed using a commercially available opto-coupler. Some ringing was present at the gate drive signal and this was due to the connecting wire inductance. The schematic diagram of the gate drive circuitry is shown by Figure 6.7.

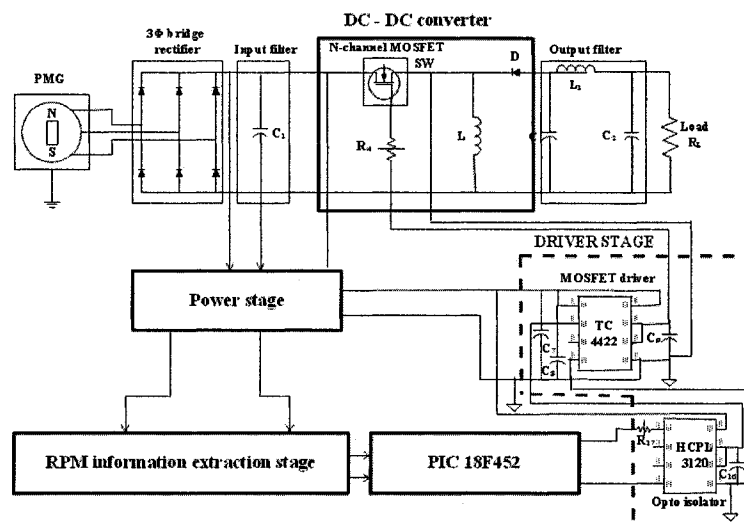


Figure 6.7 Schematic of the driver stage of DC – DC converter

6.3.4 Extraction of the RPM Information from the Generator

To supply the RPM information to the PIC, the output of the generator voltage was lowered using a transformer which has a turn cycle of 4:1. The variable voltage and variable frequency produced by the wind turbine was compared to a dc level and passed through a Schmitt trigger circuit. The output of the Schmitt trigger produced a square wave of the same frequency as produced by the wind turbine generator and the frequency applied to a commercially available F/V converter. The variation of the frequency from the generator was limited to 0 to 60 Hz and within this range, the F/V converter gives a voltage between 0 to 1 volt. As a result, an amplifier stage was necessary to amplify the

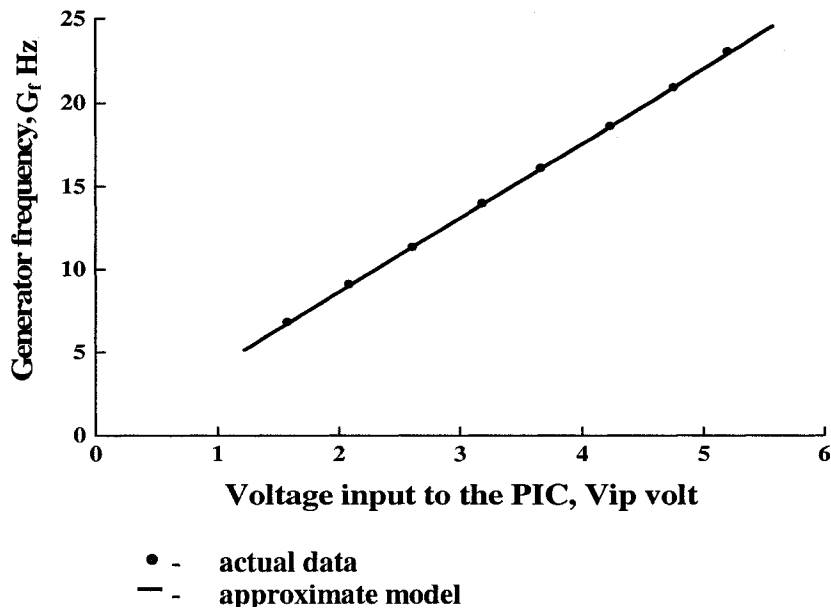


Figure 6.8 Characteristic of the RPM signal extraction circuit

voltage between 0 to 5 volts, i.e., acceptable range for the PIC. A simple low pass filter was used in conjunction with the amplifier to remove the noise. To reduce the voltage spikes of the output signal, a protection circuit was used. To acquire the RPM information inside the PIC, a calibcyclen equation was used and the experimental and fitted curve are given in Figure 6.8. The fitted modeling equation was found to be

$$G_f = 4.4271 * V_{ip} - 0.2933 \quad (6.24)$$

A schematic of the RPM information extraction circuit is given in Figure 6.9 and the pictorial presentation is in Figure 6.10.

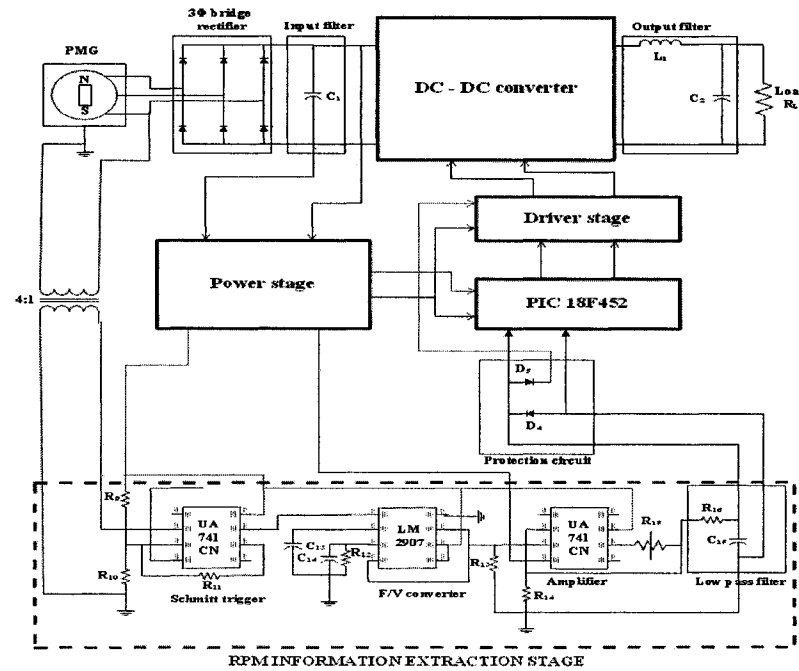


Figure 6.9 Schematic of the RPM information extraction stage with peripheral

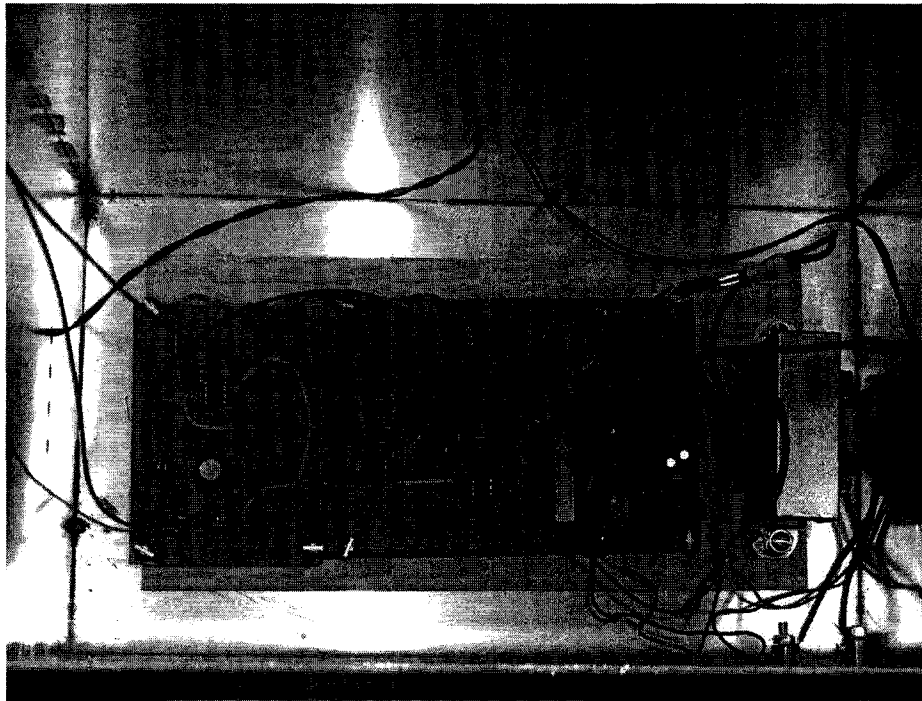


Figure 6.10 A picture of the RPM information extraction circuit

6.3.5 PIC Interfacing and Programming

After the development of the complete system, PIC programming was necessary to implement the maximum power control algorithm. The PIC 18F452 was powered up from the power stage. The PIC has two channels for PWM signal and eight analogue data-acquiring channels. The PIC was ordered along with a board which has various features, i.e., 2 independent D/A channels, RS 232 interfacing, a LCD monitor, Temperature sensor etc [69]. The maximum power control algorithm was programmed inside the PIC and it was interfaced with a PC through a serial port. The PIC was programmed using MikroBasic 2.0.0.4 as it was easy to use and similar to QBASIC that was used to develop the emulator system. A few implementation issues should be addressed. A situation can occur when the wind turbine is not rotating but the power

electronics stage is ON, or when suddenly the power is switched OFF to the power electronics stage but the wind turbine is rotating. To address these issues, MPC code was written so that it will check the input condition and jump to an appropriate section of the program as required. Also to display various data value onto the PC screen, a separate routine was created to send data to the serial port while the main loop is running. The calculated duty cycle dictated by the controller output was used to generate the PWM wave and applied to the driver circuit. To communicate between the PIC and PC a terminal emulator (TERA TERM PRO) was used. A complete flow diagram is shown in Figure 6.12 and the complete program is given in Appendix C.

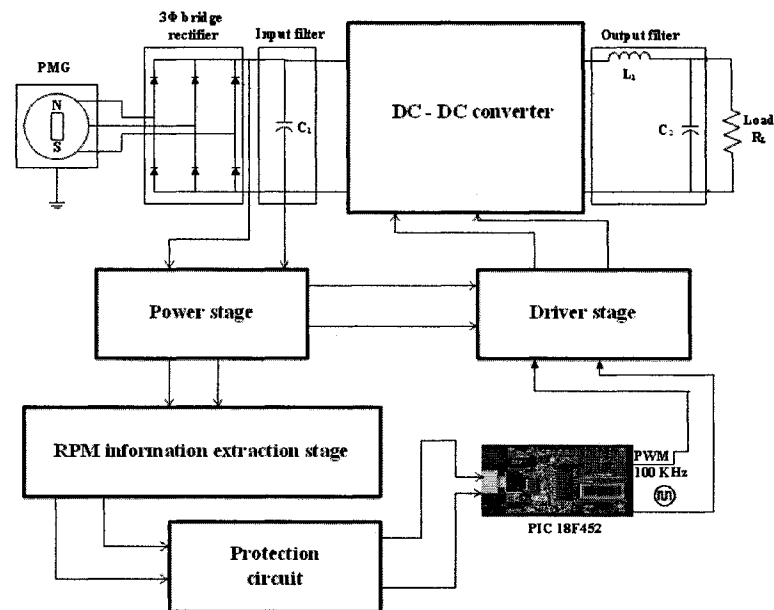


Figure 6.11 Interfacing of the PIC with peripheral

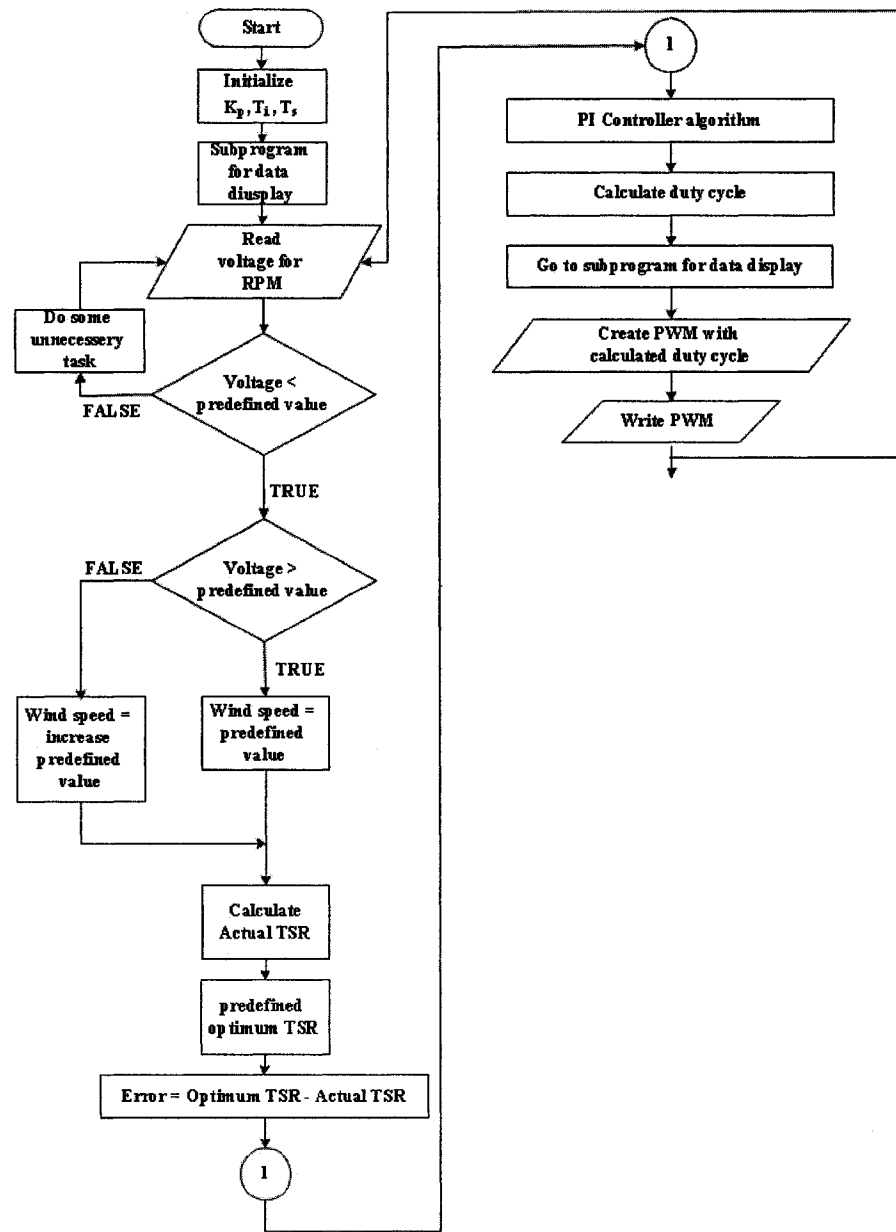


Figure 6.12 Flow chart of the maximum power controller code

A complete circuit diagram is given in Figure 6.13 and pictorial representation is in Figure 6.14.

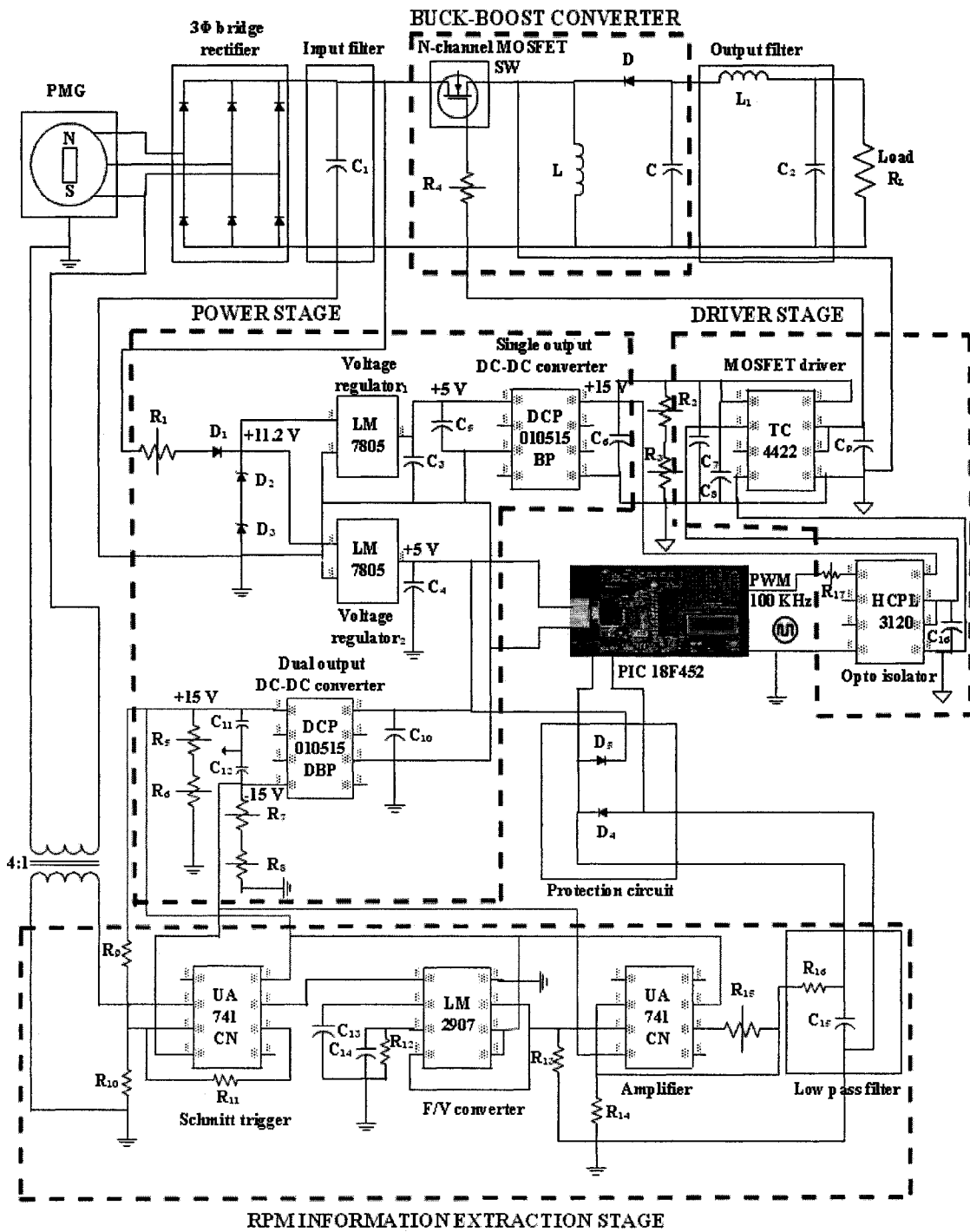


Figure 6.13 A circuit diagram of the maximum power controller power electronics



Figure 6.14 A photo of the maximum power controller power electronics

6.4 Summary

This chapter describes the implementation of a maximum power controller and related power electronics for the developed wind turbine emulator. A complete power scheme for the maximum power controller power electronics circuitries are designed. A buck-boost converter design is presented with necessary equations. The PIC based maximum power controller compares the actual TSR with an optimum TSR of the wind turbine and controls the duty cycle of the DC – DC converter to ensure the maximum power extraction from the emulator.

Chapter 7

Results and Discussions

Some test results and detailed discussion of the wind turbine emulator and maximum power controller power electronics are presented in this chapter. This can be considered as the global results of the research work. Firstly, an introduction reviews the objectives that are expected from this research. Secondly, the response of the wind turbine emulator and maximum power controller power electronics with a constant wind speed is investigated. Finally, a step change in wind speed is investigated in order to study the transient response of the system.

7.1 Introduction

The Maximum Power Controller (MPC) power electronics of the small wind turbine emulator is described (chapter 6) was implemented and tested in a laboratory environment. Digital PI controllers were designed for both the Wind Turbine Emulator (WTE) and the maximum power controller to make sure that the speed of the separately

excited DC motor is the same as the required rotation of the wind turbine rotor and also to ensure that it corresponds to the optimum tip-speed ratio (TSR) of the wind turbine. The speed control for WTE was implemented in QBASIC 4.5 and the MPC was implemented using MikroBasic 2.0.0.4. It was expected that the entire emulator would reflect the characteristics of a wind turbine and ensure maximum power extraction by maintaining the optimum TSR. Besides this, several investigations were necessary to ensure that the MPC power electronics is working as expected. Due to these reasons, an evaluation of the RPM extraction and the expected RPM, generation of the PWM signal from the PIC, change of the duty cycle at the output of the PIC, and the driving signal for the MOSFET were necessary. The following sections are the discussion of the results obtained from the emulator system.

7.2 Constant Input Response

When the integrated system was working, several step by step investigations were performed. Two sets of reading were recorded for two different constant inputs of wind speed. The detail of the results are discussed below:

7.2.1 Response to a Constant Wind Speed of 7 m/s

7.2.1.1 Wind Turbine Emulator Characteristics

The primary objective of the emulator was to follow the theoretical wind turbine rotor rotational speed. Besides this, limiting the motor armature current was also an issue. For a constant wind speed of 7 m/s (Figure 7.1), the armature current is shown in Figure 7.2. It was found that the limiting nature of the armature current and the system reaches stable

states within 6 minutes. The corresponding reference rotor speed (upper trace), actual rotational speed (middle trace) of the motor and error (lower trace) are presented in Figure 7.3. It can be seen that after 5 minutes, the motor tracks the theoretical rotor speed and remains more or less constant (Figure 7.3). It should be noted that there are

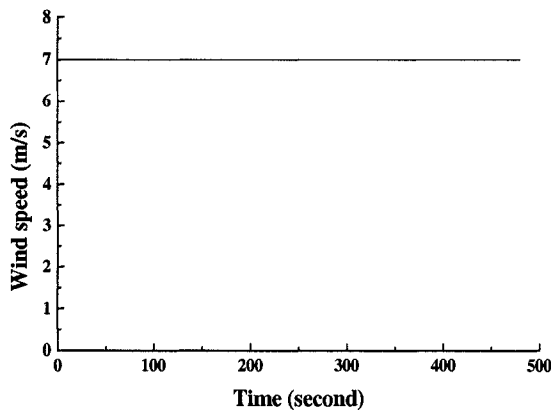


Figure 7.1 Wind speed profile applied to the wind turbine emulator

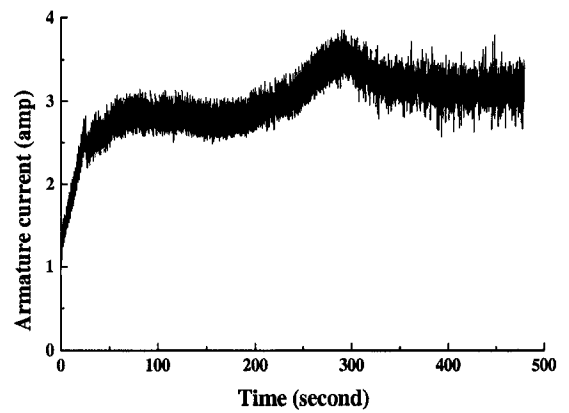


Figure 7.2 Variation of the armature current of the DC motor.

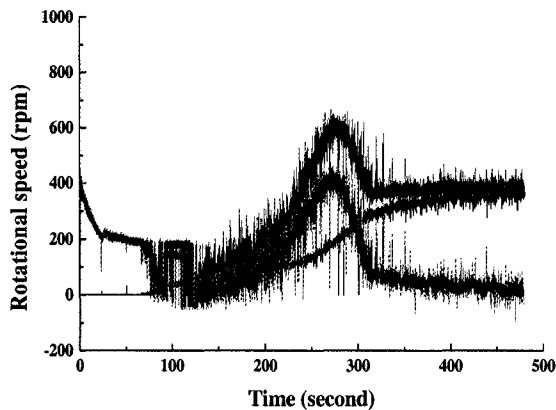


Figure 7.3 Variation of the rotational speed of the DC motor

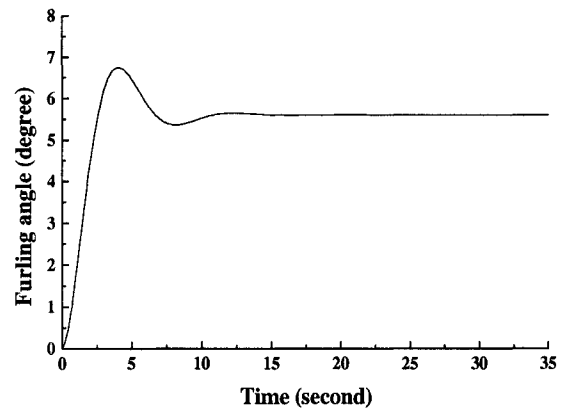


Figure 7.4 Expected furling dynamics of the wind turbine emulator

some initial transients exist on RPM and this is due to the large inertia of the inertia disk.

As far as the furling is concerned, the expected furling dynamics was attained (Figure 7.4)

and the final value of the furling angle is 5.6° from (2.5).

7.2.1.2 Maximum Power Control

As far as the maximum power extraction is concerned, it was expected that the WT will maintain an optimum TSR. Recalled from the Figure 2.1, maximum power will be extracted if the WTE can maintain an optimum TSR of 7. Figure 7.5 concludes that as soon as the system speeds up, the TSR of the emulator gradually increases towards the optimum TSR (black) and consequently error decreases (green). The TSR curve of Figure 7.5 ensures the maximum

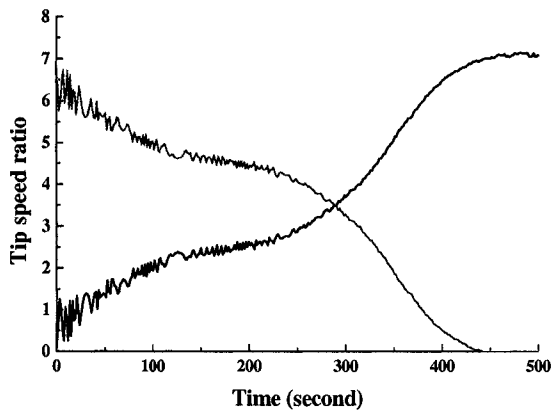


Figure 7.5 Variation of the tip-speed ratio with time

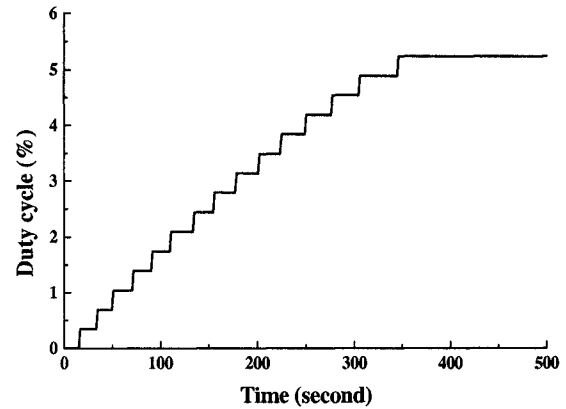


Figure 7.6 Duty cycle variation from the PIC with time power

extraction from the proposed small WTE. The corresponding duty cycle of the PWM wave and the generated PWM from the PIC are given in Figures 7.6 and 7.7. It can be observed that the system reaches a stable duty cycle and remains constant.

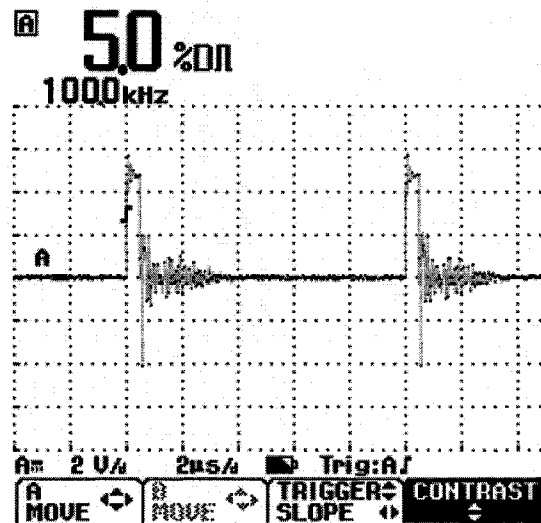


Figure 7.7 PWM output of the PIC

7.2.1.3 Maximum Power Controller Power Electronics Performances

The implementation of the MPC power electronics should make sure that the expected signals will be produced. For a wind speed of 7 m/s, the voltage input to the PIC via the RPM extraction stage is given in Figure 7.8. The corresponding signal from the transformer (upper trace) and Schmitt trigger (lower trace) are given in Figure 7.9. Recalled from section 6.3.4, there is a good agreement existing between the experimental frequency (Figure 7.9) and expected frequency (equation (6.24)) for the experimental PIC input voltage and acceptable performance are ensured. The driving signal to the MOSFET gate is given in Figure 7.10. It can be seen that some ringing exists on the driving signal, mainly due to the EM noise

from other stages of the system. Also it should be mentioned that the driver signal is almost the same as the PWM signal generated from the PIC (Figure 7.7).

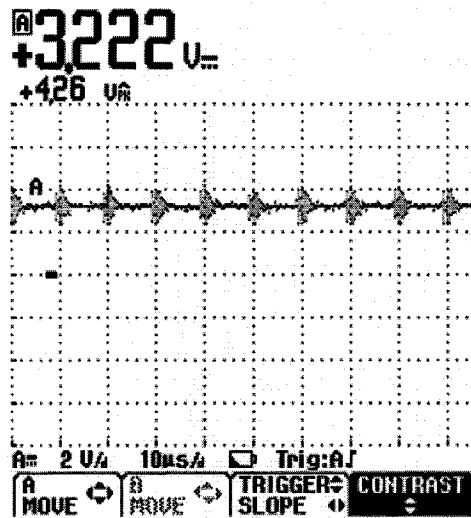


Figure 7.8 Amplified signal applied to the PIC

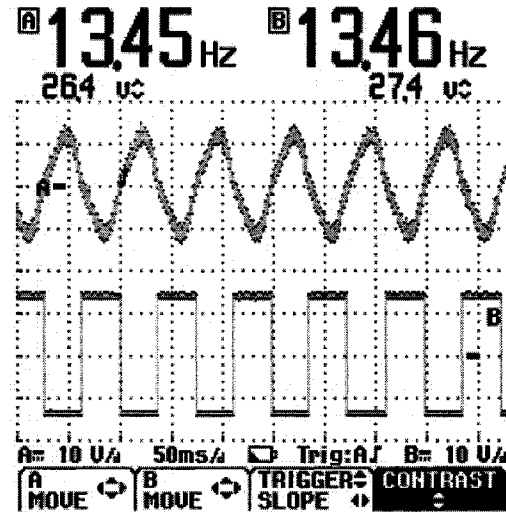


Figure 7.9 Transformer output (upper) and Schmitt trigger output (lower)

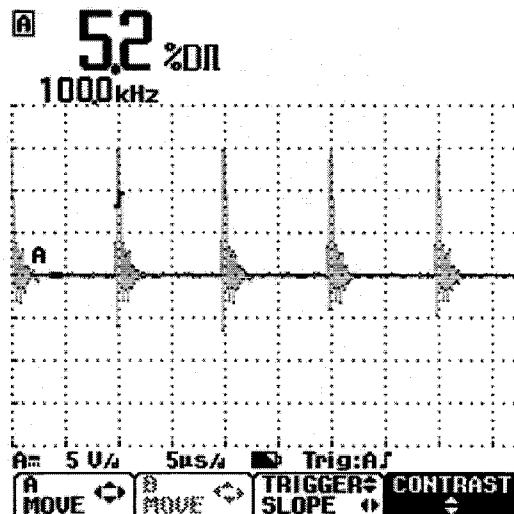


Figure 7.10 Gate drive signal for the MOSFET switch

7.2.2 Response to a Constant Wind Speed of 8 m/s

Investigation was performed for another wind speed of 8 m/s (Figure 7.11) and it was found that all the expected outputs were achieved. The armature current, rotor variation, and furling dynamics are presented in Figures 7.12, 7.13 and 7.14 respectively. Maximum power extraction was achieved by maintaining the optimum TSR (Figure 7.15) and the duty cycle settles to a

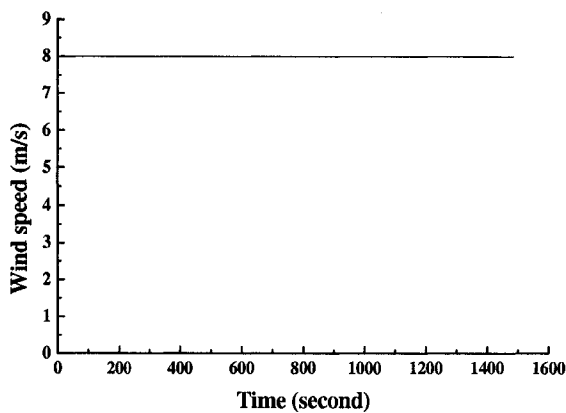


Figure 7.11 Wind speed profile applied to the wind turbine emulator.

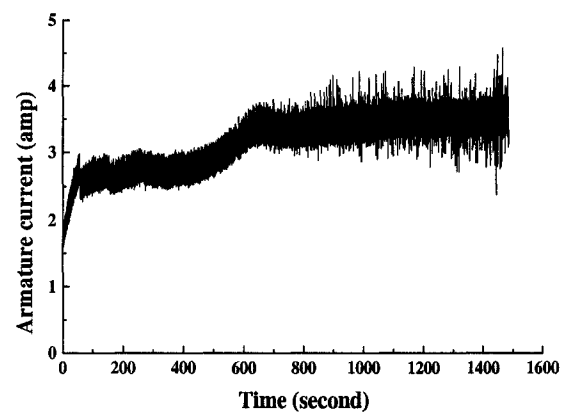


Figure 7.12 Variation of the armature current of the DC motor

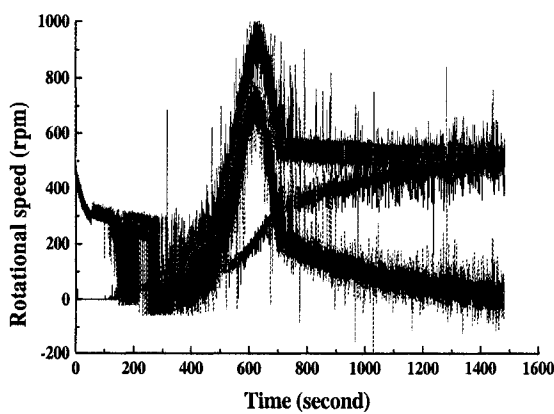


Figure 7.13 Variation of the rotational speed of the DC motor

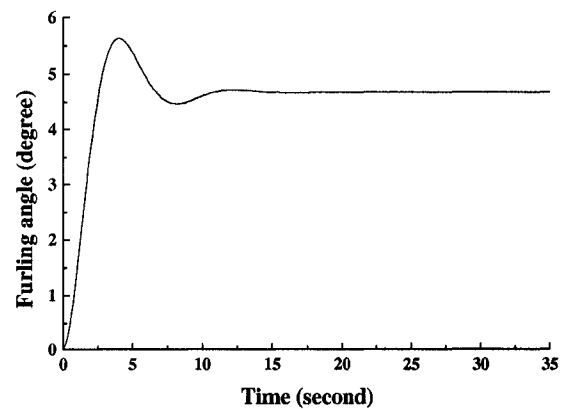


Figure 7.14 Expected furling dynamics of the wind turbine emulator

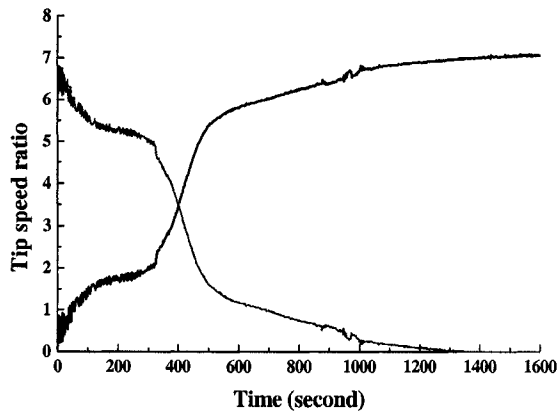


Figure 7.15 Variation of the TSR with time

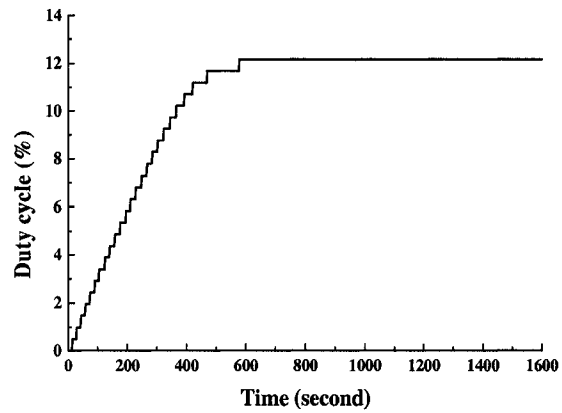


Figure 7.16 Duty cycle variation from

the PIC with time

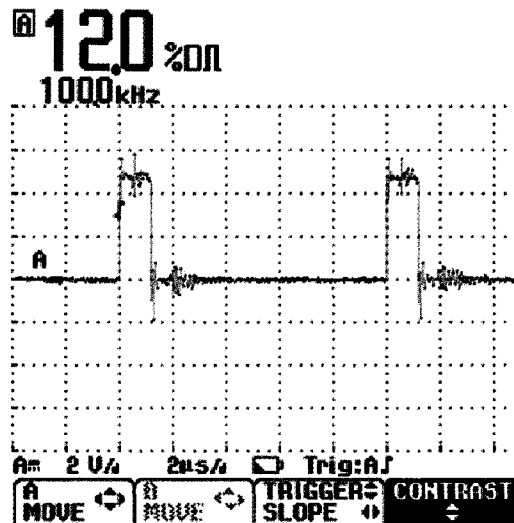


Figure 7.17 PWM wave from the PIC

stable (Figure 7.16) state. Generation of the PWM wave is also attained (Figure 7.17). The MPC power electronics performances are ensured because of a good agreement between the expected (equation (6.24)) and the experimental frequency (Figure 7.19) and because of the corresponding voltage (Figure 7.18) from the RPM extraction stage. Driver circuit performance (Figure 7.20) is also achieved with some ringing at the output due to the wiring inductance and EM noise.

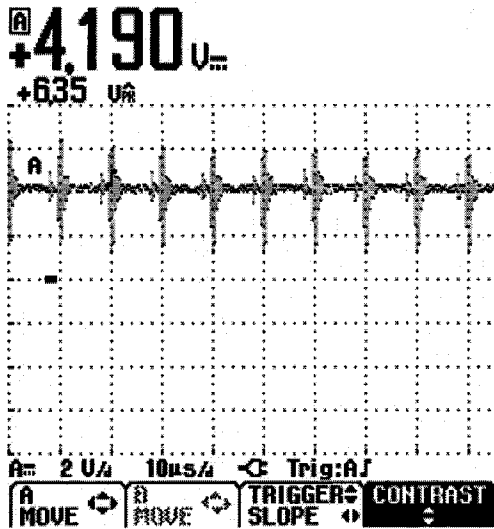


Figure 7.18 Amplified signal

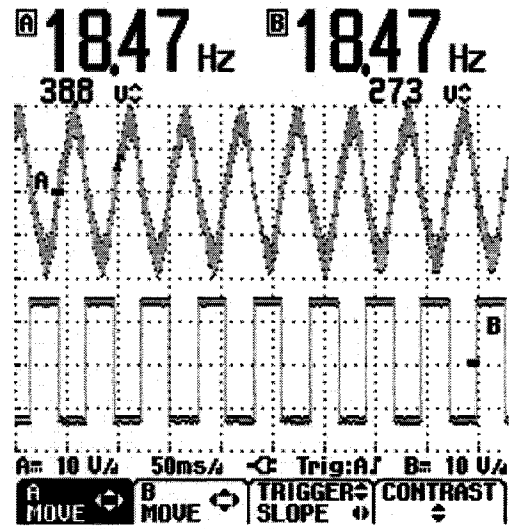


Figure 7.19 Transformer (upper) and

applied to the PIC

Schmitt trigger output (lower)

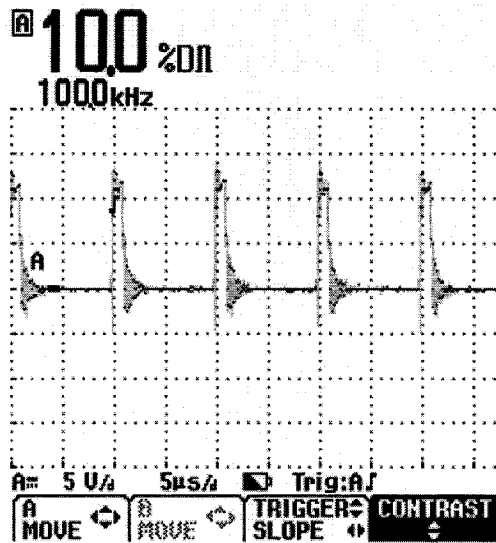


Figure 7.20 Gate drive signal for the MOSFET switch

7.3 Sudden Change Response

It has already been mentioned that a step input can give more insight into the system performances. The input to the WTE was the wind speed and was applied to the system. The objectives of the proposed WTE and MPC are discussed in chapter 6 and the results are describes below:

7.3.1 Response to a step change in wind speed from 7 to 8 m/s

7.3.1.1 Wind Turbine Emulator Characteristics

A step increase in wind speed (from 7 to 8 m/s at $t=480$ seconds) was applied to the emulator as shown in Figure 7.21. With a step change in wind speed, the armature current (Figure 7.22) slightly increases. Also, as far as the emulator receives a step change, reference rotor speed (upper trace) increases and the actual rotational speed (middle trace) of the motor starts to follow the reference rotor speed, and error (lower trace) becomes more or less zero within 13 minutes (Figure 7.23). Figure 7.24 represents the expected furling dynamics of the WTE. After a step input, the rotor comes to a new stable state of 4.6° within 20 seconds. The above discussions ensures the WT performances.

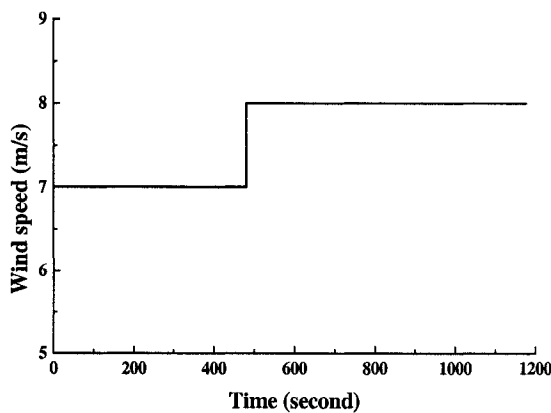


Figure 7.21 Wind speed profile applied to

the wind turbine emulator (Wind speed increases from 7m/s to 8m/s at $t=480$ s).

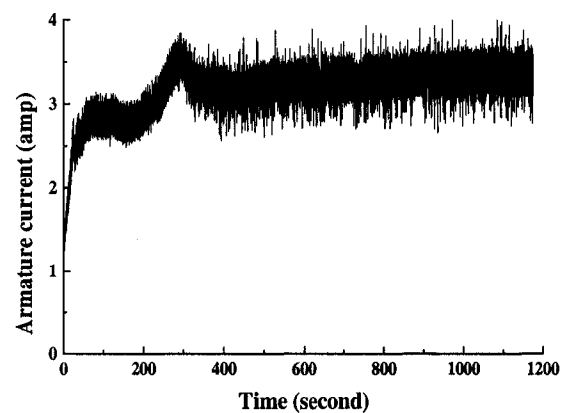


Figure 7.22 Variation of the armature

current of the DC motor

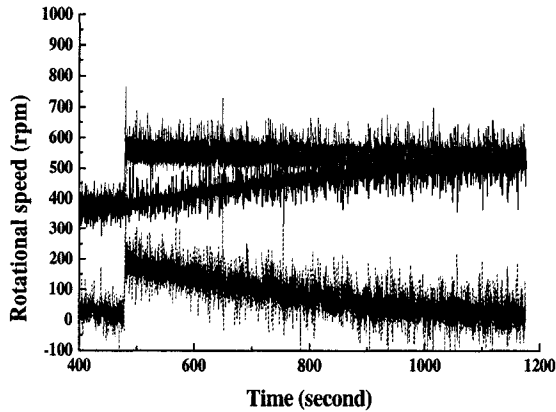


Figure 7.23: Variation of the rotational speed of the DC motor

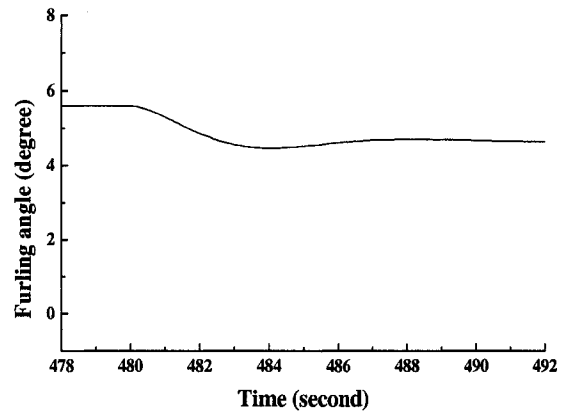


Figure 7.24: Expected furling dynamics of the wind turbine emulator

7.3.1.2 Maximum Power Control

In order to extract the maximum power, WT should have the ability to remain operating at the optimum TSR, even if the wind speed changes. As soon as the wind speed changes, the TSR of the wind turbine drops and starts to increase for the optimum TSR (Figure 7.25) and the system remains more or less constant at the optimum TSR. The PWM wave and driving signal are also presented in Figures 7.26 and 7.27 and a good agreement exists between them. It should be noted that several experimental results of the MPC power electronics for step change in wind speed are not necessary because the results for 7 and 8 m/s were performed and described in section 7.2.

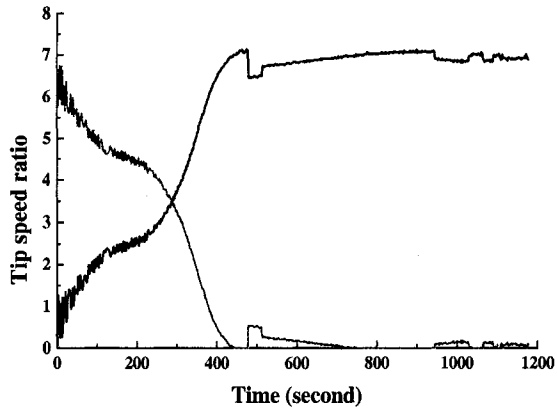


Figure 7.25 Variation of the tip-speed ratio with time

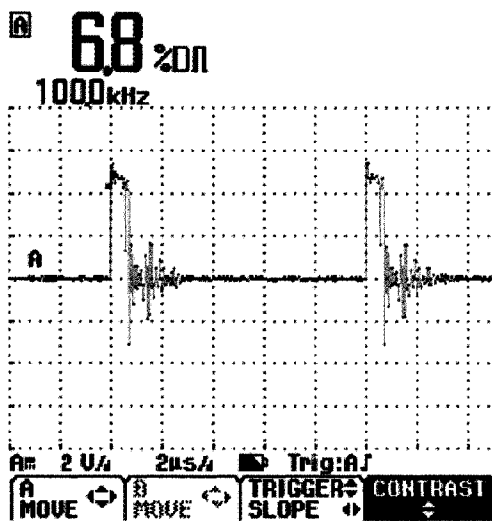


Figure 7.26: PWM wave from the PIC

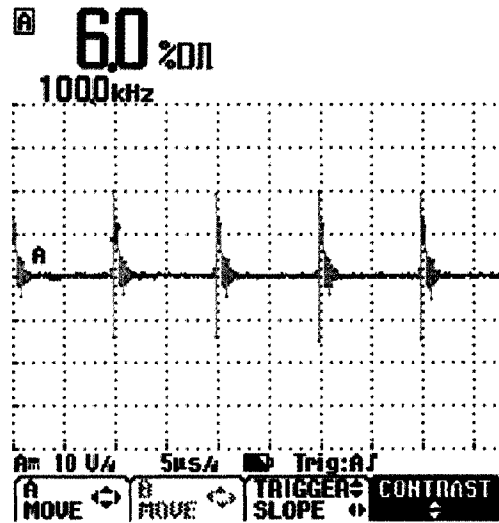


Figure 7.27 Gate drive signal for the MOSFET Switch

7.4 Summary

Implementation of the WTE and MPC are described in the previous chapters (chapter 4 and chapter 6) and the global results are described in this chapter. It was found that the

proposed WTE can emulate the characteristics of a wind turbine and, with the proposed MPC power electronics scheme, it can extract the maximum power from the system. The system works accurately with a constant wind speed and as well as a step change in wind speed.

Chapter 8

Conclusions

8.1 General Summary

Electricity generation using the renewable energy sources has great potential, as such sources are abundant in nature and environmentally friendly. In Canada, wind power is a great prospect. As it is easy to install small wind turbine systems, which require less effort to maintain, interests in the small wind turbines use are increasing dramatically. Small wind turbine systems can meet the load demand of a single user as well as they can be used for community wind. Remote or isolated places are ideal locations for applications of small wind turbines. Selection of a proper control strategy is essential to acquiring maximum output from a wind turbine system. Dynamic modeling and simulation is required to determine the suitable controller for a wind turbine connected to a load. Also, before deploying any wind turbine system for use, several tests need to be

performed to observe the steady state and dynamic aspects, as well as power electronics and controller performance.

A small wind energy conversion system model is developed in a Matlab/ Simulink environment and simulations are performed to investigate the energy capture capability of the system. In the second phase of the research, an isolated small Wind Turbine Emulator (WTE) emulator with a Maximum Power Controller (MPC) is implemented and tested in the laboratory environment. Such an emulator is very helpful for testing and observing a wind turbine and associated power electronics.

8.2 Achievements

- Dynamic modeling and control of a small wind turbine with furling dynamics is investigated. The wind turbine is modeled based on a permanent magnet synchronous generator; two controllers employing the Tip-Speed Ratio (TSR) control and the Hill Climbing (HC) control algorithm are used. A PID controller is used to control the load during the TSR control. A proportional controller is used for the HC control. With the use of Simulink blocks, simulation time is greatly reduced. Expected system stabilization and furling dynamics are attained.
- The effectiveness of these two control strategies for Small Wind Energy Conversion (SWEC) system with respect to their annual energy capture is investigated. A procedure to calculate the annual energy capture from the SWEC system is described using the Bin's power curve method. Two dynamic controllers are designed and their operations are investigated through simulation. Furling action is initiated in the case of high wind speed and reaches a steady state within

10 second. Practical wind speed data and Rayleigh distribution of St. John's, Newfoundland, are used to determine the annual energy capture. It has been found that HC control leads to a better annual energy capture than the TSR control.

- To emulate a wind turbine in a laboratory environment a small WTE is developed based on a separately excited DC machine and the over speed situation is handled by the furling control method. Dynamics due to the furling action are also introduced and it is found acceptable. To reflect the large inertia of such a wind turbine, an inertia disk is designed and coupled to the motor shaft thus rotor dynamics are also incorporated. Instead of the manufacturer's manual, parameter values are determined through experimentation. Test results on the emulator are performed and show acceptable performance. Such an emulator is a strong platform for testing and observing the wind turbine behavior.
- The developed WTE is used to test the power electronics and controller performance. Maximum power control for the emulator is investigated. The TSR control was selected and the duty cycle of the DC - DC converter is controlled to ensure the operation of the wind turbine in an optimum TSR. Various outputs of the maximum power controller power electronics are observed to ensure the system operation and found that the WTE performances are acceptable.

During the course of the thesis work, some of the results have been published in the following publications.

1. Md. Arifujjaman, M. Tariq Iqbal, John E. Quaicoe, M. Jahangir Khan, 'Modeling and control of a small wind turbine,' Proceedings, 18th Annual IEEE Canadian Conference on Electrical and Computer Engineering, CCECE05, May 1-4, 2005, Saskatoon, Saskatchewan Canada

Modeling of the small wind energy conversion system with two dynamic controllers was published in this paper. This paper is based upon the modeling equation and controller strategy described in chapter 2.

2. Md. Arifujjaman M. T. Iqbal John E. Quaicoe, 'Energy capture from a small wind energy conversion system,' 21st Annual Canadian Wind Energy Association Conference and Trade Show, October 16-19, 2005, Toronto, Canada.

Energy capture for St. John's, Newfoundland using Bin's Power Curve method was described in this paper. A comparison of annual energy capture was performed with the TSR and hill-climbing controller and the result were published. These results are based upon the results of chapter 2.

3. Md. Arifujjaman, Eranda Harinath, Scott X. Fang, M.T. Iqbal, 'Design and Comparison of different controllers for a DC position servo system,' Proceedings, The 15th Annual IEEE Newfoundland Electrical and Computer Engineering Conference, November 8, 2005 St. John's, NL.

5 different controllers for a DC position servo system were designed and a comparison was performed according to their performance parameter. This paper was the initial step of starting the implementation of the WTE system.

4. Md. Arifujjaman, M. T. Iqbal, J. E. Quaicoe, 'A Novel Small Wind Turbine Emulator,' Proceedings, The 15th Annual IEEE Newfoundland Electrical and Computer Engineering Conference,, November 8, 2005 St. John's, NL

The preliminary test results of the WTE were published in this paper. The modeling equations and wind turbine side power electronics were described in this paper and discussed in chapter 4.

5. Md. Arifujjaman, M. Tariq Iqbal, John E. Quaicoe, 'An isolated small wind turbine emulator,' Proceedings, Annual IEEE Canadian Conference on Electrical and Computer Engineering, CCECE 06, Ottawa 7-10 May, 2006.

After the accepted performance of the WTE system, this paper was published. A complete description of the load side power electronics was also described with necessary diagrams. This paper is discussed in chapter 6.

6. Md. Arifujjaman, M. Tariq Iqbal, John E. Quaicoe, 'Maximum Power Extraction from a Small Wind Turbine Emulator Using a DC – DC Converter Controlled by a Microcontroller," Accepted for presentation and publication on ICECE 2006, December 19-22, 2006, Dhaka, Bangladesh.

The maximum power extraction through the designed power electronics has been assured and results have been described in this paper. The results of this paper have been described in chapter 7.

8.3 Further Work

- The transient response of the PMSG and rectifier is neglected during the simulation of the modeled SWEC system, which is developed in Matlab/Simulink

environment. In actual practice, such a phenomenon is necessary for a better understanding of the overall system behavior. Instead of using a wind speed vs. furling angle curve, a complete furling model can be developed to reflect the furling mechanism more accurately. Limiters and memory elements are placed at several nodes to eliminate convergence problems and this limits the range of effective parameter variations. Instead of using a fixed wind speed, real time series wind speed data can be applied to the model and left for a possible future work.

- A gain schedule PI controller is designed for the WTE to follow the rotor speed, which might not work for a range of wind speed data. An optimum design of the PI controller is left for further investigation.
- A straightforward design is done for the DC – DC converter, which needs further improvement. Several dynamic aspects need to be considered and left for future research.
- Voltage spikes on several component outputs are observed and need further attention. Specifically, ringing on the gate drive signal and spikes on the voltage waveform on the RPM extraction stage. A proper grounding of the system component could improve the EM noise and need to be considered.
- The implemented emulator can extract maximum power from a resistive load, but in actual practice a load contains both inductive and capacitive component; thus investigation of inductive and capacitive loads needs to be performed.

References

- [1] www.gwec.net
- [2] <http://windenergynews.blogspot.com>
- [3] www.smallwindenergy.ca
- [4] Pena, R., Cardenas, R., Asher, G., Clare, J., Rodriguez, J., Cortes, P., “Vector control of a diesel-driven doubly fed induction machine for a stand-alone variable speed energy system,” IEEE Annual Conference of the Industrial Electronics Society, vol. 2, pp. 985–990, Nov. 5–8, 2002,
- [5] Hoffmann, R., Mutschler, P., “The influence of control strategies on the energy capture of wind turbines,” Industry Applications Conference, 2000. vol. 2, pp. 886 – 893, Oct 8-12, 2000.
- [6] Carlson, O., Hylander, J., Thorborg, K., “Survey of variable speed operation of wind turbines,” Proc. of European Union Wind Energy Conference, Sweden, pp. 406–409, May 20 – 24, 1996
- [7] Zinger, D. S., Muljadi, E., “Annualized wind energy improvement using variable speeds,” IEEE Trans. Ind. Applicat., vol. 33, no. 6, pp. 1444–1447, Nov./Dec. 1997.

- [8] Mutschler, P., Hoffmann, R., "Comparison of wind turbines regarding their energy generation," Proc. 2002 IEEE 33rd Annual IEEE Power Electronics Specialists Conference, vol. 1, Cairns, Qld., Australia, pp. 6–11, June 23–27, 2002.
- [9] Leithead, W., S. de la Salle, Readon, D., "Wind turbine control objectives and design," European Community Wind Energy Conference, Madrid, pp. 510–515, Sep. 1990.
- [10] Simmons, A.D., Freris, L.L., Bleijs, J.A.M., "Comparision of energy capture and structural implications of various policies of controlling wind turbines," EWEC '91, Amsterdam, pp. 99-103, 1991.
- [11] Iqbal, M.T., "Modeling and simulation of a small wind turbine," NECEC 2003, November 12, 2003, St. John's, NL
- [12] Bialasiewicz, J.T., "Furling control for small wind turbine power regulation," Industrial Electronics, 2003. ISIE '03. 2003 ,pp. 804 – 809
- [13] Muljadi,E., Forsyuth, T,. Butterfield, C.P., "Soft–stall control versus furling control for small wind turbine power regulation," 12 pp.; NREL Report No. CP-500-25100
- [14] Wang, Q., Chang, L., "An intelligent maximum power extraction algorithm for inverter-based variable speed wind turbine systems," IEEE Transactions on Power Electronics,vol. 19, no. 5, pp. 1242-1249, Sep 2004
- [15] Ermis, M., Ertan, H.B., Akpınar, E., Ulgut, F., "Autonomous wind energy conversion system with a simple controller for maximum-power transfer,"

Electric Power Applications, IEE Proceedings B, vol. 139, Issue 5, Sept. 1992
pp.421 – 428

- [16] Tanaka, T., Toumiya, T., “Output control by Hill-Climbing method for a small wind power generating system,” *Renewable Energy*, vol. 12, no.4, pp. 387–400, 1997.
- [17] Enslin, J. H., Wyk, J. V., “A study of a wind power converter with micro-computer based maximum power control utilizing an over-synchronous electronic Scherbius cascade,” *Renewable Energy*, vol. 2, no. 6, pp. 551–562.,1992.
- [18] Paul Gipe, “Wind power for home and business: Renewable Energy for the 1990s and Beyond,” Chelsa Green Publishing Company, White River Junction, Vermont, Totnes, England
- [19] Paul Gipe, “Wind Energy Basics-A Guide to Small and Micro Wind Turbines,” Chelsa Green Publishing Company, White River Junction, Vermont.
- [20] Paul Gipe, “Wind power- Renewable Energy for Home, Farm, and Business,” Chelsa Green Publishing Company, White River Junction, Vermont.
- [21] Farret, F. A., Gules, R., Marian, J., “Micro-turbine simulator based on speed and torque of a DC motor to drive actually loaded generators,” *Devices, Circuits and Systems*, 1995. Proceedings of the 1995 First IEEE International Caracas Conference , pp. 89 – 93, 12-14 Dec. 1995.
- [22] Chang, L., Doraiswami, R., Boutot, T., Kojabadi, H., “Development of a wind turbine simulator for wind energy conversion systems,” *Electrical and Computer*

Engineering, 2000 Canadian Conference on vol. 1, pp. 550 – 554, 7-10 March 2000.

- [23] Kojabadi, H.M., Liuchen Chang, Boutot, T., “Development of a novel wind turbine simulator for wind energy conversion systems using an inverter-controlled induction motor,” IEEE Transactions on Energy Conversions, vol. 19, no. 3, pp. 547 – 552, Sept. 2004.
- [24] Kojabadi, H.M.; Liuchen Chang, “A novel steady state wind turbine simulator using an inverter controlled induction motor,” Wind Engineering, vol. 28, no. 4, pp. 433-446, 2004.
- [25] Jian, Lu., Cheng Xu, Wang, “The simulation system of wind turbine performance using a microcontroller controlled SCR_DC motor,” BICEM Paper, August 1987, pp. 865-868
- [26] Nunes, Alexandre Augusto Cançado Seixas, Paulo Fernando Cortizo, Porfírio Cabaleiro Silva, Selênio Rocha, “Wind turbine simulator using a DC machine and a power reversible converter,” ICEMA, Adelaide, Australia, pp. 536-540, 14-16 September 1993.
- [27] Rodríguez-Amenedo, J.L., Rodríguez-García, J.L., Burgos, J.C., Chinchilla, M., Arnalte, S., Veganzones, C., “Experimental rig to emulate wind turbines,” ICEM 98, Istanbul, Turkey, vol. 3/3, pp. 2033-2038, 2- 4 September 1998.
- [28] Rabelo, B., Hofmann, W., Gluck, M., “Emulation of the static and dynamic behaviour of a wind-turbine with a DC- machine drive,” Power Electronics Specialists Conference, 2004. PESC 04. vol. 3, pp. 2107 – 2112, 2004.

- [29] Battaiotto, P. E., Mantz, R. J., and Puleston, P. F., "A wind turbine emulator based on a dual DSP processor system," *Control Engineering Practice*, vol 4, no. 5, pp. 1261-1266, 1996.
- [30] Diop, D. , Nichita, C. , Belhache, J. J., Dakyo, B., and Ceanga, E. , "Modeling variable pitch HAWT characteristics for a real time wind turbine simulator," *Wind Engineering* , vol. 23, no. 4, pp. 225-243, 1999.
- [31] F. Barrero, Mora, J.L., Perales, M., Marchante, A., Galván, E., Carrasco, J.M., Torralba, A., and Franquelo, L.G., "A Test-Rig to evaluate a wind turbine generation control system based on DSP," *7th European Conference on Power Electronics and Applications*. ISBN 90-75815-02-6 Trondheim, Noruega, septiembre de, 1997.
- [32] Pierik, J.T.G., Hoeijmakers, M.J., Vleeshouwers, J.M., Van Engelen, T.G., Baltus, C.W.A., Veltman, A.T., Warmenhoven, A., "A variable speed system with integral control for wind turbines (IRFLET): Design of the test-rig," *Wind Energy: Technology and Implementation* , Amsterdam EWEC '91, pp. 90-93
- [33] Diop, D. , Nichita, C. , Belhache, J. J., Dakyo, B., and Ceanga, E. , "Error evaluation for models of real time wind turbine simulators," *Wind Engineering* , vol. 24, no. 3, pp. 203-221, 2000.
- [34] Bhowmik, S., Spee, R., "Wind speed estimation based variable speed wind power generation, " *Industrial Electronics Society*, 1998. IECON '98. vol. 2, pp.596 - 601 31 Aug.-4 Sept. 1998

- [35] Wang, Q., Chan, L., “An independent maximum power extraction strategy for wind energy conversion systems,” *Electrical and Computer Engineering, 1999 IEEE Canadian Conference on* vol. 2, pp.1142 – 1147, 9-12 May 1999.
- [36] Yamamura, N., Ishida, M., Hori, T., “A simple wind power generating system with permanent magnet type synchronous generator,” *Power Electronics and Drive Systems, 1999. PEDS '99*, vol. 2, pp.849 – 854, 27-29 July 1999.
- [37] Papadopoulos, M. P., Papathanassiou, S. A., Boulaxis, N. G. , Tentzerakis, S. T., “Voltage quality change by grid-connected wind turbines,” *European Wind Energy Conference, Nice, France*, pp. 783–785, 1999.
- [38] Petru, T., Thiringer, T., “Active flicker reduction from a sea-based 2.5 MW wind park connected to a weak grid,” *Proc. Nordic Workshop on Power and Industrial Electronics, Aalborg, Denmark*, June, 13–16, 2002
- [39] Larsson, Å., Sørensen, P. , Santjer, F. , “Grid impact of variable speed wind turbines,” *Proc. of European Wind Energy Conference and Exhibition (EWEC'99), Nice, France, Mar.*, 1–5, 1999.
- [40] Sun, T., Chen, Z., Blaabjerg, F., “Flicker mitigation of grid connected wind turbines using STATCOM” *Power Electronics, Machines and Drives, 2004. (PEMD 2004)*, vol. 1, pp.175 – 180, 31 March-2 April 2004.
- [41] www.windpower.org
- [42] Welfonder, E., Neifer, R., Spanner, M., “Development and experimental identification of dynamic models for wind turbines,” *Control Engineering Practice*, vol. 5, no. 1, pp. 63 – 73, 1997.

- [43] Borowy B.S., Salameh, Z.M., “Dynamic response of a stand-alone wind energy conversion system with battery energy storage to a wind gust”, IEEE Transactions on Energy Conversion, vol. 12, no. 1, March 1997.
- [44] Bikdash, M., “Modeling and control of a Bergey-Type furling wind turbine,” Department of Electrical Engineering, North Carolina A&T State University, Greensboro, NC 27410
- [45] Corbus, D., Prascher, D., “Analysis and comparison of test results from the small wind research turbine test project,” Conference Paper, November 2004, NREL/CP-500-36891
- [46] Eggers Jr., A.J., Chaney, K., Holley, W.E., Ashley, Holt, James Green, H. , Sencenbaugh, Jim , “Modeling and Yawing and furling behavior of small wind turbines,” American Institute of Aeronautics and Astronautics (AIAA) 2000-0022
- [47] Park, R.H., “Two-Reaction Theory of Synchronous Machines- Generalized Method of Analysis – Part I,” AIEE Transaction vol. 48, pp. 716-727, July 1929.
- [48] Krause, P.C., “Analysis of Electric Machinery,” McGraw-Hill Book Company, New York, NY, 1986
- [49] Peterson, H.A., Krause, P.C. “A Direct- and Quadrature- Axis representation of a Parallel AC and DC system,” IEEE Transaction Power Apparatus and Systems, vol. PAS-85, pp. 210-225, March 1966.
- [50] Paul Gipe, “Wind power- Renewable Energy for Home, Farm, and Business,” Chelsea Green Publishing Company, White River Junction, Vermont.

- [51] Manwell, J.F., McGowan, J.G., Rogers, A.L., "Wind Energy Explained – Theory, Design and Application," University of Massachusetts, USA, John Wiley & Sons, LTD, August 2003.
- [52] Nichita, Cristian., Diop, D Amadou , Belhache, Jean J., Dakyo, Brayima., and Protin, Ludovic. , "Control Structure Analysis for a Real Time Wind System Simulator," Wind Engineering , vol. 22, no. 6, 1998,
- [53] Manwell, J.F., McGowan, J.G., Rogers, A., Stein, W., "Developments in Experimental Simulation of Wind/Diesel Systems," Proceedings of the European Wind Energy Conference '89, Glasgow, Scotland, July, 1989.
- [54] Ogata, Katsuhiko., "Modern control engineering," 3rd edition. ©1997 by Prentice-Hall, Inc., Upper Saddle River, New Jersey 07458, U.S.A.
- [55] www.labmaster.com
- [56] El Zawawi, A.M.O., Ashour, H.A., "A fast acting current limit for a PC based DC drive," Electrotechnical Conference, 1996. MELECON '96., vol. 1, pp.332 – 336, 13-16 May 1996.
- [57] El Zawawi, "A PC controlled DC drive using parallel port interfacing," Alexandria Eng. Journal, vol. 34, no. 1, pp. 1-9, Jan 1995.
- [58] Zelenka, K.R., Barton, T.H., "A fast acting current limit for DC motor drive," IEEE Transaction on Industrial Applications, vol. 22, no. 5, pp. 798-804, Sep/Oct 1986.
- [59] Minkova, M. , Minkov, D., Rodgeron, J.L., Harley, R.G., "Current limitation in the adaptive neural speed control of a DC motor, "AFRICON, 1996., IEEE FRICON 4th vol. 2, pp. 837 – 842, 24-27 Sept. 1996 .

- [60] Lin, P. I. H., Messal, E. E., “Design of a real-time rotor inertia estimation system for DC motors with a personal computer,” Instrumentation and Measurement Technology Conference, 1991. IMTC-91. pp. 292 – 296, 14-16 May 1991.
- [61] Castelli, F. , “Dynamic test method for the speed-torque characteristic of DC motors,” Instrumentation and Measurement Technology Conference, 1996. IMTC-96. vol.1, pp. 464 – 468, 1996.
- [62] <http://hyperphysics.phy-astr.gsu.edu>
- [63] Dr.-Ing. Andreas Jochheim, Dr.-Ing. Michael Gerke
Dipl.-Ing. Andreas Bischoff “Modeling and simulation of robotic systems,” Control Systems Engineering group, Department of Electrical Engineering, University of Hagen, D-58084 Hagen, Germany
- [64] www.national.com
- [65] www.coilcraft.com
- [66] www.aimtron.com.tw
- [67] Kazimierczuk, M.K., Nguyen, S.T., “Small-signal analysis of open-loop PWM flyback dc-dc converter for CCM,” Aerospace and Electronics Conference, 1995. NAECON 1995.,vol. 1, pp. 69-76, 22-26 May 1995.
- [68] <http://archive.ericsson.net>
- [69] www.picbook.com

Appendix A

MATLAB/Simulink Wind Energy

Conversion System Subsystem Blocks

This appendix provides the MATLAB/Simulink block diagrams for the wind energy conversion system subsystems described in Chapter 3. Most of the blocks and parameters are symbolized with almost similar notations found in chapter 3.

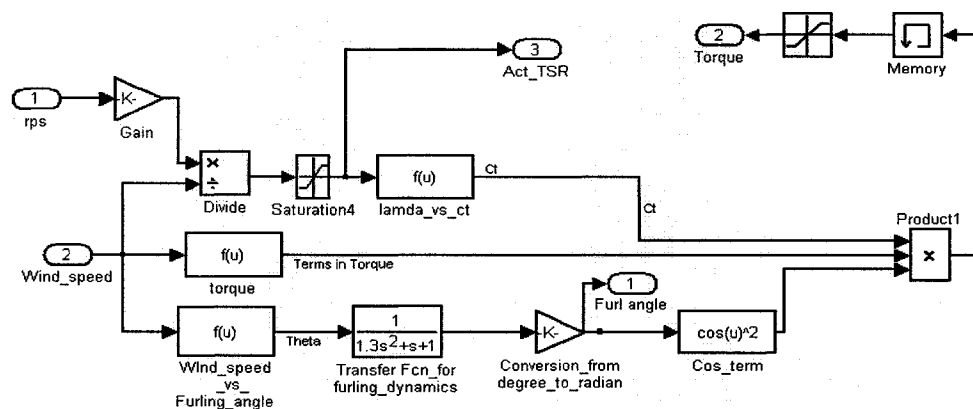


Figure A.1 Subsystem “Wind Turbine”

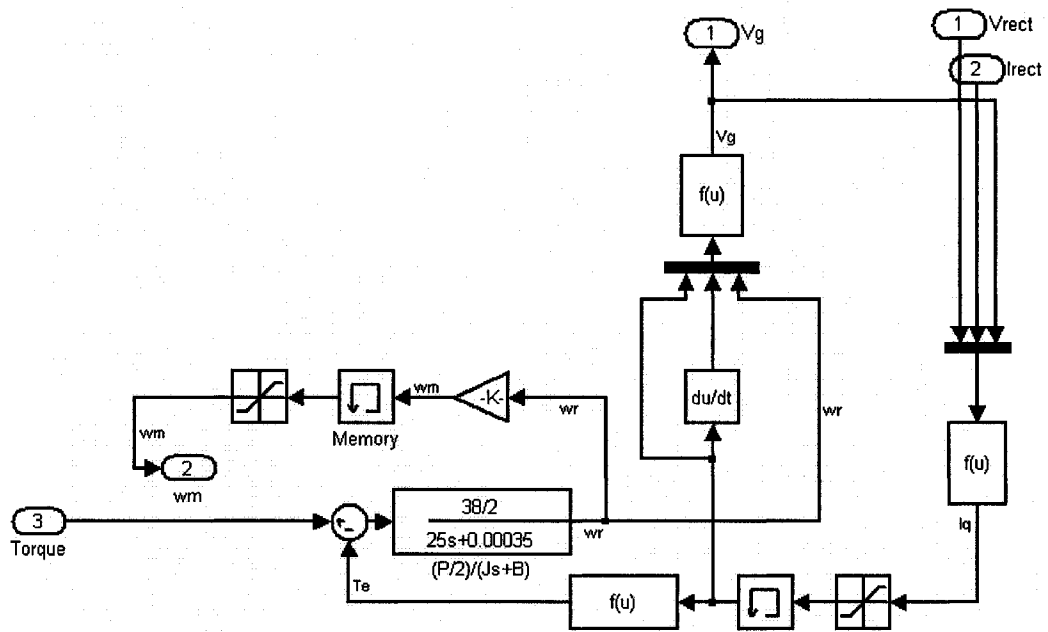


Figure A.2 Subsystem “Permanent Magnet Generator”

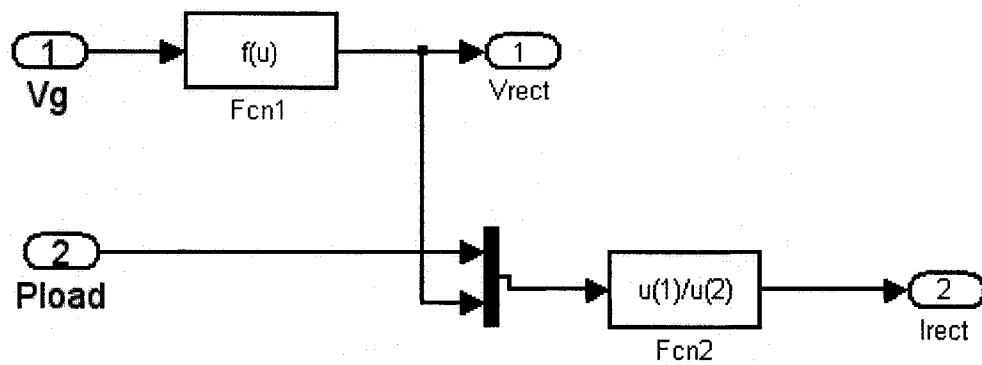


Figure A.3 Subsystem “Rectifier”

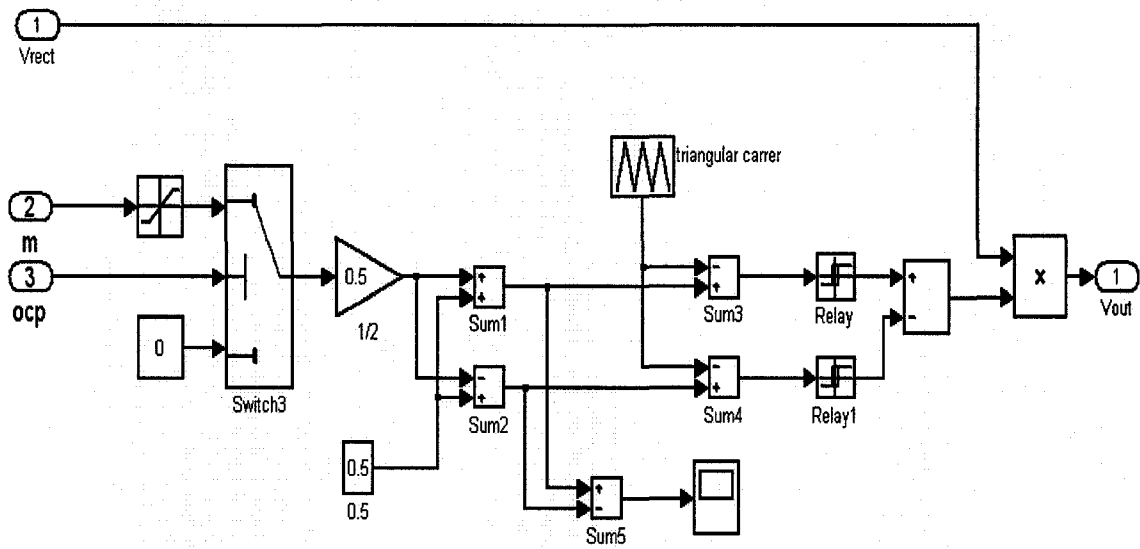


Figure A.4 Subsystem "Inverter"

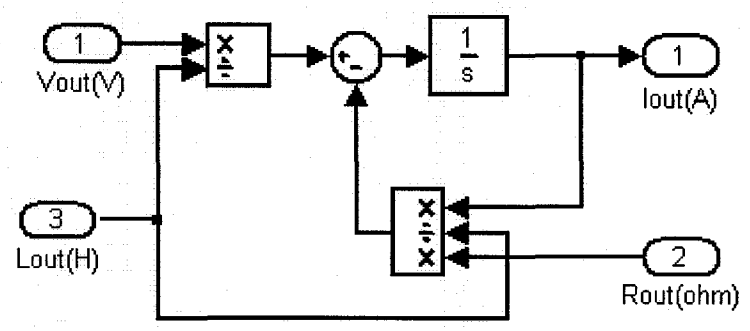


Figure A.5 Subsystem "Load"

Appendix B

Wind Turbine Emulator Control Program

In this Appendix, copies of some test programs and wind turbine emulator control program written in Quick Basic 4.5 are provided. Notations used are similar to the notations described in chapter 2 and 4.

B.1 Analogue Input Test Program

```
10 REM DEM01 Perform continuous analogue to digital conversions of the channel
20 REM      specified .The input range is assumed to be 0 to 10 volt. The board must
30 REM      be in the I/O mapped mode.
40 CLS
50 INPUT "Starting address of the board in decimal", ADDRESS
```

```

60 INPUT "Number of input channel to convert", CHANNEL
70 REM Disable auto-incrementing, external start conversions and all
80 Interrupts Gain = 1
90 OUT ADDRESS + 4, 128
100 REM Output channel number
110 OUT ADDRESS + 5, CHANNEL
120 REM Start Conversion
130 OUT ADDRESS + 6, 0
140 REM Wait until bit 7 of status byte is a 1
150 REM signaling done converting
160 IF INP(ADDRESS + 4) < 128 THEN 160
170 REM Read in data
180 LOW = INP(ADDRESS + 5) AND 255
190 HIGH = INP(ADDRESS + 6) AND 15
200 REM Convert from 2's complement to a number between 0 and 10
210 X = 256 * HIGH + LOW
220 IF HIGH > 7 THEN Y = Y - 4096
230 VOLTAGE = X / 204.8
240 PRINT 'Channel = ', CHANNEL "Voltage = "; VOLTAGE
250 GOTO 140

```

B.2 Analogue Output Test Program

```

10 REM DEM02 Program to input a voltage to a digital to analogue

```

```

20 REM converter. The board must be mapped I/O mapped mode
30 CLS
40 INPUT " Starting address of board in decimal "; ADDRESS
50 PRINT "1 0 to 10 volts"
60 PRINT "2 -10 to 10 volts"
70 PRINT "3 0 to 5 volts"
80 PRINT "4 -5 to 10 volts"
90 PRINT "5 -2.5 to +2.5 volts"
100 INPUT "Range of DAC 0"; RANGE0
110 INPUT "Range of DAC 1"; RANGE1
120 PRINT
130 INPUT "Enter DAC number, voltage", NUMBER, VOLTAGE
140 REM "Convert to a decimal number between -2048 to 2047"
150 IF NUMBER = 0 THEN ON RANGE0 GOTO 170, 180, 190, 200, 210
160 IF NUMBER = 1 THEN ON RANGE0 GOTO 170, 180, 190, 200, 210
170 DECIMAL = 409.5 * VOLTAGE - 2048: GOTO 230
180 DECIMAL = 204.7 * VOLTAGE: GOTO 230
190 DECIMAL = 819 * VOLTAGE - 2048: GOTO 230
200 DECIMAL = 409.4 * VOLTAGE - 2048: GOTO 230
210 DECIMAL = 818.8 * VOLTAGE - 2048: GOTO 230
220 REM "convert to 2's complement"
230 DECIMAL = INT (DECIMAL)
240 HIGH = INT (DECIMAL / 256)

```

```
250 LOW = DECIMAL - 256 + HIGH
260 IF HIGH < 0 THEN HIGH = 16 + HIGH
270 REM "Output the data to DAC"
280 IF NUMBER = 0 THEN OUT ADDRESS + 1, HIGH: OUT ADDRESS, LOW
290 IF NUMBER = 1 THEN OUT ADDRESS + 3, HIGH: OUT ADDRESS + 2, LOW
300 PRINT "The data has been written to DAC"
310 GOTO 180
```

B.3 Program for Control of Wind Turbine

Emulator

```
10 CLS
DIM A(2), y(3), e(2), u(2), k(2), l(2), d(2)
OPEN "wind.DAT" FOR INPUT AS #1
'OPEN "result.DAT" FOR OUTPUT AS #2
A(1) = 0: A(2) = 0
y(1) = 0: y(2) = 0: y(3) = 0
e(1) = 0: e(2) = 0
u(1) = 0: u(2) = 0
l(1) = 0: l(2) = 0
d(1) = 0: d(2) = 0
c = .9
m = .65
```

```
t0 = .1
ti = .556
kp = .03#
q0 = kp
q1 = kp * (t0 / ti - 1)
ti1 = 0.235
kp1 = .00009#
q2 = kp1
q3 = kp1 * (t0 / ti1 - 1)

ti2 = .15
kp2 = .00000005#
q4 = kp2
q5 = kp2 * (t0 / ti2 - 1)
R = 2.286

'PRINT "Program for AD conversion"
80 SOUND 21000, 1.82

FOR DELAY = 1 TO 10500: NEXT DELAY

INPUT #1, W
PRINT "w ="; W

OUT 1812, 128
OUT 1813, 1
OUT 1814, 0
```

```

90 IF INP(1812) < 128 THEN 90

LOW& = INP(1813) AND 255

HIGH& = INP(1814) AND 15

X = (256 * HIGH&) + LOW&

IF HIGH& > 7 THEN X = X - 4096

VOLTAGE1 = X / 204.8

PRINT "Channel = 1"; "voltage1 = "; VOLTAGE1

OUT 1813, 2

OUT 1814, 0

120 IF INP(1812) < 128 THEN 120

LOW% = INP(1813) AND 255

HIGH% = INP(1814) AND 15

y = (256 * HIGH%) + LOW%

IF HIGH% > 7 THEN y = y - 4096

RPM = 216 * VOLTAGE

IF RPM < 0 THEN RPM = 1 ELSE IF RPM > 1750 THEN RPM = 1750

CURRENT = 1.63 * VOLTAGE1 + .2508

TOR = .698304 * CURRENT

IF TOR < 0 THEN TOR = .1 ELSE IF TOR > 206 THEN TOR = 206

CON1 = (R / W)

TSR = (RPM * CON1 * 3.14) / 30

IF TSR < 0 THEN TSR = 0 ELSE IF TSR > 9.772 THEN TSR = 9.772

CP = .00044 * (TSR) ^ 4 - .012 * (TSR) ^ 3 + .097 * (TSR) ^ 2 - .2 * TSR + .11

```

IF CP < 0 THEN CP = .1 ELSE IF CP > .59 THEN CP = .59

A(1) = A(2)

A(2) = (-.00017327# * W ^ 5 + 8.500799999999999D-03 * W ^ 4 - .12034 * W ^ 3 +
.4501 * W ^ 2 + 1.0592 * W - .38972) * .0174532#

y(1) = y(2)

y(2) = y(3)

y(3) = (1.919 * y(2) - .926 * y(1) + .003747 * A(2) + .003652 * A(1))

ANG = (COS(y(3))) ^ 3 * W ^ 3

CON2 = .5 * 1.293 * 3.14 * R ^ 2

RES1 = CP * ANG * CON2

RPM1 = RES1 / TOR

e(1) = e(2)

e(2) = RPM1 - RPM

PRINT "e(1) ="; e(2)

u(1) = u(2)

IF W = 7 THEN u(2) = u(1) + q0 * e(2) + q1 * e(1)

IF W = 8 THEN u(2) = u(1) + q2 * e(2) + q3 * e(1)

k(1) = k(2)

k(2) = -2.9 * u(2) ^ 2 + 54 * u(2) - 130

IF k(2) < 24.48 THEN k(2) = 24.48 ELSE IF k(2) > 125 THEN k(2) = 125

l(1) = l(2)

l(2) = .00001 * k(2) ^ 3 - .0021 * k(2) ^ 2 + .18 * k(2) - .64

d(1) = m * l(1) + c

$d(2) = m * l(2) + c$

$chy = d(2) - d(1)$

$cho = l(2) - l(1)$

If $chy > cho$ THEN $ou = d(2)$ else $ou = l(2)$

$500 \text{ DECIMAL\%} = 409.5 * ou - 2048$

$600 \text{ DECIMAL\%} = \text{INT}(\text{DECIMAL\%})$

$\text{HIGH\%} = \text{INT}(\text{DECIMAL\%} / 256)$

$\text{LOW\%} = \text{DECIMAL\%} - (256 * \text{HIGH\%})$

IF $\text{HIGH\%} < 0$ THEN $\text{HIGH\%} = 16 + \text{HIGH\%}$

OUT 1809, HIGH\%

OUT 1808, LOW\%

WRITE #2, RPM, RPM1, A(2), y(3), e(2), CURRENT, CP

GOTO 80

Appendix C

Program for the Maximum Power Control

In this Appendix, PIC 18F452 program to extract maximum power from the wind turbine emulator is provided. Details may be found in chapter 6. This program was written in MikroBasic version 2.0.0.4.

C.1 Program for the Maximum Power Control

```
program load_controller  
  
dim AD_Res1 as word  
  
dim Value1,Value2 as longint  
  
dim Value1_view,Value2_view as word  
  
dim t0,ti,kp as float
```

dim q0,q1,q2 as float
dim q01 as float
dim q03 as float
dim q02 as word
dim q04 as word
dim rps2 as longint
dim rps1 as longint
dim rps as word
dim rarious as word
dim wind_speed as word
dim wind1 as word
dim lamda as longint
dim lamda_final as word
dim lam as word [2]
dim lam_dummy as word
dim lam_dummy1 as word
dim lam_dummy2, lam_dummy3 as longint
dim lamr as longint [2]
dim lamrt as float
dim outm as word
dim rps_view as longint
dim lamda_view as longint
dim wind1_view as longint

```

dim Value21, Value22, Value23 as longint

dim la as longint

sub procedure Write_str_usart(dim strx as word)

dim p as ^word

dim ij as byte

p=strx

ij=0

while p^ > 0

if p^ > 0 then

usart_write(p^)

end if

ij=ij+1

p=strx+ij

wend

end sub

sub procedure writeByte(dim datillo as word)

dim strz as string[5]

WordToStr(datillo, strz )

Write_str_usart(@strz)

end sub

main:

TRISA = $FF

```

```

PORTC = $FF

ADCON1= $80

' parameter decleration

t0 = 1.5

ti = 0.01

kp = 0.0001

q0 = kp

q01 = q0 * 1000

q02 = float(q01)

q1 = kp*(t0/ti - 1.0)

q2 = q1 *1000

q04 = float(q2)

'Initialization

lam[0] = 0

lam[1] = 0

lamr[0] = 0

lamr[1] = 0

outm = 0

eloop:

Usart_init(19200)           ' init rs232

AD_Res1 = ADC_read(4)      'read input from wind turbine

'Delay_ms(1000)

Value1 = (AD_Res1 * 5000)/1023

```

```
IF Value1 <= 90 THEN
    goto level1
ELSE
    goto level2
END IF

level1:
writeByte(Value1)
USART_write(13)
USART_write(10)
goto eloop

level2:
Value1_view = longint(Value1)
Value2 = 4.4571 * Value1 - 293.3
wind_speed = 7
IF Value1 > 3300 THEN
    wind_speed = 8
    END IF
Value2_view = longint(Value2)
rps2 = Value2 * 30
rps1 = rps2 * 0.104719755
rps = longint(rps1)
Pwm_Init(100000)
Pwm_Start
```

```

radius = 2286

wind1 = radius / wind_speed

lamda = (rps * wind1)/1000

lamda_final = longint(lamda)

lamda_view = (lamda_final)/10

lam[0] = lam[1]

lam[1] = 7000 - lamda_final

IF lam[0] < 50 THEN           'limits
    lam[0] = 0
END IF

IF lam[0] > 7000 THEN        'limits
    lam[0] = 0
END IF

IF lam[1] < 50 THEN         'limits
    lam[1] = 0
END IF

IF lam[1] > 7000 THEN       'limits
    lam[1] = 0
END IF

lamr[0] = lamr[1]

lam_dummy = float(q0 * lam[1])

lam_dummy2 = word(lam_dummy)

lam_dummy1 = float(q1 * lam[0])

```

```
lam_dummy3 = word(lam_dummy1)

lamr[1] = lamr[0]+lam_dummy2 + lam_dummy3

IF lamr[1] < 0 THEN          'limits
    lamr[1] = 0
ELSE
    IF lamr[1] > 127500 THEN
        lamr[1] = 127500
    END IF
END IF

writeByte(Value1_view)

outm = lamr[1]/1000

writeByte(outm)

USART_write(13)

USART_write(10)

Pwm_Change_Duty(outm)

Delay_us(5000)

delay_ms(1000)

goto eloop

end.
```